Aus dem Institut für Neuropathologie
der Medizinischen Fakultät Charité – Universitätsmedizin Berlin

DISSERTATION

Cellular targets and downstream effector mechanisms of IL-12/IL-23 signalling in Alzheimer‘s disease

zur Erlangung des akademischen Grades
Doctor of Philosophy (PhD)

vorgelegt der Medizinischen Fakultät
Charité – Universitätsmedizin Berlin

von

Pascale Eede

aus Bonn

Datum der Promotion: 18.12.2020

Index

List of figures and tables 3

Abstract 4

Zusammenfassung 5

Supporting text “Cellular targets and downstream effector mechanisms of IL-12/IL-23 signalling in Alzheimer‘s disease” 6-32

- Background 6-7
- Aims 7-8
- Results & Discussion 8-23
- Conclusion 23
- Materials & Methods 24-28
- References 29-32

Statutory Declaration 33

Declaration of contribution 34

Journal Summary List 35

Publication Eede *et al*., 2020 36-53

Curriculum vitae 54-55

List of publications 56-57

Acknowledgements 58

List of figures

Figure 1. Graphical summary illustrating the effect of IL12p40 deletion in male and female APP23 mice 10

Figure 2. IL-12/IL-23 receptor expression in the brain 13

Figure 3. Graphical illustration of APPPS1;Nestin^{Cre};IL23R$^{fl/fl}$ and APPPS1;Aldh1l1^{CreERT};IL23R$^{fl/fl}$ mouse breedings 15

Figure 4. Analysis of Aβ pathology and targeting efficiency in APPPS1;Nestin^{Cre};IL23R$^{fl/fl}$ mice 17

Figure 5. Analysis of targeting efficiency and Aβ pathology in APPPS1;Aldh1l1^{CreERT};IL23R$^{fl/fl}$ mice 19

Figure 6. Graphical illustration of APPPS1;Nestin^{Cre};IL12Rβ2$^{fl/fl}$ and APPPS1;Aldh1l1^{CreERT};IL12Rβ2$^{fl/fl}$ mouse breedings 21

Figure 7. Validation experiments of APPPS1;Nestin^{Cre};IL12Rβ2$^{fl/fl}$ and APPPS1;Aldh1l1^{CreERT};IL12Rβ2$^{fl/fl}$ mouse lines 22

List of tables

Table 1. PCR primer sequences for the detection of exon-specific gene recombination 24

Table 2. PCR program for floxed *Il23r* gene amplification 25

Table 3. PCR program for floxed *Il12rb2* gene amplification 25

Table 4. Overview of RNAscope® target probes 27

Abstract

Alzheimer's disease (AD) is a severe neurodegenerative disorder characterised by the accumulation of aggregated amyloid-β (Aβ) and tau proteins as well as the activation of inflammatory processes in the brain, leading to neuronal cell death. Modulation of inflammatory factors presents an attractive therapeutic target since a direct interplay between inflammation and AD pathogenesis has been identified. In this study, we confirm previously published data showing that inhibition of the interleukin (IL)-12 and IL-23 signalling pathway leads to an amelioration of Aβ pathology. Genetic deletion of the shared IL-12/IL-23 IL12p40 subunit in APP23 AD-like mice caused a gender-specific reduction in Aβ burden, highlighting the significance of the IL-12/IL-23 pathway as well as gender considerations in AD. Furthermore, we identified neurons and oligodendrocytes as the IL-12/IL-23 receptor-bearing cells, uncovering a yet unknown intercellular inflammatory signalling pathway. Based on these observations, we generated AD-like mouse lines deleting the IL-23-specific receptor (APPPS1;Nestin^{Cre};IL23R$^{fl/fl}$ and APPPS1;Aldh1l1^{CreERT};IL23R$^{fl/fl}$) as well as the IL-12-specific receptor (APPPS1;Nestin^{Cre};IL12Rβ2$^{fl/fl}$ and APPPS1;Aldh1l1^{CreERT};IL12Rβ2$^{fl/fl}$) only in neural cells. Since initial results indicate that IL-23 signalling is not the key player in IL-12/IL-23-driven pathogenic aspects of AD, future research is required to prove the importance of IL-12 signalling in AD. Obtaining a detailed understanding of the precise downstream signalling mechanisms of the IL-12/IL-23 pathway is essential since it can provide a basis for target-directed therapy of AD, a disease that is not yet curable.

Zusammenfassung

Die Alzheimer Erkrankung (AE) ist eine schwerwiegende neurodegenerative Erkrankung, die charakterisiert wird durch die Akkumulation von aggregierten Amyloid-β (Aβ) und Tau Proteinen sowie der Aktivierung inflammatorischer Prozesse im Gehirn, welche schließlich zu neuronalem Zelltod führen. Modulierung von inflammatorischen Faktoren gilt als attraktiver therapeutischer Angriffspunkt, da ein direkter Zusammenhang zwischen Inflammation und AE Pathogenese besteht. In dieser Arbeit konnten wir bereits publizierte Daten validieren, welche zeigten, dass die Inhibition des Interleukin (IL)-12/IL-23 Signalwegs zu einer Verbesserung der Aβ Pathologie führte. Genetische Deletion der von IL-12/IL-23 geteilten IL12p40 Untereinheit im APP23 AE-Mausmodell erwirkte eine geschlechter-spezifische Reduktion der Aβ Belastung, welches die Signifikanz des IL-12/IL-23 Signalwegs sowie von Geschlechterunterschieden in der AE hervorhebt. Zusätzlich identifizierten wir, dass Neurone und Oligodendrozyten die IL-12/IL-23 Rezeptoren exprimierten, und entdeckten somit einen neuen interzellulären inflammatorischen Signalweg. Basierend auf diesen Ergebnissen generierten wir AE-ähnliche Mauslinien, in denen der IL-23-spezifische Rezeptor (APPPS1;Nestin^{Cre};IL23R$^{fl/fl}$ und APPPS1;Aldh1l1^{CreERT};IL23R$^{fl/fl}$) sowie der IL-12-spezifische Rezeptor (APPPS1;Nestin^{Cre};IL12Rβ2$^{fl/fl}$ und APPPS1;Aldh1l1^{CreERT};IL12Rβ2$^{fl/fl}$) ausschließlich auf neuralen Zellen deletiert ist. Erste Ergebnisse zeigten, dass IL-23 wohl nicht das entscheidende Zytokin im pathogenetisch relevanten IL-12/IL-23 Signalweg darstellt, weshalb sich unsere weiteren Forschungsvorhaben auf die Rolle von IL-12 in der AE fokussieren werden. Ein exaktes Verständnis der nachgeschalteten Mechanismen des IL-12/IL-23 Signalwegs ist essentiell um eine valide und präzise Grundlage für künftige Therapieansätze der bislang unheilbaren AE zu entwickeln.

Cellular targets and downstream effector mechanisms of IL-12/IL-23 signalling in Alzheimer‘s disease

Background

Alzheimer’s disease (AD) is the most common form of dementia with an increasing prevalence in the elderly population. Clinical symptoms include memory loss as well as deterioration of language and emotional control, which are caused by the dysfunction of synapses and degeneration of neurons in cortical regions and the hippocampus (McKhann *et al*., 2011). The pathophysiology of AD is characterised by the aberrant accumulation of the amyloid-β (Aβ) protein into extracellular plaques, which can already be noted approximately 20 years before the appearance of cognitive impairment (Gordon *et al*., 2018). Another pathological hallmark is the appearance of intracellular tangles of the tau protein found within neurons (Montine *et al*., 2012). In recent years, the role of the immune system in AD has also become a large research focus, since genetic variants of genes linked to the innate immune system have been ascribed to an increased risk for the development of sporadic AD (Bradshaw *et al*., 2013; Guerreiro *et al.,* 2013). The main innate immune cells of the brain are microglia and astrocytes that both regulate brain homeostasis and respond to pathogenic stimuli or cellular changes by secreting pro- and anti-inflammatory cytokines and chemokines or engulfing pathogens or cellular debris (reviewed in Colonna & Butovsky, 2017 and Sofroniew & Vinters, 2010). Both microglia and astrocytes have been shown to associate with Aβ plaques in the brains of AD patients (Serrano-Pozo *et al*., 2011), yet the exact nature of their role in AD pathogenesis is still far from clear and an area of active research.

Mouse models of AD provide a very useful tool in identifying and elucidating mechanisms influencing AD development or progression. Commonly used models overexpress human mutated forms of the amyloid precursor protein (APP) and/or presenilin 1 (PSEN1) genes that lead to familial AD in patients under the control of neuronal promoters (reviewed in Myers & McGonigle, 2019). These lines are characterised by amyloidogenesis in the brain parenchyma as well as plaque-associated activation of microglia and astrocytes, mimicking early pathological processes observed in the brains of AD patients. AD mouse models thus present very useful tools for genetic manipulation of specific cell types or pathways and for testing pharmacological compounds and their effect upon Aβ pathology.

Making use of the APPPS1 mouse line harbouring the Swedish (KM670/671NL) APP mutation and PSEN1 L166P mutation under the control of the Thy1 promoter (Radde *et al*., 2006), our lab has previously reported an upregulation of the pro-inflammatory cytokines interleukin (IL)-12 and IL-23 by microglia (vom Berg *et al*., 2012). When targeting IL12p40, the common subunit of both IL-12 and IL-23, by genetic deletion or pharmacological blockage, Aβ pathology was reduced and cognitive deficits were ameliorated (vom Berg *et al*., 2012). Tan *et al*. (2014) also found a positive effect of blocking IL-12/IL-23 signalling upon AD-like pathology and analysis of AD patient material also found a link between these pathways and the human disease condition (Hu *et al*., 2012; vom Berg *et al*., 2012; Chen *et al*., 2014; Wood *et al*., 2015).

Another important observation derived from epidemiological studies of AD patients is the increased risk to develop AD in female subjects (Mayeda, 2019). Additionally, differences in both the innate and adaptive immune response between males and females (reviewed in Klein & Flanagan, 2016), including microglial phenotypes (Guneykaya *et al*., 2018; Villa *et al*., 2018), have been described. Single-cell transcriptome analyses confirmed these notions by finding a gender-specific response within all brain cell populations of male and female AD patients (Mathys *et al*., 2019).

Aims

1. **Assessing the lack of IL-12/IL-23 signalling upon Aβ pathogenesis in APP23 mice**

In light of these observations, this study firstly aimed at identifying whether the beneficial effect of blocking the IL-12/IL-23 pathway upon AD pathogenesis is model- and/or gender-specific. We thus crossed mice deficient in IL12p40 (Magram *et al*., 1996) to the APP23 mouse model of AD harbouring the Swedish (KM670/671NL) mutation in the *APP* gene (Sturchler-Pierrat *et al*., 1997). APP23 mice recapitulate more closely the Aβ pathology of human AD patients with respect to the Aβ accumulation time course and histopathological Aβ composition. Similar to human AD patient populations (Mayeda, 2019), gender differences in plaque deposition have been described in this mouse model (Sturchler-Pierrat & Staufenbiel, 2000). We therefore assessed gender-specific properties of Aβ deposition as well as Aβ processing, neuritic dystrophy and glial activation in male and female APP23 mice lacking or harbouring the IL-12/IL-23 signalling pathway.

2. Investigation of downstream IL-12/IL-23 signalling mechanisms in AD

The second aim of this study was to further analyse the downstream signalling mechanisms of IL-12/IL-23 signalling. Vom Berg *et al*. (2012) could show that the IL12p40 receptor, namely IL12Rβ1, was expressed in non-microglial cell populations, suggesting an intercellular signalling pathway. We therefore aimed at localising the IL-12/IL-23 receptors in brain tissue of AD mouse lines. Additionally, it is of major therapeutic interest to identify whether it is IL-12 or IL-23 specifically that exerts its detrimental effect upon AD pathology. We thus generated mouse lines targeting specifically IL-12 or IL-23 signalling in neural cells to identify and target the cytokine and the cell type most relevant to AD pathology.

Results & Discussion

Aim 1 – Assessing the lack of IL-12/IL-23 signalling upon Aβ pathogenesis in APP23 mice

Female APP23 mice show increased Aβ pathology and astrogliosis compared to male APP23 mice

We and others have linked IL-12/IL-23 signalling to AD pathology by identifying an increase of this pathway in AD-like mouse models (vom Berg *et* al., 2012; Tan *et al*., 2014) as well as CSF (vom Berg *et al*., 2014), plasma (Hu *et al*., 2012) and brain tissue (Wood *et al*., 2015) of AD patients. However, the role of IL-12/IL-23 signalling in a gender-specific context has not been analysed so far. The APP23 mouse model has been reported to show gender differences in Aβ pathology and behavioural characteristics (Sturchler-Pierrat & Staufenbiel, 2000), yet no side-by-side comparison of male and female APP23 mice at late stages of pathology has been undertaken to date. We thus quantified pathological hallmarks in male versus female APP23 mice at 21 months of age using biochemical and histological methods. We quantified both diffuse and core plaque pathology via immunohistochemistry and identified that female mice have a 2-fold higher plaque burden than male mice (Eede *et al*., 2020). Using biochemical techniques, we also saw increased levels of both soluble and insoluble levels of the $A\beta_{1\text{-}40}$ and $A\beta_{1\text{-}42}$ isoforms as well as an increased amount of aggregated Aβ in the insoluble protein fractions of female APP23 mice (Eede *et al*., 2020). Despite this increase in Aβ pathology, there were no gender-specific differences found in plaque-associated neuritic dystrophy or

Aβ-processing enzymes (Eede *et al*., 2020). A possible explanation for the observed gender differences could be a faster disease course in female APP23 mice. It was previously suggested that hormonal variances could account for gender-specific differences in spatial learning paradigms (D'Hooge & de Deyn, 2001), however an effect of hormones upon Aβ burden has not been described to date. The underlying reasons for gender-specific pathogenesis in AD mouse models thus remains to be elucidated.

Similar to human pathology, APP23 mice also show activated microglia and astrocytes associated with Aβ deposits in the brain (Sturchler-Pierrat *et al*., 1997; Stalder *et al*., 1999). Compared to male mice, we found an increase in the cortical astrocyte number in female mice, which correlated with the increase in plaque burden. Microglial characteristics such as peri-plaque accumulation, expression of the activation marker Clec7a (Keren-Shaul *et al*., 2017; Krasemann *et al*., 2017) and Aβ uptake did not differ between male and female APP23 mice (Eede *et al.,* 2020). We also analysed the cytokine milieu of the brain and plasma which showed that, compared to male mice, female APP23 mice had higher levels of IL-4 in the plasma, IL-10 in both plasma and brain as well as TNF-α and CXCL1 in brain. We also noted a positive correlation between CXCL1 levels in the brain and both soluble and insoluble $A\beta_{1\text{-}40}$ levels (Eede *et al*., 2020). These results indicate that deregulated cytokine secretion could be a confounding factor and biomarker for gender-specific differences of Aβ burden.

Similar to APPPS1 mice, we also identified the IL12p40 subunit to be a relevant immune target in the APP23 mouse model, since microglial IL12p40 (*Il12b*) gene expression as well as IL12p40 protein levels in the brain were increased compared to wildtype littermates. To validate the protective effects of IL12p40 deletion seen in APPPS1 mice in another mouse model, we crossed APP23 mice to $IL12p40^{-/-}$ mice ($APP23p40^{-/-}$), lacking IL12p40 expression.

IL12p40 deficiency differentially affects pathology in male and female APP23 mice

Due to the vast gender differences observed in APP23 mice, the effect of IL12p40 deficiency upon pathology was assessed separately in male and female $APP23p40^{-/-}$ mice, where indeed, gender-specific effects of IL12p40 deletion were found (summary in *Fig. 1*). Male $APP23p40^{-/-}$ mice had significantly less diffuse and core Aβ plaques compared to APP23 littermates, yet $A\beta_{1\text{-}40}$ levels and Aβ aggregation properties were unchanged (Eede *et al*., 2020). In female mice, on the other hand, lack of IL12p40 led to

a significant reduction in TBS- and Triton-X-soluble $A\beta_{1-40}$ species, the main Aβ isoform found in APP23 mice (Sturchler-Pierrat & Staufenbiel, 2000), whilst Aβ plaque burden was unaffected (Eede *et al*., 2020). Despite these reductions in Aβ pathology, other pathological hallmarks such as neurite dystrophy and the number of cortical astrocytes were not affected by IL12p40 deletion. Similarly, the number of plaque-associated microglia, their expression of the activation marker Clec7a as well as the amount of Aβ uptake were unchanged in APP23p40$^{-/-}$ mice (Eede *et al*., 2020). We also observed that the reduction in Aβ pathology was not mediated by changes in Aβ-processing enzymes (Eede *et al*., 2020). Interestingly, IL12p40 deficiency led to changes in the pro- and anti-inflammatory cytokine milieu of the brain and plasma. Compared to APP23 mice, plasma levels of IFNγ were reduced in male APP23p40$^{-/-}$ mice, whilst in female APP23p40$^{-/-}$ mice, IL-5 and IL-6 were reduced and IL-1β and CXCL1 levels were increased in the plasma, and CXCL1 levels were decreased in the brain (Eede *et al*., 2020).

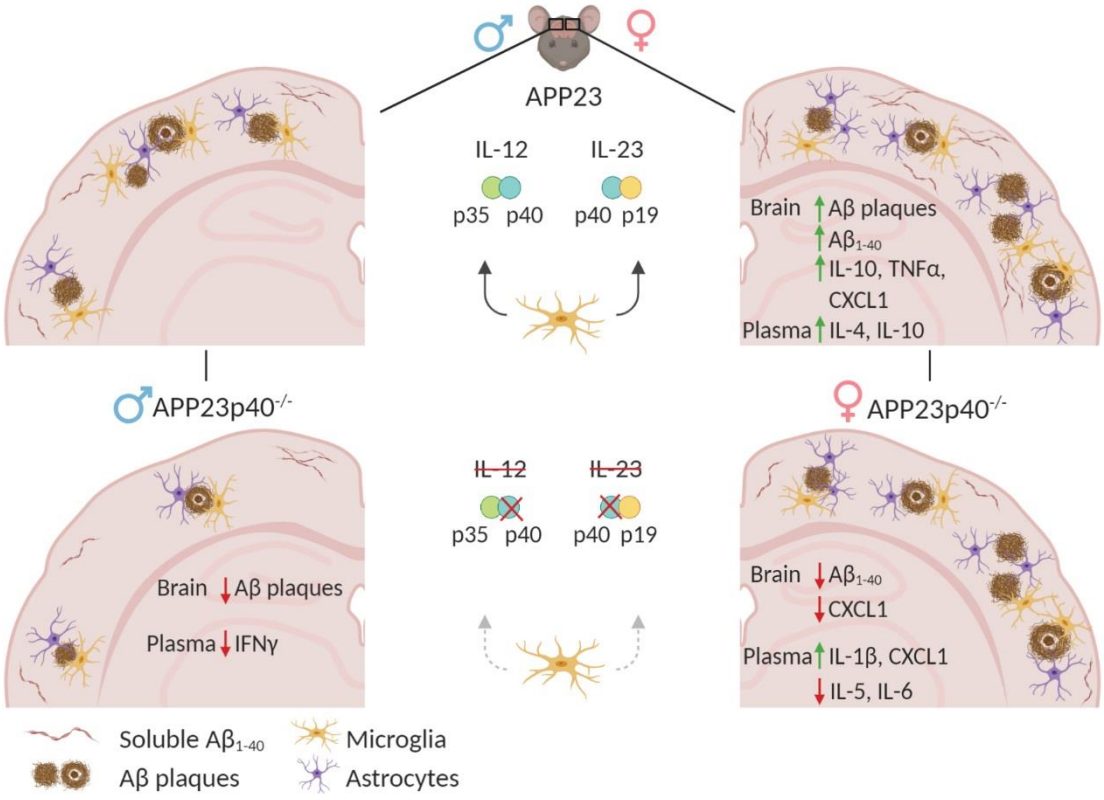

Figure 4. Graphical summary illustrating the effect of IL12p40 deletion in male and female APP23 mice. Image adapted from Eede et al., 2020, made with Biorender.

This might indicate that the beneficial effect of IL12p40 deletion upon Aβ pathology is not mediated by changes in microglial function or Aβ processing, but rather by an indirect effect of IL12p40-mediated intercellular signalling via cytokine modulation. CXCL1 secretion by astrocytes, for example, has been shown to increase disease severity in a mouse model of multiple sclerosis by enhancing neutrophil recruitment (Grist *et al*., 2018). Additionally, blocking neutrophil entry in a mouse model of AD could ameliorate Aβ pathogenesis (Zenaro *et al*., 2015).

In summary, our results provide further evidence on the detrimental role of IL-12/IL-23 signalling in the context of AD. Yet to successfully target IL12p40 in AD, there is an obvious need to further dissect specific signalling characteristics and downstream mechanisms of IL-12 and IL-23.

Aim 2 – Investigation of downstream IL-12/IL-23 signalling mechanisms in AD

In the brain, IL-12/IL-23 receptors are expressed by oligodendrocytes and neurons

Previous data showed that the IL12p40 receptor, namely IL12Rβ1, was expressed on non-microglial cells (vom Berg *et al*., 2012), supporting the idea of an intercellular IL-12/IL-23 signalling pathway. We therefore assessed IL-12/IL-23 receptor localisation in the AD context in more detail. IL-12 and IL-23 both share the IL12p40 subunit (*Il12b*), which forms a heterodimer with either IL12p35 (*Il12a*) or IL23p19 (*Il23a*), respectively. IL12p40 binds to the IL12Rβ1 (*Il12rb1*) receptor, which in turn either dimerises with the receptor subunit IL12Rβ2 (*Il12rb2*) to enable IL-12 signalling or the IL23R (*Il23r*) receptor subunit to enable IL-23 signalling (summarised in *Fig. 2A*). In the peripheral immune system, IL-12 and IL-23 are expressed by antigen-presenting cells such as dendritic cells and play a large role in T cell-mediated immune responses by initiating the expansion and activation of T_H1 and T_H17 T helper cells respectively (reviewed in Croxford *et al*., 2014). In the brains of wildtype or AD-like mice, however, no infiltration of dendritic cells and T cells takes place, and instead, IL-12/IL-23 signalling is mediated by microglia (vom Berg *et al*., 2012; Eede *et al*., 2020). The exact localisation of the IL-12/IL-23 receptors in the brain, however, has not been identified so far, also due to the lack of functional antibodies targeting the receptor subunits. We therefore used an *in situ* hybridisation approach to stain receptor mRNA molecules on brain tissue from 21-month-old APP23 mice and 4-month-old APPPS1 mice as well as their age-matched wildtype littermates.

The RNAscope® *in situ* hybridisation system allows for co-labelling of three different mRNA-binding probes. We thus co-stained probes for each of the three receptor subunits (i.e. *Il12rb1*, *Il12rb2*, *Il23r*) either with probes targeting astrocytic (*Gfap*, *Slc1a3*, *Aldh1l1*) and neuronal (*Map2*, *Rbfox3*) cell markers or with probes specific for cell markers for oligodendrocytes (*Sox10*) and microglia (*Tmem119*, *Sall1*). Signal for all three receptor subunits was found in wildtype, APPPS1 and APP23 brain tissue with regional specificity and no obvious expression differences between genotypes (subjective, non-quantitative observation). In APP23 mice and aged-matched wildtype animals, receptor expression did not seem to be as pronounced as in APPPS1 mice and wildtype littermates, which could be explained by the differences in age and disease stage.

Signal positive for *Il12rb1* was found in cortical regions (especially the entorhinal cortex), hippocampus and corpus callosum and co-staining with cell markers revealed *Il12rb1* expression by oligodendrocytes in both APPPS1 and APP23 mice (*Fig. 2B*). *Il12rb2* expression was found throughout the cortex and co-localised with neuronal cell markers in both AD-like models and wildtype littermates (*Fig. 2C*). Lastly, *Il23r*-positive signal was detected in the midbrain of wildtype and AD-like mice and co-localised with neuronal cell markers (*Fig. 2D*). For the first time, we could therefore provide evidence for region- and cell type-specific expression of IL-12/IL-23 receptors in wildtype and AD-like mice, with *Il12rb1* being expressed by oligodendrocytes and *Il12rb2* and *Il23r* being expressed by neurons.

Oligodendrocytes in AD pathogenesis have not received the same attention as microglia and astrocytes. However, some studies have linked oligodendrocyte dysfunction, changes in myelination patterns as well as demyelination to AD progression (Mitew *et al*., 2010). Additionally, blocking of oligodendrocyte precursor cell (OPC) senescence has recently been linked to reduction of neuroinflammation and AD pathology in an AD-like mouse model (Zhang *et al*., 2019). Neurons have of course been of major focus in the study of AD, since neuronal production and secretion of Aβ, intracellular tau accumulation and resulting neurodegeneration are central events in AD pathogenesis (Montine *et al*., 2012). Nonetheless, the direct role of oligodendrocytes and neurons in modulating AD-associated neuroinflammation remains unclear, highlighting the novelty of IL-12/IL-23 receptor expression by these cells.

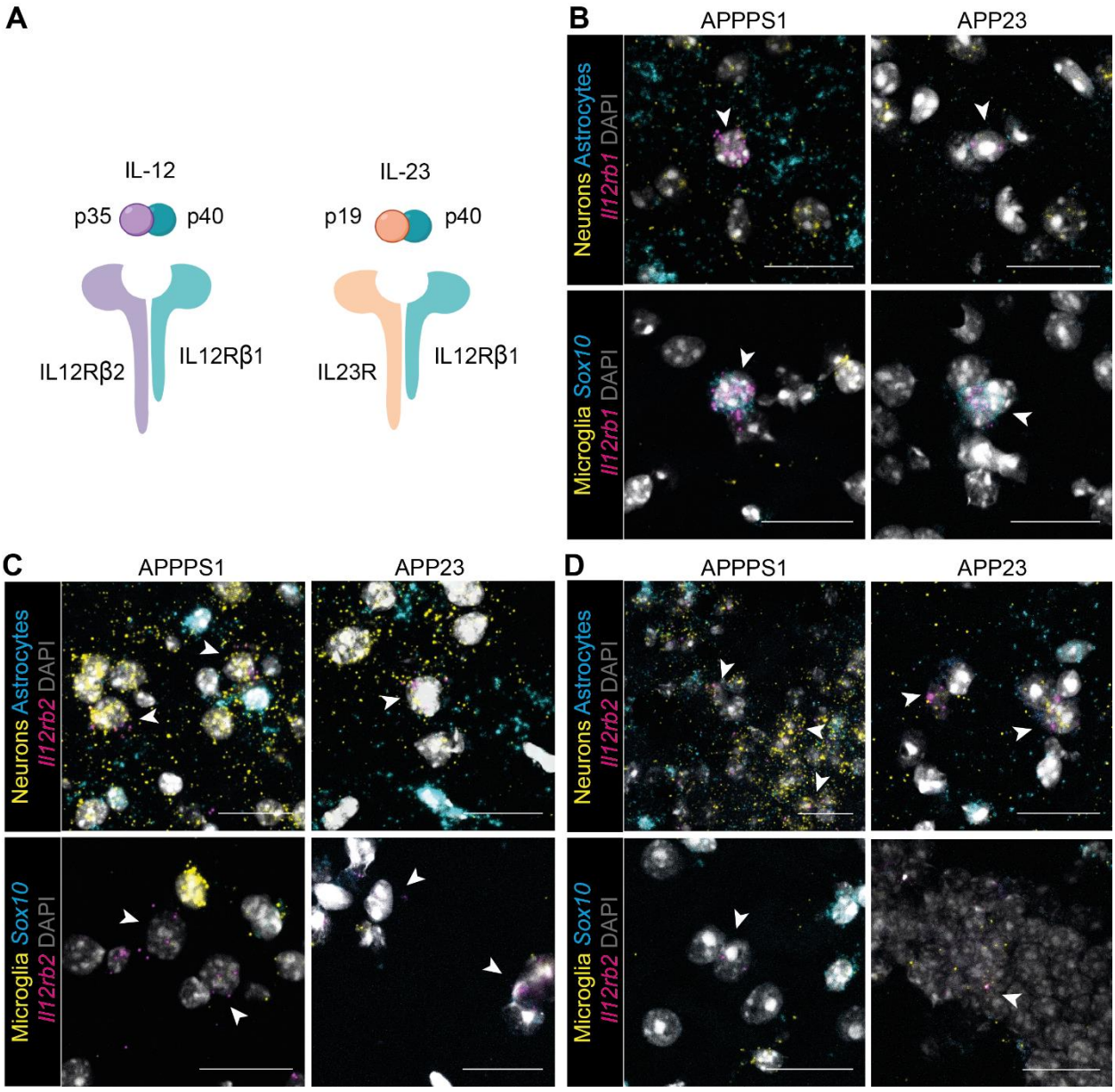

Figure 5. IL-12/IL-23 receptor expression in the brain. (A) Schematic representation of IL-12/IL-23 signalling components. Made with Biorender. (B-D) Representative images of RNAscope® staining of brain tissue from APPPS1 and APP23 mice using probes targeting cell markers for neurons (*Map2, Rbfox3)* and astrocytes (*Gfap, Slc1a3, Aldh1l1*) (top images) as well as microglia (*Sall1, Tmem119*) and *Sox10* for oligodendrocytes (bottom images). Cell markers were co-stained with probes for *Il12rb1* (B), *Il12rb2* (C) and *Il23r* (D) as highlighted by arrowheads. Scale bars = 25 µm.

It is of note, that the shared *Il12rb1* subunit is expressed on oligodendrocytes and in regions different to the neurons expressing *Il12rb2* and *Il23r*. Future work is thus aimed at co-labelling *Il12rb1* with both *Il12rb2* and *Il23r* to confirm whether the IL-12/IL-23 receptor subunits are indeed not co-expressed on the same cell. Should this be the case,

one needs to hypothesise whether in the brain, the receptor subunits can dimerise with other receptors and signal via mechanisms that are so far unknown.

What also remains unclear is whether the amelioration of Aβ pathology by IL12p40 deficiency is mediated specifically by IL-12 or by IL-23. Dissection of the exact molecular mechanisms of IL-12 and IL-23 signalling are of high therapeutic relevance since biologicals that inhibit IL-12 and/or IL-23 have already been approved by the US Food and Drug Administration (FDA) for other diseases such as psoriasis and Crohn's disease, thus providing the possibility of repurposing existing drugs for the treatment of AD. To dissect the role of IL-12 and IL-23 and their downstream signalling components in AD, we generated AD-like mouse models targeting either the IL-12-specific IL12Rβ2 receptor or the IL-23-specific IL23R receptor in various neural cell types. In this study, the effect of inhibiting IL-23 signalling upon Aβ pathology was the main focus. Since we observed similar receptor expression patterns in both APP23 and APPPS1 mice, we continued our studies using the APPPS1 mouse model for operational reasons, namely due to their accelerated disease time course. It is of note that unlike APP23 mice, APPPS1 mice do not appear to exhibit gender-specific AD pathogenesis which is why both genders were used in the following analyses.

Cell-specific deletion of IL23R in neural cells does not alter Aβ pathology in APPPS1 mice

In order to analyse whether IL-23 is the cytokine modulating AD pathology and to investigate the downstream cellular players in this signalling pathway, we generated two mouse lines based on the Cre-loxP system. We crossed APPPS1 mice to IL23R$^{fl/fl}$ mice (Aden *et al*., 2016), in which exon 4 of the *Il23r* gene is flanked by two loxP sites, a sequence recognised by the Cre recombinase, leading to site-specific recombination. These mice were firstly crossed to Nestin^{Cre} mice (Tronche *et al*., 1999), which constitutively express Cre recombinase under the control of the Nestin promoter, generating APPPS1;Nestin^{Cre};IL23R$^{fl/fl}$ mice. Nestin is a promoter active in neural stem cells, thus APPPS1;Nestin^{Cre};IL23R$^{fl/fl}$ mice harbour an IL23R deletion specifically in neural cells such as astrocytes, neurons and oligodendrocytes. Since we previously identified neurons and oligodendrocytes to be relevant downstream mediators of IL-12/IL-23 signalling, this mouse model is useful in targeting both these cell types. In order to exclude an unspecific effect mediated by astrocytes, we also generated APPPS1;Aldh1l1^{CreERT};IL23R$^{fl/fl}$ mice, which harbour a tamoxifen-inducible Cre

recombinase under the control of the astrocyte-specific Aldh1l1 promoter (Winchenbach *et al*., 2016), leading to an astrocyte-specific IL23R deletion upon tamoxifen administration. A schematic overview of the mouse crossings is depicted in *Fig. 3*.

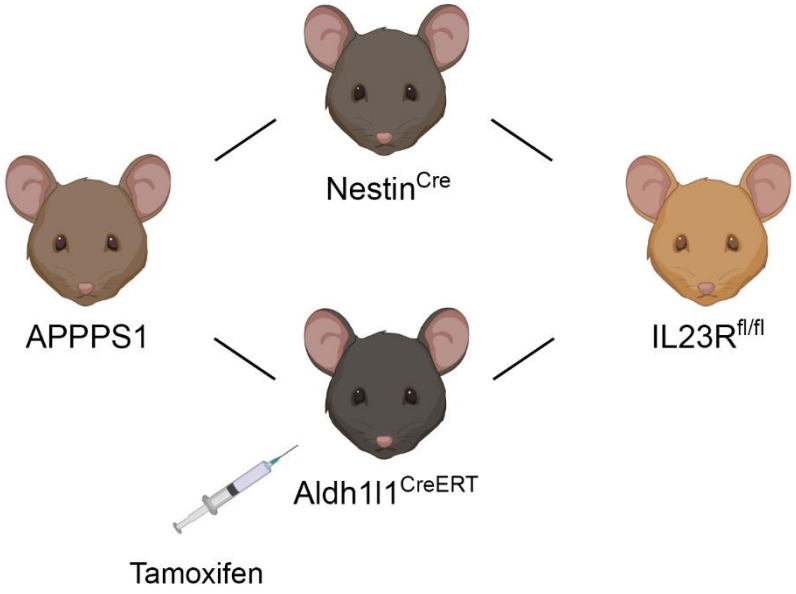

Figure 6. Graphical illustration of APPPS1;Nestin^{Cre};IL23R$^{fl/fl}$ and APPPS1;Aldh1l1^{CreERT};IL23R$^{fl/fl}$ mouse breedings. Made with Biorender.

To assess the effect of IL-23 receptor deficiency in Nestin-positive cells upon Aβ pathology, APPPS1;Nestin^{Cre};IL23R$^{fl/fl}$ mice and APPPS1;IL23R$^{fl/fl}$ control littermates were aged to 4 and 8 months, stages of early and robust plaque pathology (Radde *et al*., 2006). Firstly, protein extracts of varying solubility were extracted from brains of 4-month-old APPPS1;Nestin^{Cre};IL23R$^{fl/fl}$ mice and APPPS1;IL23R$^{fl/fl}$ control littermates and Aβ$_{1-40}$ and Aβ$_{1-42}$ levels were biochemically quantified. Here, we could not detect an effect of neural cell-specific IL23R deletion upon Aβ load (*Fig. 4A*). In order to validate *Il23r* gene excision in our experimental groups, we genotyped biopsies of each mouse via PCR using primers specific to the excised loxP locus. Surprisingly, we noted that the excised gene product was also present in Nestin^{Cre}-negative APPPS1;IL23R$^{fl/fl}$ control mice (*Fig. 4B*). Indeed, Zhang *et al*. (2013) have shown that in the Nestin^{Cre} strain, the germline can also be mutated, leading to the excised gene to be passed on to offspring, irrespective of their Nestin^{Cre} genotype. We thus re-assigned the experimental animals based on their exon-specific genotype, yet still no effect of a neural cell-specific IL23R deletion upon Aβ levels was seen (*Fig. 4C*). When re-analysing the experimental mice of the 8-month time

point for their exon-specific genotype, we observed that all Nestin^{Cre}-negative APPPS1;IL23R$^{fl/fl}$ mice harboured the exon-specific deletion and could thus not be used as an adequate control group. In order to draw conclusions about the effect of a Nestin-specific IL23R deletion at this later disease stage, we will need to carefully select for APPPS1;IL23R$^{fl/fl}$ control mice with an un-excised *Il23r* gene.

To rule out that Aβ pathology is unchanged in 4-month-old APPPS1;Nestin^{Cre};IL23R$^{fl/fl}$ mice due to inefficient gene recombination in Nestin-positive neural cells, we performed an *in vitro* study of *Il23r* targeting efficiency in this mouse line. Here, we purified microglia and astrocytes from neonatal APPPS1;Nestin^{Cre};IL23R$^{fl/fl}$ and APPPS1;IL23R$^{fl/fl}$ mice, whereby gene recombination should occur in Nestin-expressing astrocytes yet not in Nestin-negative microglia. Since no baseline gene expression of the IL-12/IL-23 receptors is present in astrocytes and microglia in these mice, expression was induced by treatment with LPS and IFNγ, a known stimulus for IL-12/IL-23 receptor upregulation. Using qPCR and TaqMan primers specifically binding to the exon 4-5 junction of the *Il23r* mRNA, we could show that induction of *Il23r* expression upon LPS/IFNγ stimulation did not take place in astrocytes derived from APPPS1;Nestin^{Cre};IL23R$^{fl/fl}$ mice, indicating high targeting efficiency (*Fig. 4D*). However, *Il23r* induction did also not take place in the APPPS1;IL23R$^{fl/fl}$ control group and genotyping revealed that unspecific gene recombination again took place in these Nestin^{Cre}-negative mice. Thus, cells derived from these animals cannot not serve as a proper control. Experiments will thus need to be repeated with APPPS1;IL23R$^{fl/fl}$ animals not harbouring unspecific *Il23r* gene excision. In microglia, on the other hand, *Il23r* upregulation could be noted, showing that off-target recombination in Nestin-negative cells did not occur (*Fig. 4D*).

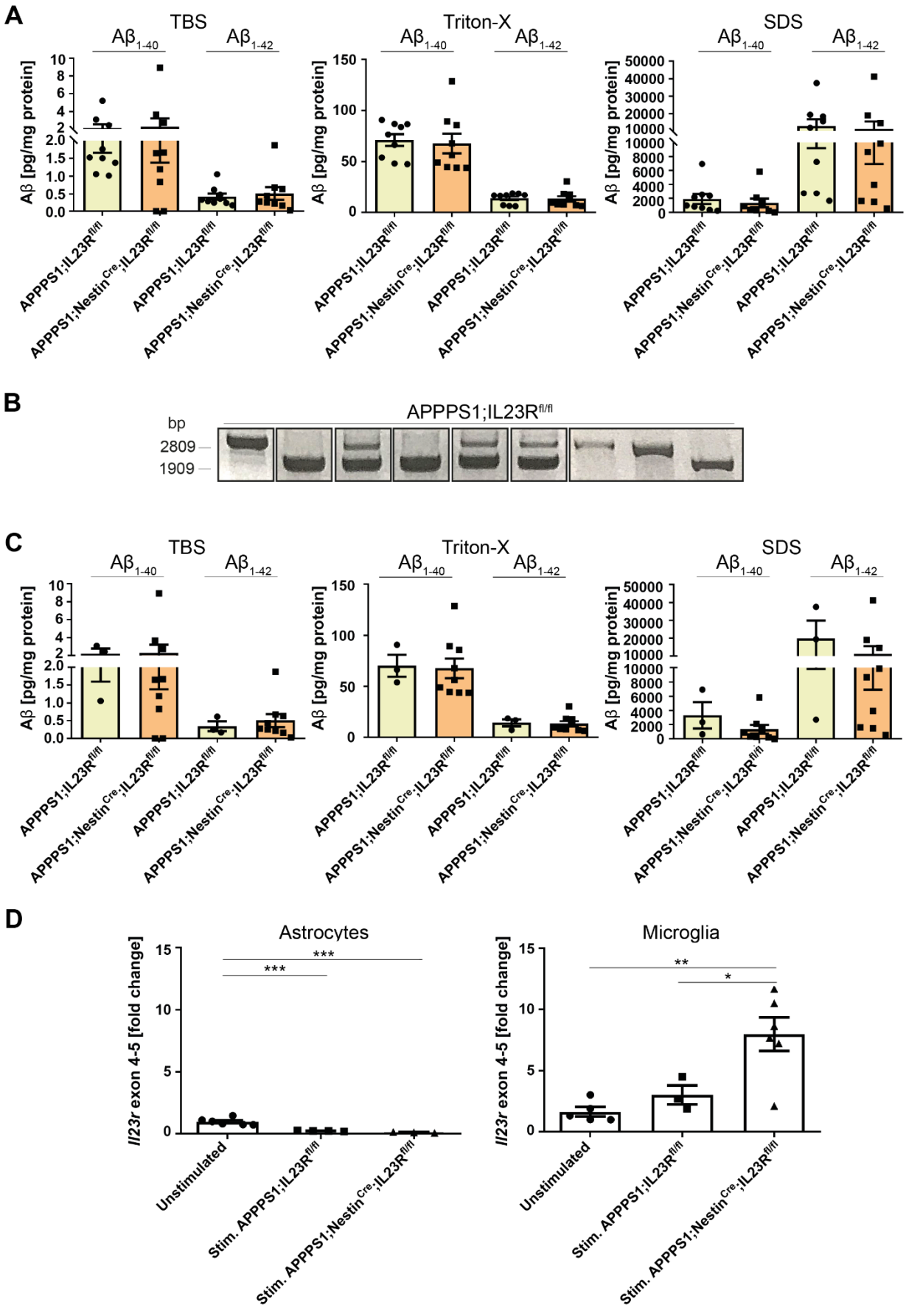
A
TBS
Triton-X
SDS
Aβ1-40
Aβ1-42
Aβ [pg/mg protein]
APPPS1;IL23Rfl/fl
APPPS1;NestinCre;IL23Rfl/fl
B
APPPS1;IL23Rfl/fl
bp
2809
1909
C
TBS
Triton-X
SDS
Aβ1-40
Aβ1-42
Aβ [pg/mg protein]
APPPS1;IL23Rfl/fl
APPPS1;NestinCre;IL23Rfl/fl
D
Astrocytes
Microglia
Il23r exon 4-5 [fold change]
***
***
**
*
Unstimulated
Stim. APPPS1;IL23Rfl/fl
Stim. APPPS1;NestinCre;IL23Rfl/fl

Figure 4. Analysis of Aβ pathology and targeting efficiency in APPPS1;Nestin^{Cre};IL23R$^{fl/fl}$ mice. (A) Quantitative analysis of the $A\beta_{1-40}$ and $A\beta_{1-42}$ proteins in the TBS ($A\beta_{1-40}$ p=0.8562; $A\beta_{1-42}$ p=0.6723), Triton-X ($A\beta_{1-40}$ p=0.7626; $A\beta_{1-42}$ p=0.8588) and SDS ($A\beta_{1-40}$ p=0.5632; $A\beta_{1-42}$ p=0.7584) fractions of brain homogenates from APPPS1;IL23R$^{fl/fl}$ (n=9) and APPPS1;Nestin^{Cre};IL23R$^{fl/fl}$ (n=9) mice. Measurements were normalised to total protein content. Mean ± s.e.m., statistical analysis: two-tailed unpaired t-test between $A\beta_{1-40}$ and $A\beta_{1-42}$ measurements respectively. (B) Representative gel electrophoresis images of PCR analyses of the exon-specific *Il23r* gene recombination in APPPS1;IL23R$^{fl/fl}$ mice. Top band (2809 bp) represents the wildtype *Il23r* gene locus whilst the bottom band (1909 bp) shows the excised *Il23r* gene following Cre recombination. (C) Quantitative analysis of the $A\beta_{1-40}$ and $A\beta_{1-42}$ proteins in the TBS ($A\beta_{1-40}$ p=0.8562; $A\beta_{1-42}$ p=0.6723), Triton-X ($A\beta_{1-40}$ p=0.7626; $A\beta_{1-42}$ p=0.8588) and SDS ($A\beta_{1-40}$ p=0.5632; $A\beta_{1-42}$ p=0.7584) fractions of brain homogenates from APPPS1;IL23R$^{fl/fl}$ (n=3) and APPPS1;Nestin^{Cre};IL23R$^{fl/f}$ (n=9) mice with correct exon-specific genotypes. Measurements were normalised to total protein content. Mean ± s.e.m., statistical analysis: two-tailed unpaired t-test between $A\beta_{1-40}$ and $A\beta_{1-42}$ measurements respectively. (D) Gene expression analysis of the exon 4-5 junction of the *Il23r* gene in cultured neonatal astrocytes (left) and microglia (right) from APPPS1;IL23R$^{fl/fl}$ (astrocyte n=4; microglia n=3) and APPPS1;Nestin^{Cre};IL23R$^{fl/fl}$ (astrocyte n=3; microglia n=6) mice. Cells were treated with control medium ("unstimulated") or LPS/IFNγ ("stim.") for 24 hours. The unstimulated control group was set as baseline and incorporates data points from both APPPS1;IL23R$^{fl/fl}$ and APPPS1;Nestin^{Cre};IL23R$^{fl/fl}$ mice (astrocyte n=6; microglia n=5). *Gapdh* was used as internal reference gene. Mean ± s.e.m., statistical analysis: One-way ANOVA with Tukey post-hoc test (***p≤0.0005; **p=0.0028, *p=0.0331). All data was generated by M. Foerster (MD student supervised by P. Eede).

Unlike the APPPS1;Nestin^{Cre};IL23R$^{fl/fl}$ mouse line, IL23R deletion in the APPPS1;Aldh1l1^{CreERT};IL23R$^{fl/fl}$ line needs to be induced by tamoxifen administration. We chose to intraperitoneally inject the animals at an age of 30 days, a time point before disease onset, with either 75 mg/kg tamoxifen or a vehicle solution (olive oil) daily for 5 days, whilst one experimental group was left untreated. To firstly validate targeting efficiency, we injected APPPS1;Aldh1l1^{CreERT};IL23R$^{fl/fl}$ and littermate APPPS1;IL23R$^{fl/fl}$ control animals with tamoxifen and at 30 days post-injection isolated and cultured astrocytes and microglia from their brains. *Il23r* expression was induced by treatment with LPS/IFNγ and a deletion efficiency of 80 % was detected in the astrocytes of tamoxifen-treated APPPS1;Aldh1l1^{CreERT};IL23R$^{fl/fl}$ mice, compared to Aldh1l1^{CreERT}-negative tamoxifen-treated APPPS1;IL23R$^{fl/fl}$ control littermates, confirming high targeting efficiency (*Fig. 5A*). Microglial *Il23r* induction was unchanged between experimental groups, highlighting that off-target recombination did not take place (*Fig. 5A*).

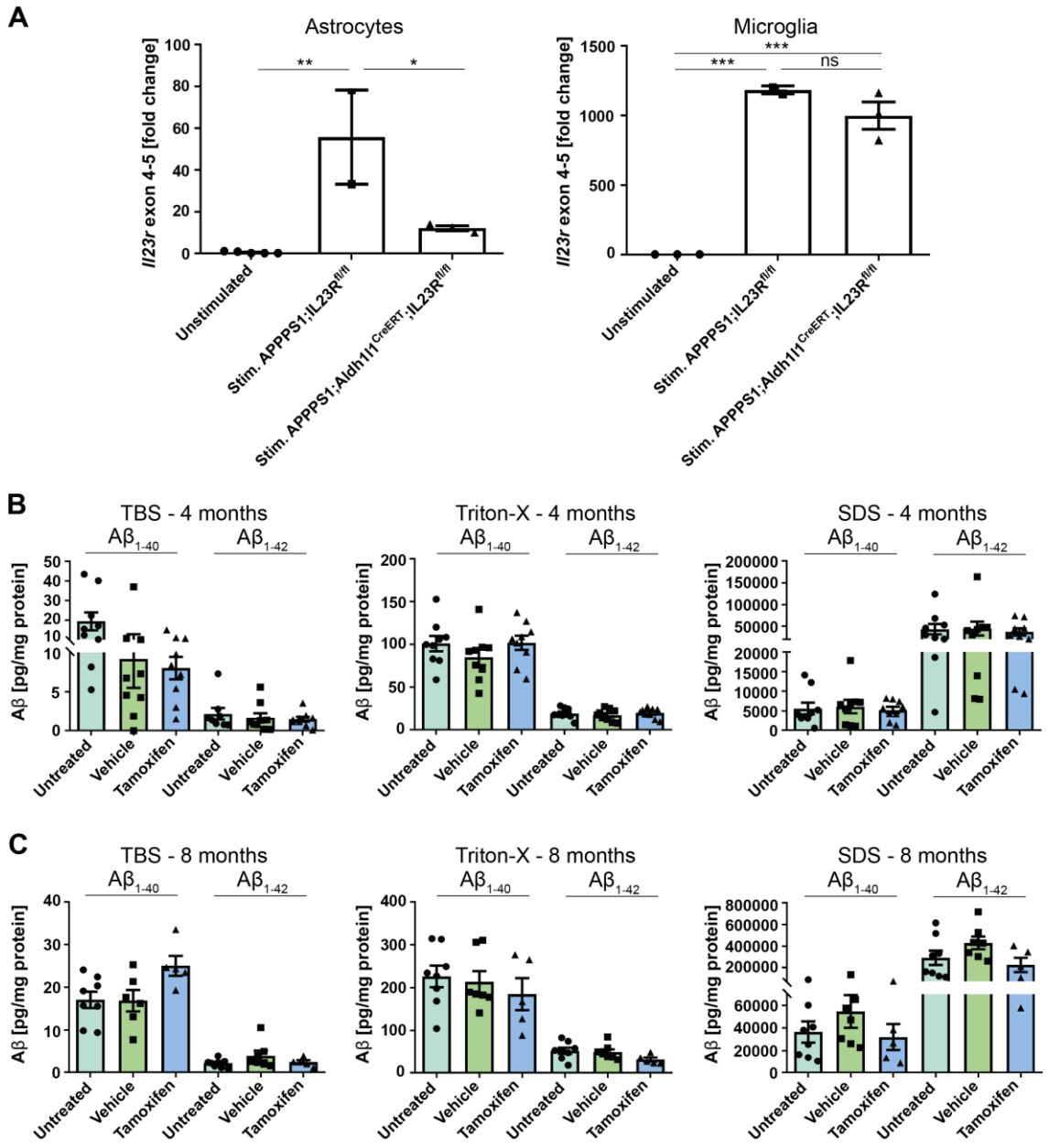

Figure 5. Analysis of targeting efficiency and Aβ pathology in APPPS1;Aldh1l1^{CreERT};IL23R$^{fl/fl}$ mice. (A) Gene expression analysis of the exon 4-5 junction of the *Il23r* gene in cultured adult astrocytes (left) and microglia (right) isolated from tamoxifen-treated APPPS1;IL23R$^{fl/fl}$ (n=2) and APPPS1;Aldh1l1^{CreERT};IL23R$^{fl/fl}$ (n=3) mice. Cells were treated with control medium ("unstimulated") or LPS/IFNγ ("stim.") for 24 hours. The unstimulated control group was set as baseline and incorporates data points from both APPPS1;IL23R$^{fl/fl}$ and APPPS1;Aldh1l1^{CreERT};IL23R$^{fl/fl}$ mice. *Gapdh* was used as internal reference gene. Mean ± s.e.m., statistical analysis: One-way ANOVA with Tukey post-hoc test (***p=0.0002; **p=0.0023, *p=0.0133, ns p=0.2467). (B) Quantitative analysis of the Aβ$_{1-40}$ and Aβ$_{1-42}$ proteins in the TBS, Triton-X and SDS fractions of brain homogenates from 4-month-old APPPS1;Aldh1l1^{CreERT};IL23R$^{fl/fl}$ mice treated with tamoxifen (n=9), vehicle solution (n=9) or left untreated (n=9). Measurements were normalised to total protein content. Mean ± s.e.m., statistical analysis: One-way ANOVA with Tukey post-hoc test (p≥0.05). (C) Quantitative analysis of the Aβ$_{1-40}$ and Aβ$_{1-42}$ proteins in the TBS, Triton-X and SDS fractions of brain homogenates from 8-month-old APPPS1;Aldh1l1^{CreERT};IL23R$^{fl/fl}$ mice treated with tamoxifen (n=5), vehicle solution (n=7) or left untreated (n=8). Measurements were normalised to total protein content. Mean ± s.e.m., statistical analysis: One-way ANOVA with Tukey post-hoc test (p≥0.05).

Having confirmed efficient and specific targeting in the APPPS1;Aldh1l1^{CreERT};IL23R$^{fl/fl}$ mouse line, we analysed the experimental animals aged to 4 and 8 months of age for their levels of soluble and insoluble Aβ_{1-40} and Aβ_{1-42} species. Here, we did not see any differences in Aβ levels between untreated, vehicle-injected and tamoxifen-injected APPPS1;Aldh1l1^{CreERT};IL23R$^{fl/fl}$ mice (*Figs. 5B&C*), indicating that an astrocyte-specific deletion of the IL23R receptor subunit does not affect Aβ pathology at early and late stages of disease.

Taken together, these preliminary data indicate that the disruption of IL-23 signalling specifically in oligodendrocytes, neurons and astrocytes does not affect Aβ pathology in APPPS1 mice. This therefore highlights the relevance of specifically studying IL-12 signalling in the AD context, since this might be the cytokine specifically leading to the amelioration of pathological processes in IL12p40 deficient mice.

Assessing neural cell-mediated IL12Rβ2 signalling in Aβ pathogenesis in APPPS1 mice

Future work is aimed at investigating the role of IL-12 signalling and its downstream mediators in AD pathogenesis. A similar mouse breeding strategy as used for studying IL-23 has been set up already. Here, APPPS1 mice were crossed either to Nestin^{Cre} or Aldh1l1^{CreERT} mice, which in turn were crossed to IL12Rβ2$^{fl/fl}$ mice, where exon 7 of the *Il12rb2* gene is flanked by two loxP sites (unpublished). The two mouse models enabling the study of IL12Rβ2 signalling in neural cells are thus the APPPS1;Nestin^{Cre};IL12Rβ2$^{fl/fl}$ mouse line, in which all neural cells are targeted by Cre recombinase, as well as the APPPS1;Aldh1l1^{CreERT};IL12Rβ2$^{fl/fl}$ line, in which tamoxifen administration induces *Il12rb2* recombination in astrocytes only. A schematic overview of the mouse crossings is depicted in *Fig. 6*.

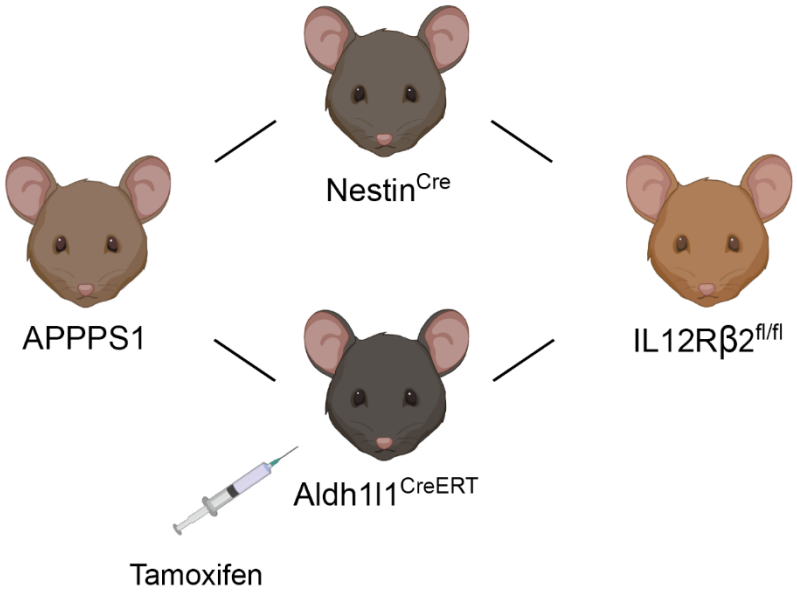

Figure 6. Graphical illustration of APPPS1;Nestin^{Cre};IL12Rβ2$^{fl/fl}$ and APPPS1;Aldh1l1^{CreERT};IL12Rβ2$^{fl/fl}$ mouse breedings. Made with Biorender.

We performed initial validation experiments for each mouse line by characterising the exon-specific *Il12rb2* gene deletion. For APPPS1;Nestin^{Cre};IL12Rβ2$^{fl/fl}$ mice, we genotyped tissue biopsies via PCR with primers specific for the excised exon 7 of the *Il12rb2* gene. Similar to the APPPS1;Nestin^{Cre};IL23R$^{fl/fl}$ mouse line, a high proportion of Nestin^{Cre}-negative APPPS1;IL12Rβ2$^{fl/fl}$ control mice exhibited exon-specific gene recombination, indicating germline transmission of the excised *Il12rb2* gene (*Fig. 7A*). Therefore, experimental mice will need to be carefully selected based on their exon-specific *Il12rb2* genotype. Additionally, future experiments are aimed at quantifying targeting efficiency by isolating adult microglia and astrocytes and inducing *Il12rb2* mRNA expression *in vitro*. Using qPCR in combination with TaqMan primers specifically targeting the exon 6-7 junction, recombination efficiency and potential off-target recombination can thus be assessed.

In APPPS1;Aldh1l1^{CreERT};IL12Rβ2$^{fl/fl}$ mice, gene recombination is dependent on Cre activation by tamoxifen. For initial validation of the model, we again used an *in vitro* approach using neonatal APPPS1;Aldh1l1^{CreERT};IL12Rβ2$^{fl/fl}$ and APPPS1;IL12Rβ2$^{fl/fl}$ control littermates. Neonatal microglia and astrocytes were purified and stimulated firstly with vehicle solution or 4-Hydroxytamoxifen (4-OHT), the active form of tamoxifen suitable for use *in vitro*, to induce Cre recombinase. After 24 hour incubation, cells were stimulated with control medium or LPS/IFNγ to induce *Il12rb2* gene expression.

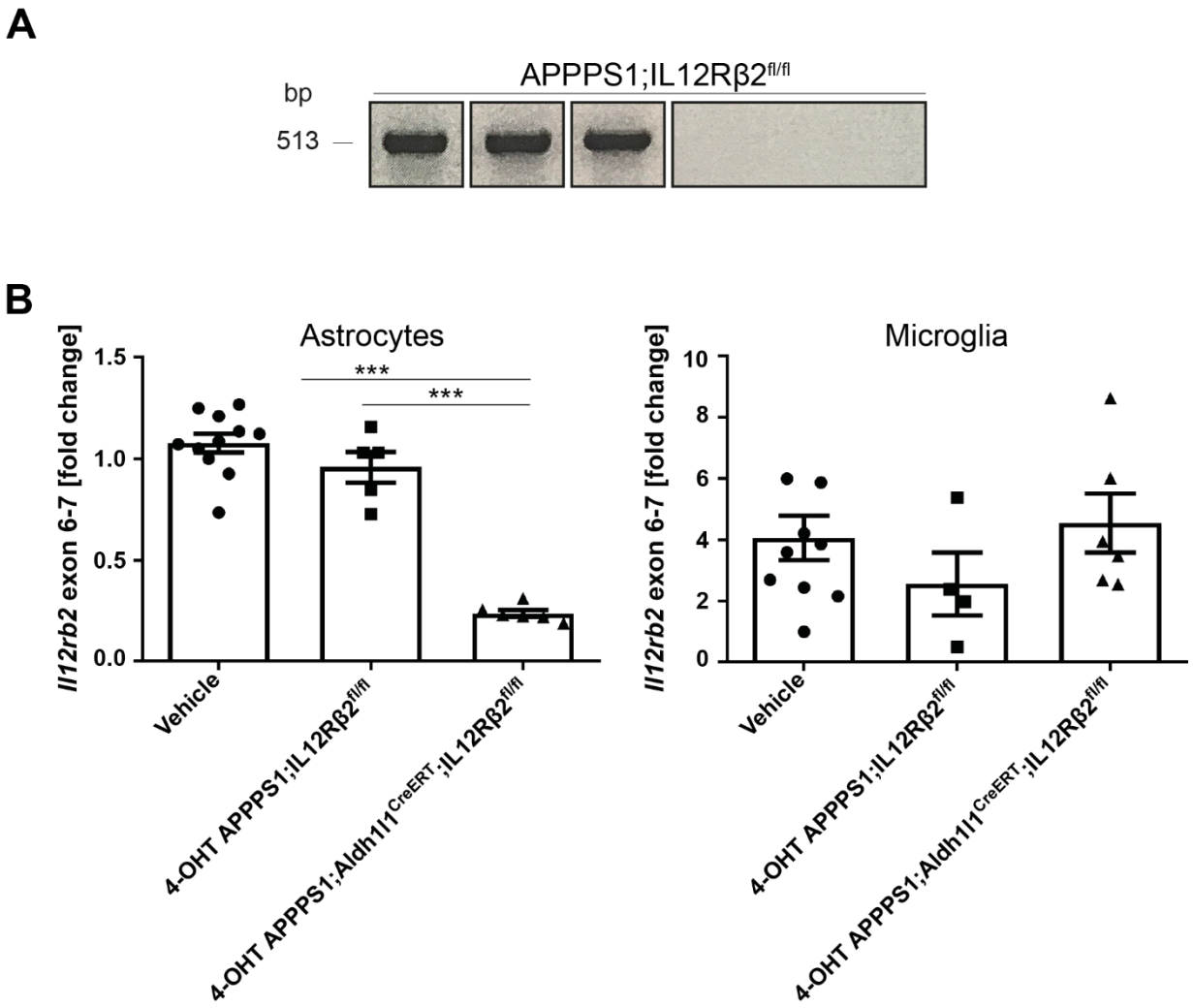

Figure 7. Validation experiments of APPPS1;Nestin^{Cre};IL12Rβ2$^{fl/fl}$ and APPPS1;Aldh1l1^{CreERT};IL12Rβ2$^{fl/fl}$ mouse lines. (A) Representative gel electrophoresis images of PCR analyses of the exon-specific *Il12rb2* gene recombination in APPPS1;IL12Rβ2$^{fl/fl}$ mice derived from the APPPS1;Nestin^{Cre};IL12Rβ2$^{fl/fl}$ line. Presence of a band (513 bp) represents the excised *Il12rb2* gene following Cre recombination whilst no band is present when the wildtype *Il12rb2* gene locus is still existent. (B) Gene expression analysis of the exon 6-7 junction of the *Il12rb2* gene in cultured neonatal astrocytes (left) and microglia (right) from APPPS1;IL12Rβ2$^{fl/fl}$ (astrocyte n=5; microglia n=4) and APPPS1;Aldh1l1^{CreERT};IL12Rβ2$^{fl/fl}$ (astrocyte n=6; microglia n=6) mice. Cre recombinase was induced with 4-OHT treatment and controlled for with vehicle medium. Then, cells were treated with LPS/IFNγ for 24 hours. The vehicle group was set as baseline and incorporates data points from both APPPS1;IL12Rβ2$^{fl/fl}$ and APPPS1;Aldh1l1^{CreERT};IL12Rβ2$^{fl/fl}$ mice (astrocyte n=11; microglia n=10). *Gapdh* was used as internal reference gene. Mean ± s.e.m., statistical analysis: One-way ANOVA with Tukey post-hoc test (***p≤0.0001).

Vehicle-treated microglia and astrocytes from APPPS1;Aldh1l1^{CreERT};IL12Rβ2$^{fl/fl}$ and APPPS1;IL12Rβ2$^{fl/fl}$ stimulated with LPS/IFNγ showed *Il12rb2* upregulation, similar to Aldh1l1^{CreERT}-negative APPPS1;IL12Rβ2$^{fl/fl}$ cells stimulated with 4-OHT and LPS/IFNγ. Microglia from APPPS1;Aldh1l1^{CreERT};IL12Rβ2$^{fl/fl}$ mice treated with 4-OHT and LPS/IFNγ

also showed increased *Il12rb2* expression, indicating that off-target gene recombination does not occur in non-Aldh1l1 expressing cells (*Fig. 7B*). On the other hand, astrocytes from APPPS1;Aldh1l1^{CreERT};IL12Rβ2$^{fl/fl}$ mice treated with 4-OHT and LPS/IFNγ showed a 75% reduction of *Il12rb2* gene expression, indicating a high targeting efficiency in astrocytes (*Fig. 7B*). Future experiments are aimed at treating 30-day-old animals with tamoxifen, followed by isolation, culturing and stimulation of adult microglia and astrocytes, in order to assess *in vivo* targeting efficiency, similar to the regimen described for APPPS1;Aldh1l1^{CreERT};IL23R$^{fl/fl}$ mice.

In summary, first data confirm the suitability of the APPPS1;Nestin^{Cre};IL12Rβ2$^{fl/fl}$ and APPPS1;Aldh1l1^{CreERT};IL12Rβ2$^{fl/fl}$ mouse lines in studying IL12Rβ2 signalling in neural cells in the context of AD pathology. Next, experimental mice for each mouse line will be aged to 4 and 8 months of age in order to analyse pathological parameters at early and late disease stages. This study could provide important information on IL-12-dependent signalling mechanisms and could identify potential therapeutic targets for the treatment of AD.

Conclusion

The work presented here provides further evidence for a pathogenic role of IL-12 and IL-23 signalling in AD and delivers insights into the cellular players mediating this signalling pathway. Firstly, we could show that genetic ablation of IL-12/IL-23 signalling ameliorated Aβ burden differentially in male and female APP23 mice, a mouse model of slow and gender-specific temporal Aβ pathogenesis. Additionally, we could identify both neurons and oligodendrocytes as the IL-12/IL-23 receptor-bearing cells, uncovering a yet unknown brain-intrinsic intercellular inflammatory signalling pathway. When dissecting whether IL-12 or IL-23 specifically affects AD pathology, we did not see an effect of deleting the IL-23 receptor in neural cells upon Aβ burden, pointing towards IL-12 to be the more relevant cytokine in the context of amyloidosis. Further studies are thus required to pinpoint the exact downstream signalling dynamics of brain-specific IL-12/IL-23 signalling in order to pave the way for new therapeutics targeting disease progression of AD.

Materials & Methods

Methods from the data published by Eede *et al*., 2020 are already described extensively in the publication and are not repeated here.

Animals

The following mouse lines were used in the described experiments: APP23 (Tg(Thy1-APPKM670/671NL)23) (Sturchler-Pierrat *et al*., 1997), APPPS1 (Tg(Thy1-APPSw,Thy1-PSEN1*L166P)21Jckr (Radde *et al*., 2006), Nestin^{Cre} (B6.Cg-Tg(Nes-cre)1Kln/J) (Tronche *et al*., 1999), Aldh1l1^{CreERT} (Tg(Aldh1l1-cre/ERT2)02Kan) (Winchenbach *et al*., 2016), IL23R$^{fl/fl}$ (B6.129/SvPas-Il23rtm1Kuv/Orl) (Aden *et al*., 2016) and IL12RB2$^{fl/fl}$ (Tg(Il12rb2tm1a(KOMP)Wtsi) (unpublished).

Mice were group housed under specific pathogen–free conditions on a 12 h light/dark cycle, food and water were provided *ad libidum*. All animal experiments were performed in accordance to the national animal protection guidelines approved by the regional offices for health and social services in Berlin (LaGeSo, license numbers T 0276/07, O 0132/09 & G 0278/15).

For tamoxifen administration in APPPS1;Aldh1l1^{CreERT};IL23R$^{fl/fl}$ mice, tamoxifen (13258, Cayman) was dissolved in olive oil (O1514, Merck) at a concentration of 20 mg/ml and injected intraperitoneally at 75 mg/kg body weight on 5 consecutive days. As vehicle treatment, olive oil only was injected into the animals.

Genotyping for loxP-mediated gene recombination

Exon-specific gene recombination of the *Il23r* gene in APPPS1;Nestin^{Cre};IL23R$^{fl/fl}$ and APPPS1;Aldh1l1^{CreERT};IL23R$^{fl/fl}$ mice as well as the *Il12rb2* gene in APPPS1;Nestin^{Cre};IL12Rβ2$^{fl/fl}$ and APPPS1;Aldh1l1^{CreERT};IL12Rβ2$^{fl/fl}$ mice was done using the PCR primers described in *Table 1*.

DNA from tissue biopsies was isolated using the NucleoSpin® Tissue kit (740952, Macherey Nagel) and amplified using the 5x HOT FIREPol® Master Mix with 12.5 mM $MgCl_2$ (04-11-00125 Solis Biodyne). Primers were used at a concentration of 10 pg/ml and the PCR programs for each set of primers are listed in *Tables 2 & 3*. Finally, PCR products were separated on 1.5 % agarose gels and visualised on a Syngene imager.

Table 2. PCR primer sequences for the detection of exon-specific gene recombination.

Mouse line	Primer name	Primer sequence 5'-3'	Expected size of PCR product in allele	
			Wildtype	Knock-out
IL23R$^{fl/fl}$	15531cre-NGF12	GCGTGCCTTGAAATAGTTCTCTGAATACC	2809 bp	1909 bp
	15532cre-NGF12	ACCTAGCAATGGGTCTCAGCAATGG		
IL12Rβ2$^{fl/fl}$	CSD-F	GATTGCCTTAATGAGTAAGAACCTGG	-	513 bp
	CSD-R	CATTTGGAGAAAAGAGACAATGTTGG		

Table 2. PCR program for floxed *Il23r* gene amplification.

Temperature (°C)	Time	
95	15 min	
95	30 sec	35x
65	30 sec	
72	5 min	
72	8 min	
10	∞	

Table 3. PCR program for floxed *Il12rb2* gene amplification.

Temperature (°C)	Time	
94	5 min	
94	15 sec	10x (decrease 1 °C/cycle)
65	30 sec	
72	40 sec	
94	15 sec	30x
55	30 sec	
72	40 sec	
72	5 min	
10	∞	

Brain homogenisation and quantification of Aβ load

For tissue collection, mice were deeply anaesthetised and transcardially perfused with PBS. The brain was rapidly removed from the skull, divided sagittally in half and the cerebellum and olfactory bulbs were removed. The right hemisphere was snap-frozen in liquid nitrogen and stored at -80 °C. For analysis of protein levels, frozen hemispheres were subjected to a protein extraction protocol using buffers with increasing stringency (Kawarabayashi *et al*., 2001). In brief, hemispheres were homogenised consecutively in Tris-buffered saline (TBS) buffer (20 mM Tris, 137 mM NaCl, pH = 7.6), Triton-X buffer

(TBS buffer containing 1 % Triton X-100) and SDS buffer (2 % SDS in ddH2O). Immediately before use, cOmplete™ Mini Protease Inhibitor Cocktail Tablets (11836153001, Roche, 1 tablet per 10 ml) were added to all buffers. Initial homogenization occurred using a handheld tissue homogeniser (VWR) followed by passing the solution through a 2 ml syringe and G25 cannula. Brain extracts were incubated 30 minutes on ice (only the SDS homogenate was incubated at RT) and centrifuged at 100,000 g for 45 minutes at 4 °C in an Optima MAX-TL ultracentrifuge (Beckman Coulter). The supernatant was collected, aliquoted, snap frozen in liquid nitrogen and stored at -80 °C until further use. The remaining pellet was re-suspended in subsequent buffers. Protein concentrations of each fraction were determined using the Pierce™ BCA Protein Assay Kit (23225, Thermo Fisher) according to manufacturer's protocol and measured on the Tecan Infinite® 200M Photometer (Tecan).

Quantification of Aβ levels

Brain extracts of TBS, Triton-X and SDS fractions were analysed for $A\beta_{1-40}$ and $A\beta_{1-42}$ levels using the 96-well MultiSpot Human 6E10 Ab Triplex Assay Kit (K15200E-2, Meso Scale Diagnostics, MSD). In brief, samples were analysed in duplicate and were diluted to fit the standard curve (Aβ Peptide 3-Plex). After blocking the MSD plate with 1 % Blocker A Solution, the detection antibody solution and sample or calibrator were added and incubated for 2 hours. After washing the plate with 0.05 % Tween-20 in PBS, 2x Reading Buffer was added to the wells and the plate was analysed on a MS6000 machine (MSD).

RNAscope® *in situ* hybridisation

Frozen brain tissue was placed in a tissue mold (SA62534-15, Sakura) and submerged in Tissue-Tek® freezing medium (4583, Sakura). 10 µm tissue sections were cut using a cryostat (Thermo Scientific HM 560), placed on SuperFrost Plus slides (500621, R. Langenbrink) and dried for 1 hour at -20 °C. Tissue processing for RNAscope® multiplex staining was done following manufacturer's protocol for fresh frozen sections. In brief, tissue was fixed in freshly prepared 4 % PFA (pH 7.4) for 30 minutes at 4 °C, followed by alcohol dehydration. Tissue was exposed at room temperature to 10 minute H_2O_2 and 30 minute Protease IV treatment (322340, Bio-Techne) and then incubated for two hours with target probes (*Table 4*) at 40 °C in a HybEZ™ Hybridisation System (321711, Bio-Techne). Signal amplification was achieved using the RNAscope® Multiplex

Fluorescent Kit v2 (323110, Bio-Techne), following the exact protocol. Probes were labelled with Opal™ 520 (1:500, C2 probe, FP1487001KT, Perkin Elmer), Opal™ 570 (1:500, C1 probe, FP1488001KT, Perkin Elmer) and Opal™ 690 (1:500, C3 probe, FP1497001KT, Perkin Elmer) and three-dimensional image stacks (1 µm step size, 40x objective) of stained sections were taken on a Leica TCS SP5 confocal laser scanning microscope using a HCX PL APO lambda blue 63× oil UV objective controlled by LAS AF scan software (Leica Microsystems).

Table 4. Overview of RNAscope® target probes (all by Bio-Techne).

RNAscope® Probes	Catalog number
Mm-Il12rb1	488761
Mm-Il12rb2	451301
Mm-Il23r	403751
Mm-Aldh1l1-C2	405891-C2
Mm-Slc1a3-C2	430781-C2
Mm-Gfap-C2	313211-C2
Mm-Sox10-C2	435931-C2
Mm-Tmem119-C3	472901-C3
Mm-Sall1-C3	469661-C3
Mm-Rbfox3-C3	313311-C3
Mm-Map2-C3	431151-C3

Quantitative real-time PCR

Gene expression analysis was performed on 12 ng cDNA per reaction using the TaqMan Fast Universal Master Mix (4364103, Applied Biosystems) and TaqMan primers for *Il23r* (Mm01186168_m1, Thermo Fisher), *Il12rb2* (Mm00434198_m1, Thermo Fisher) and *Gapdh* (Mm99999915_g1, Thermo Fisher). Quantitative PCR analysis was performed on a QuantStudio 6 Flex Real-Time PCR System (Applied Biosystems). Data was analysed using the Double Delta Ct method to determine fold change expression changes between samples.

Astrocyte & microglia culture

For neonatal glia cultures, brains of p 2-4 animals were dissociated in 0.005 % Trypsin-EDTA (15400054, Thermo Fisher) for 15 minutes at 37°C. Cells were cultivated at 37 °C in 95 % O_2, 5 % CO_2 in DMEM (41966-029, Invitrogen) supplemented with 10 % fetal bovine serum (FBS) (P40-37500, PAN-Biotech) and 1 % penicillin/streptomycin (Pen/Strep) (15140122, Thermo Fisher) for 7 days. To induce microglial proliferation, the culture was stimulated from day 7 onwards with 5 ng/ml GM-CSF (130-095-746, Miltenyi Biotec). Microglia and astrocytes were harvested after 10-14 days *in vitro*. To isolate

microglia, cells were detached from the confluent cell layer by mechanical shaking for 6 minutes and cultivated in 24-well plates at a density of 100.000 cells/well in DMEM, 10 % FBS, 1 % Pen/Strep. After 24 hour incubation, cells were used for downstream applications. For astrocyte isolation, cells were detached from the flask by incubation with 0.05 % Trypsin-EDTA for 5 minutes at 37 °C. The cell suspension was depleted from remaining microglia using Magnetic-Activated Cell Sorting (MACS) by incubating with CD11b MicroBeads (130-093-634, Miltenyi Biotec) according to manufacturer's protocol. Samples were passed over LS columns (130-042-401, Miltenyi Biotec) and the astrocyte-containing CD11b-negative flow through was collected and plated in 24-well plates at a density of 100.000 cells/well in DMEM, 10 % FBS, 1 % Pen/Strep for 48 hours until further use.

Adult astrocytes and microglia were isolated using MACS. Mice were deeply anaesthetised and transcardially perfused with PBS at an age of 60 days. Brain tissue was dissociated using the Adult Brain Dissociation Kit (130-107-677, Miltenyi Biotec) on a gentleMACS Octo Dissociator with Heaters (130-096-427, Miltenyi Biotec) according to manufacturer's protocol. The resulting single cell suspension was labelled with ACSA2 MicroBeads (130-097-678, Miltenyi Biotec) and passed consecutively over two MS columns (130-042-201, Miltenyi Biotec) to positively select for astrocytes. Astrocytes were cultivated in 24-well plates at a density of 100.000 cells/well in AstroMACS medium (130-117-031, Miltenyi Biotec) supplemented with 0.25 % L-glutamine (0.5 mM) (A2916801, Thermo Fisher) and 1 % Pen/Strep for 7 days until further use. The ACSA2-negative flow through derived from isolating astrocytes was collected and labelled with CD11b MicroBeads. To positively select for microglia, the cell suspension was passed over one MS column and were microglia cultivated in 24-well plates at a density of 100.000 cells/well in conditioned medium collected from neonatal astrocytes (see above) for 7 days until further use.

To induce Cre recombination in neonatal cells derived from APPPS1;Aldh1l1^{CreERT};IL12Rβ2$^{fl/fl}$ mice, 4-Hydroxytamoxifen (OHT) (7904, Merck) was reconstituted in 100 % EtOH to generate a 5 mM stock solution. Cells were treated with 1 µM 4-OHT or 0.1 % EtOH as control treatment for 24 hours. Induction of IL-12/IL-23 receptor expression was performed by treating cells with 1 µg/ml Lipopolysaccharides (LPS) (L4391-1MG, Merck) and 100 u/ml IFN-γ (315-05, Peprotech) for 24 hours.

References

Aden, K., Rehman, A., Falk-Paulsen, M., Secher, T., Kuiper, J., Tran, F., Pfeuffer, S., Sheibani-Tezerji, R., Breuer, A., Luzius, A., Jentzsch, M., Häsler, R., Billmann-Born, S., Will, O., Lipinski, S., Bharti, R., Adolph, T., Iovanna, J. L., Kempster, S. L., Blumberg, R. S., Schreiber, S., Becher, B., Chamaillard, M., Kaser, A.&Rosenstiel, P. (2016). Epithelial IL-23R Signaling Licenses Protective IL-22 Responses in Intestinal Inflammation. *Cell Rep* **16,** 2208-2218.

Bradshaw, E. M., Chibnik, L. B., Keenan, B. T., Ottoboni, L., Raj, T., Tang, A., Rosenkrantz, L. L., Imboywa, S., Lee, M., Von Korff, A., Morris, M. C., Evans, D. A., Johnson, K., Sperling, R. A., Schneider, J. A., Bennett, D. A. & De Jager, P. L. (2013). CD33 Alzheimer's disease locus: altered monocyte function and amyloid biology. *Nat Neurosci* **16,** 848-850.

Chen, J. M., Jiang, G. X., Li, Q. W., Zhou, Z. M. & Cheng, Q. (2014). Increased Serum Levels of Interleukin-18, -23 and -17 in Chinese Patients with Alzheimer's Disease. *Dement Geriatr Cogn* **38,** 321-329.

Colonna, M. & Butovsky, O. (2017). Microglia Function in the Central Nervous System During Health and Neurodegeneration. *Annu Rev Immunol* **35,** 441-468.

Croxford, A. L., Kulig, P. & Becher, B. (2014). IL-12-and IL-23 in health and disease. *Cytokine Growth F R* **25,** 415-421.

D'Hooge, R. & de Deyn, P. P. (2001). Applications of the Morris water maze in the study of learning and memory. *Brain Res Rev* **36,** 60-90.

Eede, P., Obst, J., Benke, E., Yvon-Durocher, G., Richard, B. C., Gimber, N., Schmoranzer, J., Böddrich, A., Wanker, E. E., Prokop, S. & Heppner, F. L. (2020). Interleukin-12/23 deficiency differentially affects pathology in male and female Alzheimer's disease-like mice. *EMBO Rep*, e48530.

Gordon, B. A., Blazey, T. M., Su, Y., Hari-Raj, A., Dincer, A., Flores, S., Christensen, J., Mcdade, E., Wang, G., Xiong, C., Cairns, N. J., Hassenstab, J., Marcus, D. S., Fagan, A. M., Jack, C. R., Jr., Hornbeck, R. C., Paumier, K. L., Ances, B. M., Berman, S. B., Brickman, A. M., Cash, D. M., Chhatwal, J. P., Correia, S., Forster, S., Fox, N. C., Graff-Radford, N. R., La Fougere, C., Levin, J., Masters, C. L., Rossor, M. N., Salloway, S., Saykin, A. J., Schofield, P. R., Thompson, P. M., Weiner, M. M., Holtzman, D. M., Raichle, M. E., Morris, J. C., Bateman, R. J. & Benzinger, T. L. S. (2018). Spatial patterns of neuroimaging biomarker change in individuals from families with autosomal dominant Alzheimer's disease: a longitudinal study. *Lancet Neurol* **17,** 241-250.

Grist, J. J., Marro, B. S., Skinner, D. D., Syage, A. R., Worne, C., Doty, D. J., Fujinami, R. S. & Lane, T. E. (2018). Induced CNS expression of CXCL1 augments neurologic disease in a murine model of multiple sclerosis via enhanced neutrophil recruitment. *Eur J Immunol* **48,** 1199-1210.

Guerreiro, R., Wojtas, A., Bras, J., Carrasquillo, M., Rogaeva, E., Majounie, E., Cruchaga, C., Sassi, C., Kauwe, J. S., Younkin, S., Hazrati, L., Collinge, J., Pocock, J., Lashley, T., Williams, J., Lambert, J. C., Amouyel, P., Goate, A., Rademakers, R., Morgan, K., Powell, J., St George-Hyslop, P., Singleton, A. & Hardy, J. (2013). TREM2 variants in Alzheimer's disease. *N Engl J Med* **368,** 117-127.

Guneykaya, D., Ivanov, A., Hernandez, D. P., Haage, V., Wojtas, B., Meyer, N., Maricos, M., Jordan, P., Buonfiglioli, A., Gielniewski, B., Ochocka, N., Comert, C., Friedrich, C., Artiles, L. S., Kaminska, B., Mertins, P., Beule, D., Kettenmann, H. & Wolf, S. A. (2018). Transcriptional and Translational Differences of Microglia from Male and Female Brains. *Cell Rep* **24,** 2773-2783.e2776.

Heppner, F. L., Ransohoff, R. M. & Becher, B. (2015). Immune attack: the role of inflammation in Alzheimer disease. *Nat Rev Neurosci* **16,** 358-372.

Hu, W. T., Holtzman, D. M., Fagan, A. M., Shaw, L. M., Perrin, R., Arnold, S. E., Grossman, M., Xiong, C., Craig-Schapiro, R., Clark, C. M., Pickering, E., Kuhn, M., Chen, Y., Van Deerlin, V. M., Mccluskey, L., Elman, L., Karlawish, J., Chen-Plotkin, A., Hurtig, H. I., Siderowf, A., Swenson, F., Lee, V. M., Morris, J. C., Trojanowski, J. Q. & Soares, H. (2012). Plasma multianalyte profiling in mild cognitive impairment and Alzheimer disease. *Neurology* **79,** 897-905.

Kawarabayashi, T., Younkin, L. H., Saido, T. C., Shoji, M., Ashe, K. H. & Younkin, S. G. (2001). Age-dependent changes in brain, CSF, and plasma amyloid (beta) protein in the Tg2576 transgenic mouse model of Alzheimer's disease. *J Neurosci* **21,** 372-381.

Keren-Shaul, H., Spinrad, A., Weiner, A., Matcovitch-Natan, O., Dvir-Szternfeld, R., Ulland, T. K., David, E., Baruch, K., Lara-Astaiso, D., Toth, B., Itzkovitz, S., Colonna, M., Schwartz, M. & Amit, I. (2017). A Unique Microglia Type Associated with Restricting Development of Alzheimer's Disease. *Cell* **169,** 1276-1290.e1217.

Klein, S. L. & Flanagan, K. L. (2016). Sex differences in immune responses. *Nat Rev Immunol* **16,** 626-638.

Krasemann, S., Madore, C., Cialic, R., Baufeld, C., Calcagno, N., El Fatimy, R., Beckers, L., O'loughlin, E., Xu, Y., Fanek, Z., Greco, D. J., Smith, S. T., Tweet, G., Humulock, Z., Zrzavy, T., Conde-Sanroman, P., Gacias, M., Weng, Z., Chen, H., Tjon, E., Mazaheri, F., Hartmann, K., Madi, A., Ulrich, J. D., Glatzel, M., Worthmann, A., Heeren, J., Budnik, B., Lemere, C., Ikezu, T., Heppner, F. L., Litvak, V., Holtzman, D. M., Lassmann, H., Weiner, H. L., Ochando, J., Haass, C. & Butovsky, O. (2017). The TREM2-APOE Pathway Drives the Transcriptional Phenotype of Dysfunctional Microglia in Neurodegenerative Diseases. *Immunity* **47,** 566-581.e569.

Magram, J., Connaughton, S. E., Warrier, R. R., Carvajal, D. M., Wu, C. Y., Ferrante, J., Stewart, C., Sarmiento, U., Faherty, D. A. & Gately, M. K. (1996). IL-12-deficient mice are defective in IFN gamma production and type 1 cytokine responses. *Immunity* **4,** 471-481.

Mathys, H., Davila-Velderrain, J., Peng, Z., Gao, F., Mohammadi, S., Young, J. Z., Menon, M., He, L., Abdurrob, F., Jiang, X., Martorell, A. J., Ransohoff, R. M., Hafler, B. P., Bennett, D. A., Kellis, M. & Tsai, L.-H. (2019). Single-cell transcriptomic analysis of Alzheimer's disease. *Nature* **570,** 332-337.

Mayeda, E. R. (2019). Invited Commentary: Examining Sex/Gender Differences in Risk of Alzheimer Disease and Related Dementias-Challenges and Future Directions. *Am J Epidemiol* **188,** 1224-1227.

McKhann, G. M., Knopman, D. S., Chertkow, H., Hyman, B. T., Jack, C. R., Jr., Kawas, C. H., Klunk, W. E., Koroshetz, W. J., Manly, J. J., Mayeux, R., Mohs, R. C., Morris, J. C., Rossor, M. N., Scheltens, P., Carrillo, M. C., Thies, B., Weintraub, S. & Phelps, C. H. (2011). The diagnosis of dementia due to Alzheimer's disease: recommendations from the National Institute on Aging-Alzheimer's Association workgroups on diagnostic guidelines for Alzheimer's disease. *Alzheimers Dement* **7,** 263-269.

Mitew, S., Kirkcaldie, M. T., Halliday, G. M., Shepherd, C. E., Vickers, J. C. & Dickson, T. C. (2010). Focal demyelination in Alzheimer's disease and transgenic mouse models. *Acta Neuropathol* **119,** 567-577.

Montine, T. J., Phelps, C. H., Beach, T. G., Bigio, E. H., Cairns, N. J., Dickson, D. W., Duyckaerts, C., Frosch, M. P., Masliah, E., Mirra, S. S., Nelson, P. T., Schneider, J. A., Thal, D. R., Trojanowski, J. Q., Vinters, H. V. & Hyman, B. T. (2012). National Institute on Aging-Alzheimer's Association guidelines for the neuropathologic assessment of Alzheimer's disease: a practical approach. *Acta Neuropathol* **123,** 1-11.

Myers, A. & McGonigle, P. (2019). Overview of Transgenic Mouse Models for Alzheimer's Disease. *Curr Protoc Neurosci* **89,** e81.

Radde, R., Bolmont, T., Kaeser, S. A., Coomaraswamy, J., Lindau, D., Stoltze, L., Calhoun, M. E., Jäggi, F., Wolburg, H., Gengler, S., Haass, C., Ghetti, B., Czech, C., Hölscher, C., Mathews, P. M. & Jucker, M. (2006). Abeta42-driven cerebral amyloidosis in transgenic mice reveals early and robust pathology. *EMBO Rep* **7,** 940-946.

Serrano-Pozo, A., Mielke, M. L., Gómez-Isla, T., Betensky, R. A., Growdon, J. H., Frosch, M. P. & Hyman, B. T. (2011). Reactive Glia not only Associates with Plaques but also Parallels Tangles in Alzheimer's Disease. *Am J Pathol* **179,** 1373-1384.

Sofroniew, M. V. & Vinters, H. V. (2010). Astrocytes: biology and pathology. *Acta Neuropathol* **119,** 7-35.

Stalder, M., Phinney, A., Probst, A., Sommer, B., Staufenbiel, M. & Jucker, M. (1999). Association of microglia with amyloid plaques in brains of APP23 transgenic mice. *Am J Pathol* **154,** 1673-1684.

Sturchler-Pierrat, C., Abramowski, D., Duke, M., Wiederhold, K. H., Mistl, C., Rothacher, S., Ledermann, B., Burki, K., Frey, P., Paganetti, P. A., Waridel, C., Calhoun, M. E., Jucker, M., Probst, A., Staufenbiel, M. & Sommer, B. (1997). Two amyloid precursor protein transgenic mouse models with Alzheimer disease-like pathology. *Proc Natl Acad Sci U S A* **94,** 13287-13292.

Sturchler-Pierrat, C. & Staufenbiel, M. (2000). Pathogenic Mechanisms of Alzheimer's Disease Analyzed in the APP23 Transgenic Mouse Model. *Ann NY Acad Sci* **920,** 134-139.

Tan, M. S., Yu, J. T., Jiang, T., Zhu, X. C., Guan, H. S. & Tan, L. (2014). IL12/23 p40 inhibition ameliorates Alzheimer's disease-associated neuropathology and spatial memory in SAMP8 mice. *J Alzheimers Dis* **38,** 633-646.

Tronche, F., Kellendonk, C., Kretz, O., Gass, P., Anlag, K., Orban, P. C., Bock, R., Klein, R. & Schutz, G. (1999). Disruption of the glucocorticoid receptor gene in the nervous system results in reduced anxiety. *Nat Genet* **23,** 99-103.

Villa, A., Gelosa, P., Castiglioni, L., Cimino, M., Rizzi, N., Pepe, G., Lolli, F., Marcello, E., Sironi, L., Vegeto, E. & Maggi, A. (2018). Sex-Specific Features of Microglia from Adult Mice. *Cell Rep* **23,** 3501-3511.

Vom Berg, J., Prokop, S., Miller, K. R., Obst, J., Kalin, R. E., Lopategui-Cabezas, I., Wegner, A., Mair, F., Schipke, C. G., Peters, O., Winter, Y., Becher, B. & Heppner, F. L. (2012). Inhibition of IL-12/IL-23 signaling reduces Alzheimer's disease-like pathology and cognitive decline. *Nat Med* **18,** 1812-1819.

Winchenbach, J., Düking, T., Berghoff, S. A., Stumpf, S. K., Hülsmann, S., Nave, K.-A. & Saher, G. (2016). Inducible targeting of CNS astrocytes in Aldh1l1-CreERT2 BAC transgenic mice. *F1000Res* **5,** 2934-2934.

Wood, L. B., Winslow, A. R., Proctor, E. A., Mcguone, D., Mordes, D. A., Frosch, M. P., Hyman, B. T., Lauffenburger, D. A. & Haigis, K. M. (2015). Identification of neurotoxic cytokines by profiling Alzheimer's disease tissues and neuron culture viability screening. *Sci Rep* **5,** 16622.

Zenaro, E., Pietronigro, E., Della Bianca, V., Piacentino, G., Marongiu, L., Budui, S., Turano, E., Rossi, B., Angiari, S., Dusi, S., Montresor, A., Carlucci, T., Nani, S., Tosadori, G., Calciano, L., Catalucci, D., Berton, G., Bonetti, B. & Constantin, G. (2015). Neutrophils promote Alzheimer's disease-like pathology and cognitive decline via LFA-1 integrin. *Nat Med* **21,** 880-886.

Zhang, J., Dublin, P., Griemsmann, S., Klein, A., Brehm, R., Bedner, P., Fleischmann, B. K., Steinhauser, C. & Theis, M. (2013). Germ-line recombination activity of the widely used hGFAP-Cre and nestin-Cre transgenes. *PLoS One* **8,** e82818.

Zhang, P., Kishimoto, Y., Grammatikakis, I., Gottimukkala, K., Cutler, R. G., Zhang, S., Abdelmohsen, K., Bohr, V. A., Misra Sen, J., Gorospe, M. & Mattson, M. P. (2019). Senolytic therapy alleviates Aβ-associated oligodendrocyte progenitor cell senescence and cognitive deficits in an Alzheimer's disease model. *Nat Neurosci* **22,** 719-728.

Statutory Declaration

“I, Pascale Eede, by personally signing this document in lieu of an oath, hereby affirm that I prepared the submitted dissertation on the topic “Cellular targets and downstream effector mechanisms of IL-12/IL-23 signalling in Alzheimer‘s disease”, independently and without the support of third parties, and that I used no other sources and aids than those stated.

All parts which are based on the publications or presentations of other authors, either in letter or in spirit, are specified as such in accordance with the citing guidelines. The sections on methodology (in particular regarding practical work, laboratory regulations, statistical processing) and results (in particular regarding figures, charts and tables) are exclusively my responsibility.

Furthermore, I declare that I have correctly marked all of the data, the analyses, and the conclusions generated from data obtained in collaboration with other persons, and that I have correctly marked my own contribution and the contributions of other persons (cf. declaration of contribution). I have correctly marked all texts or parts of texts that were generated in collaboration with other persons.

My contributions to any publications to this dissertation correspond to those stated in the below joint declaration made together with the supervisor. All publications created within the scope of the dissertation comply with the guidelines of the ICMJE (International Committee of Medical Journal Editors; www.icmje.org) on authorship. In addition, I declare that I shall comply with the regulations of Charité – Universitätsmedizin Berlin on ensuring good scientific practice.

I declare that I have not yet submitted this dissertation in identical or similar form to another Faculty.

The significance of this statutory declaration and the consequences of a false statutory declaration under criminal law (Sections 156, 161 of the German Criminal Code) are known to me.”

Date Signature

Declaration of your own contribution to the top-journal publication for a PhD or MD/PhD degree

Pascale Eede contributed the following to the below listed publication:

Eede, P.*, Obst, J.*, Benke, E., Yvon-Durocher, G., Richard, B. C., Gimber, N., Schmoranzer, J., Böddrich, A., Wanker, E. E., Prokop, S.* & Heppner, F. L.* (2020). Interleukin-12/23 deficiency differentially affects pathology in male and female Alzheimer's disease-like mice. *EMBO Rep*, e48530.

I, Pascale Eede, contributed to the enclosed publication the composition of the majority of the methods section, results and discussion as well as the generation of all figures. Processing of tissues (sampling of organs and plasma, isolation of proteins and cells from the brain, preparation of brain sections) used for the analyses shown in figures 1, 2, 3, 4, 5, 6, 7, EV1, EV2, EV3, EV4, S1A&C and S2 was partly done by me. Histological stainings and their stereological analyses for some of the data points of figures 1B-D, 4B-D, 6B-D, EV1A, S1A and S2C&D were performed by me. Additionally, I undertook histological stainings and image acquisition for figures 2A&C, 5A&C and 7A&C. Execution of the MultiSpot Human 6E10 Aβ Triplex Assay (Figs. 1A, 4A, 6A, EV1B, S1A, S2A&B), the 10-plex Pro-inflammatory Panel 1 (mouse) Mesoscale Assay (Figs. EV1B, EV2, EV3C-K, EV4C-K), the IL-12/IL-23 total p40 enzyme-linked immunosorbent assay (ELISA) (Fig. 3B), Western Blots (Figs. EV3A&B, EV4A&B) as well as qPCR analyses (Fig. 3A) was done by me. Furthermore, I performed statistical analyses for figures 1, 2B, EV1, EV2, 3, 4, 5B, EV3, 6, 7B, EV4, S1A&B and S2.

_____

Signature of doctoral candidate

Journal Summary List

Journal Data Filtered By: **Selected JCR Year: 2017** Selected Editions: SCIE,SSCI
Selected Categories: **"CELL BIOLOGY"** Selected Category Scheme: WoS
Gesamtanzahl: 190 Journale

Rank	Full Journal Title	Total Cites	Journal Impact Factor	Eigenfactor Score
1	NATURE REVIEWS MOLECULAR CELL BIOLOGY	43,667	35.612	0.095540
2	NATURE MEDICINE	75,461	32.621	0.171980
3	CELL	230,625	31.398	0.583260
4	Cell Stem Cell	23,493	23.290	0.096030
5	CANCER CELL	35,217	22.844	0.096910
6	Cell Metabolism	29,834	20.565	0.101740
7	NATURE CELL BIOLOGY	39,896	19.064	0.092960
8	TRENDS IN CELL BIOLOGY	13,708	18.564	0.037630
9	Science Translational Medicine	26,691	16.710	0.126450
10	CELL RESEARCH	13,728	15.393	0.037450
11	MOLECULAR CELL	61,604	14.248	0.181170
12	NATURE STRUCTURAL & MOLECULAR BIOLOGY	27,547	13.333	0.081820
13	Autophagy	14,923	11.100	0.035510
14	TRENDS IN MOLECULAR MEDICINE	9,213	11.021	0.019720
15	EMBO JOURNAL	67,036	10.557	0.079780
16	CURRENT OPINION IN CELL BIOLOGY	13,339	10.015	0.027790
17	DEVELOPMENTAL CELL	26,896	9.616	0.074980
18	GENES & DEVELOPMENT	57,469	9.462	0.092720
19	CURRENT BIOLOGY	56,595	9.251	0.137200
20	Cold Spring Harbor Perspectives in Biology	13,275	9.247	0.049360
21	Annual Review of Cell and Developmental Biology	9,812	9.032	0.016870
22	Cell Systems	1,129	8.982	0.009600
23	AGEING RESEARCH REVIEWS	5,297	8.973	0.012030
24	JOURNAL OF CELL BIOLOGY	68,915	8.784	0.085170
25	EMBO REPORTS	13,293	8.749	0.031350
26	PLANT CELL	48,393	8.228	0.063640
27	MATRIX BIOLOGY	4,803	8.136	0.008500
28	Cell Reports	29,789	8.032	0.210690

Article

SOURCE DATA | TRANSPARENT PROCESS | OPEN ACCESS

EMBO reports

Interleukin-12/23 deficiency differentially affects pathology in male and female Alzheimer's disease-like mice

Pascale Eede[1,††], Juliane Obst[1,†,††], Eileen Benke[1], Genevieve Yvon-Durocher[1], Bernhard C Richard[1], Niclas Gimber[2], Jan Schmoranzer[2], Annett Böddrich[3], Erich E Wanker[3], Stefan Prokop[1,‡,§,¶,††] & Frank L Heppner[1,4,5,6,*,††]

Abstract

Pathological aggregation of amyloid-β (Aβ) is a main hallmark of Alzheimer's disease (AD). Recent genetic association studies have linked innate immune system actions to AD development, and current evidence suggests profound gender differences in AD pathogenesis. Here, we characterise gender-specific pathologies in the APP23 AD-like mouse model and find that female mice show stronger amyloidosis and astrogliosis compared with male mice. We tested the gender-specific effect of lack of IL12p40, the shared subunit of interleukin (IL)-12 and IL-23, that we previously reported to ameliorate pathology in APPPS1 mice. IL12p40 deficiency gender specifically reduces Aβ plaque burden in male APP23 mice, while in female mice, a significant reduction in soluble $A\beta_{1-40}$ without changes in Aβ plaque burden is seen. Similarly, plasma and brain cytokine levels are altered differently in female versus male APP23 mice lacking IL12p40, while glial properties are unchanged. These data corroborate the therapeutic potential of targeting IL-12/IL-23 signalling in AD, but also highlight the importance of gender considerations when studying the role of the immune system and AD.

Keywords Alzheimer's disease; gender; IL-12/IL-23; innate immunity; β-amyloid

Subject Categories Immunology; Molecular Biology of Disease; Neuroscience

DOI 10.15252/embr.201948530 | Received 21 May 2019 | Revised 19 December 2019 | Accepted 8 January 2020

EMBO Reports (2020) e48530

Introduction

Alzheimer's disease (AD) is a chronic progressive neurodegenerative disorder associated with extracellular and intracellular protein aggregates [1] which induce synaptic dysfunction and degeneration of neurons and cause a characteristic clinical syndrome with prominent cognitive impairment [2,3]. Extracellular amyloid-β (Aβ) deposits are one of the prominent hallmarks of the disease [1], and a dysregulation of Aβ metabolism is thought to be one of the earliest pathological changes observable in AD patients, decades before first clinical symptoms occur [4,5]. Mouse models of Aβ deposition provide a useful tool to study amyloidogenesis *in vivo* [6] which in these mouse models is accompanied by an activation of the innate immune response characterised by activated microglia surrounding Aβ plaques [7], mimicking microglia activation observed in the brains of AD patients [8].

In the last decade, the importance of the innate immune response in AD pathogenesis has risen, driven by the discovery of multiple variants in immune system-associated genes conferring an increased risk for the development of sporadic AD, including the microglia cell surface receptors TREM2 and CD33 [9,10]. Even though these data suggest that the innate immune system plays an important role in AD, the exact nature of this immune response and its impact on disease is still far from clear [7,11]. While the short-term depletion of microglia had no major impact on development or progression of Aβ pathology [12,13], suggesting that microglia are rather inefficient in acutely regulating Aβ load, there are numerous examples in which modulation of the microglia response towards Aβ did have a

1 Department of Neuropathology, corporate member of Freie Universität Berlin, Humboldt-Universität zu Berlin, Berlin Institute of Health, Charité – Universitätsmedizin Berlin, Berlin, Germany
2 Advanced Medical Bioimaging Core Facility (AMBIO), corporate member of Freie Universität Berlin, Humboldt-Universität zu Berlin, Berlin Institute of Health, Charité - Universitätsmedizin Berlin, Berlin, Germany
3 Neuroproteomics, Max Delbrück Center for Molecular Medicine, Berlin, Germany
4 Cluster of Excellence, NeuroCure, Berlin, Germany
5 Berlin Institute of Health (BIH), Berlin, Germany
6 German Center for Neurodegenerative Diseases (DZNE) Berlin, Berlin, Germany
*Corresponding author. Tel: +49 30 450 536 032; E-mail: frank.heppner@charite.de
††These authors contributed equally to this work
†Present address: ARUK Oxford Drug Discovery Institute, University of Oxford, Oxford, UK
‡Present address: Department of Pathology, University of Florida, Gainesville, FL, USA
§Present address: Center for Translational Research in Neurodegenerative Disease, University of Florida, Gainesville, FL, USA
¶Present address: Fixel Institute for Neurological Diseases, University of Florida, Gainesville, FL, USA

major impact on disease progression [14–16], especially in long-term depletion settings [17]. Similarly, we have reported an upregulation of the inflammatory cytokines interleukin (IL)-12 and IL-23 by microglia in the brain of AD-like APPPS1 mice and demonstrated that targeting IL12p40, the common subunit of both IL-12 and IL-23, using either genetic or pharmacological strategies reduced Aβ pathology and ameliorated cognitive deficits inherent in these mice [18]. The finding that IL12p40 levels are also de-regulated in the cerebrospinal fluid (CSF) of AD patients [18], the correlation between IL12p40 levels in plasma and mild cognitive impairment (MCI) and AD [19] and the detection of elevated levels of IL12p70 in brain tissue of AD patients [20], further emphasises the relevance of these pathways for the human disease condition.

Another observation derived from epidemiological studies implies differences in the prevalence to develop AD between male and female subjects [21–23]. Additionally, there are known differences in both the innate and adaptive immune responses between males and females [24], including gender-specific differences in male versus female microglial phenotypes [25–27]. Single-cell transcriptome analyses confirmed these notions by finding a gender-specific response within all brain cell populations of male and female AD patients, including microglia [28]. In light of these observations, our study aimed at identifying whether the effect of targeting the microglia-expressed IL12p40 on disease pathogenesis is model- and/or gender-specific. We therefore crossed mice deficient in IL12p40 to yet another AD-like mouse model, namely APP23 mice [29]. APP23 mice show a much slower rate of Aβ deposition than APPPS1 mice [30] utilised in earlier studies, which recapitulates more closely Aβ pathology of human AD patients with respect to the Aβ accumulation time course and the histopathological Aβ composition consisting of a sound mixture of "soft"/"diffuse" and "core" Aβ plaques. Similar to effects described in human AD patient populations [21–23], gender differences in plaque deposition have been described in this mouse model, although these have not been characterised thoroughly to the best of our knowledge [31,32]. To address the latter, we assessed gender-specific properties of Aβ deposition as well as Aβ processing, surrogate markers of neuritic dystrophy and glial activation in male and female APP23 mice lacking or harbouring the IL-12/IL-23 signalling pathway.

Results

Female APP23 mice show increased Aβ pathology and astrogliosis compared to male mice

We and others have previously described an increase in the IL12p40 subunit shared by the cytokines IL-12 and IL-23, in AD-like mouse models [18,33], as well as CSF [18], plasma [19] and brain tissue [20] of AD patients, but so far, no analysis of potential gender differences has been performed. In order to validate these findings in a mouse model of AD with slow Aβ accumulation, more closely representing Aβ pathology and Aβ composition in sporadic AD patients, we made use of the APP23 mouse model harbouring the Swedish (KM670/671NL) mutation in the gene encoding the amyloid precursor protein (APP) [29]. The APP23 mouse model reportedly shows gender differences when examining Aβ plaque load and behavioural characteristics [31,32], which appears to relate more closely to the pathogenetic events mimicking sporadic AD [21–23]. However, to our knowledge no gender-specific side-by-side comparison of the AD-like changes in male and female APP23 mice has been reported so far. We therefore aimed at quantifying late-stage plaque burden in 21-month-old APP23 male versus female mice using biochemical and histological methods.

In order to gain insights into Aβ accumulation, we generated consecutive protein homogenates with increased detergent stringency [34] of brains from male and female APP23 mice which were each analysed on the Meso Scale Diagnostics (MSD) platform to measure $A\beta_{1-40}$ and $A\beta_{1-42}$ content. Compared to male mice, we found that female APP23 mice contain twofold higher levels of the soluble (TBS fraction) and insoluble (SDS fraction) $A\beta_{1-40}$ isoform (Fig 1A) as well as the $A\beta_{1-42}$ isoform (Appendix Fig S1A). We could also confirm the published observation that $A\beta_{1-40}$ species are the main Aβ isoform present in brains of APP23 mice, while the more aggregation-prone $A\beta_{1-42}$ isoform is less abundant (Fig 1A; Appendix Fig S1A). Histologically, Aβ plaque burden can be characterised as being "diffuse" or "compact" [35]. Both types of plaques can be detected with antibodies targeting the Aβ protein itself, such as 4G8 or the chemical compound pFTAA [36]. Additionally, compact plaques can be visualised specifically using β-sheet-binding dyes such as Congo Red [37]. In APP23 mice, we observed that the cortical area covered by 4G8-, pFTAA- and Congo Red-positive amyloid-β plaques was twice as high in female mice compared to male mice (Fig 1B–D). Using the ratio between the area covered by 4G8-positive plaques and Congo Red-positive compact plaques, we determined that compact plaques only account for a quarter of total plaques in both male and female APP23 mice (Appendix Fig S1B).

To further investigate the differences between males and females in the APP23 model, a filter retardation assay was used to determine the presence of Aβ aggregates in protein lysates [38]. Protein homogenates from APP23 mouse brains were positively selected for aggregates larger than 0.2 μm in size. Immunostaining for 6E10, staining the Aβ protein, revealed that male mice have Aβ aggregates in the TBS-soluble protein fractions, few in the Triton-X fraction and none in the SDS fraction. However, an increased amount of aggregates was found in the FA fraction. In female mice, on the other hand, aggregates were found increasingly in the Triton-X fraction, SDS-soluble fraction and FA fraction at higher levels than in male mice (Fig 1E; Appendix Fig S1C). This indicates gender-specific Aβ aggregation properties and higher levels of insoluble Aβ aggregates in female mice. Neuritic dystrophy is another common pathological characteristic found in APP23 mice [29,39]. We thus stained tissue sections with BACE1, which has been suggested to act as a surrogate marker of neuritic dystrophy [40–43]. We noted that plaque-associated BACE1 immunoreactivity normalised to 4G8-positive Aβ plaques did not show any gender-specific differences (Fig 2A). The APP23 mouse strain also shows prominent microgliosis and astrocytosis around the amyloid deposits found in the brain [29,44–46]. Stereological analysis revealed a rise in the number of cortical astrocytes in female APP23 mice (Fig 2B), which correlated with increased Congo Red- and 4G8-positive plaque burden (Fig EV1A). To phenotype microglial characteristics, we quantified the number of plaque-associated microglia within 30 μm of the plaque border as well as their expression of Clec7a, which has been described as a marker of activated microglia in various disease contexts [47,48]. Both the number of plaque-associated microglia and the Clec7a

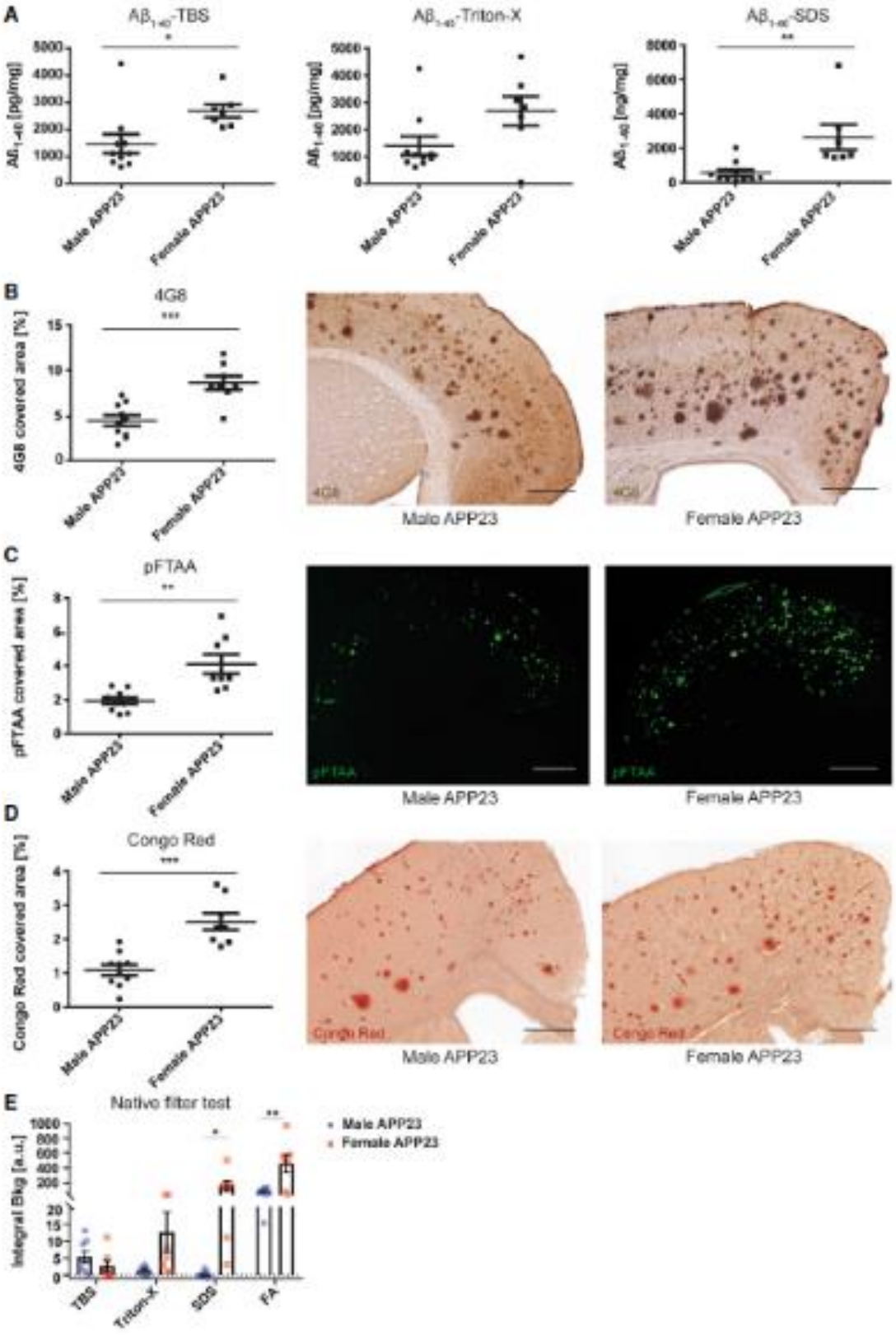
A
Aβ1-40-TBS
Aβ1-40-Triton-X
Aβ1-40-SDS
Aβ1-40 [pg/mg]
Aβ1-40 [ng/mg]
Male APP23
Female APP23
B
4G8
4G8 covered area [%]
Male APP23
Female APP23
C
pFTAA
pFTAA covered area [%]
Male APP23
Female APP23
D
Congo Red
Congo Red covered area [%]
Male APP23
Female APP23
E
Native filter test
Integral Bkg [a.u.]
Male APP23
Female APP23
TBS
Triton-X
SDS
FA

Figure 1.

Figure 1. Female APP23 mice at 21 months have higher Aβ burden than male APP23 mice.

A Quantitative analysis of the $A\beta_{1-40}$ protein in the TBS (*P = 0.0212), Triton-X (P = 0.0544) and SDS (**P = 0.0063) fractions of brain homogenates from male (n = 7) and female (n = 10) APP23 mice. Mean ± SEM, statistical analysis: two-tailed unpaired t-test.

B Stereological analysis of cortical area covered by 4G8-positive plaques in male (n = 10) and female (n = 8) APP23 mice (left) and representative images (right), scale bar = 500 μm. Mean ± SEM, statistical analysis: two-tailed unpaired t-test, ***P = 0.0004.

C Fluorescence intensity-based analysis of pFTAA-stained Aβ plaques in the cortex of male (n = 10) and female (n = 8) APP23 mice (left) and representative images (right), scale bar = 1 mm. Mean ± SEM, statistical analysis: two-tailed unpaired t-test, **P = 0.0011.

D Stereological analysis of cortical area covered by Congo Red-positive plaques in male (n = 10) and female (n = 8) APP23 mice (left) and representative images (right), scale bar = 500 μm. Mean ± SEM, statistical analysis: two-tailed unpaired t-test, ***P = 0.0001.

E Native filter assay analysis of TBS (P = 0.2453), Triton-X (P = 0.0604), SDS (*P = 0.0196) and formic acid (FA) (**P = 0.0057) fractions from male (n = 8) and female (n = 7) APP23 mouse brain homogenates. Mean ± SEM, statistical analysis: two-tailed unpaired t-test between the same fractions.

staining intensity within these cells were similar in male and female APP23 mice (Fig 2C). We used radial intensity profiling of 4G8-positive signal within Iba1-positive microglia as an indicator of microglial Aβ uptake. This analysis showed 4G8 intensity peaks inside the cell (~4 μm), but revealed no significant difference between both 4G8 traces, i.e. intracellular Aβ levels between male and female APP23 mice (Fig 2D). Analysis of pro- and anti-inflammatory cytokines (IFNγ, IL-10, IL-1β, IL-2, IL-4, IL-5, IL-6, TNF-α, CXCL1) revealed increased levels of IL-4 in the plasma, IL-10 in both plasma and brain as well as TNF-α and CXCL1 in brain homogenates of female APP23 mice, compared to male mice (Fig EV2A–I). We also noted a positive correlation between CXCL1 levels in the brain and both soluble and insoluble $A\beta_{1-40}$ levels (Fig EV1B). In summary, male and female APP23 mice show distinct differences in plaque accumulation at an age of 21 months. In both biochemical and histological analyses, female APP23 mice had twice the amount of Aβ accumulation and plaque load, and Aβ aggregates are more insoluble and more abundant than those in age-matched male APP23 mice. We also identified an Aβ burden-dependent increase in cortical astrocytes in female APP23 mice while microgliosis and BACE1-positive dystrophic neurites were unchanged between genders. Moreover, brain and plasma cytokine levels were regulated differently in male versus female APP23 mice. Due to the observed gender differences in Aβ deposition and associated pathology, the impact of IL12p40 deficiency on pathological outcomes in this mouse model was assessed separately in female and male APP23 mice.

Microglial IL12p40 is increased in APP23 mice

To examine whether the IL12p40 subunit also is a relevant interventional immune target in the APP23 mouse model, we examined IL12p40 expression in aged APP23 mice. Firstly, we could validate our previous findings [18], namely that IL12p40 (Il12b) gene expression in the brain was specific to microglia irrespective of gender (Fig 3A). On protein level, APP23 mice showed a ~45% increase in IL12p40 compared to age-matched wild-type (WT) littermates that were not influenced by the gender of the mice (Fig 3B).

To further understand the role of IL12p40 on disease pathophysiology in this mouse model, we crossed APP23 mice to IL12p40$^{-/-}$ knock out mice [49] (APP23p40$^{-/-}$) and investigated whether a lack of the IL12p40 subunit influences plaque pathology as it did in the APPPS1 model [18]. We confirmed by ELISA analysis that APP23p40$^{-/-}$ mice lack IL12p40 expression irrespective of the gender of the mice (Fig 3B).

Male APP23p40$^{-/-}$ mice exhibit reduced Aβ deposits compared to APP23 mice

To investigate the effect of IL12p40 deficiency, brain tissues of male and female APP23 and APP23p40$^{-/-}$ mice were analysed for Aβ levels, the abundance of Aβ aggregates, surrogate markers of neuritic dystrophy, astrogliosis, plaque-associated microglia, the levels of pro- and anti-inflammatory cytokines as well as Aβ processing enzymes using histological and biochemical methods.

In male mice, biochemical analysis of $A\beta_{1-40}$ levels in TBS, Triton-X and SDS-soluble protein fractions did not reveal any differences between the APP23 and APP23p40$^{-/-}$ genotypes (Fig 4A). Additionally, $A\beta_{1-42}$ concentration was not influenced by IL12p40 deficiency (Appendix Fig S2A), as was the presence of Aβ aggregates as measured by native filter test (Fig 4E; Appendix Fig S3). Histological analyses of brain sections, however, did reveal a strong reduction in the area covered of both diffuse and compact plaques. Here, genetic deficiency of IL12p40 led to a 58% decrease in the cortical area covered by 4G8-positive plaques (Fig 4B) and to a 42% reduction in the area covered by pFTAA-positive plaques (Fig 4C). Similarly, Congo Red-positive "core" plaques were reduced by 52% (Fig 4D). The presence of filtered Aβ aggregates (Fig 4E), the total ratio of diffuse versus core plaques (Appendix Fig S2C) and expression levels of APP, APP-cleaving protein BACE1 and Aβ degrading enzymes neprilysin and insulin-degrading enzyme (IDE) were not influenced by IL12p40 deficiency (Fig EV3A and B), similar to what has been reported for APPPS1 mice lacking IL12p40 [18]. Deficiency of IL12p40 also did not affect plaque-associated BACE1 immunoreactivity or astrocyte numbers in male APP23 mice (Fig 5A and B), which also showed no alteration in the number of plaque-associated microglia and of Clec7a-positive activated microglia (Fig 5C) or Aβ uptake (Fig 5D). While most pro- and anti-inflammatory cytokines assessed by us were not altered in brain homogenates of male APP23 and APP23p40$^{-/-}$ mice, we noted a threefold reduction in IFNγ levels in plasma samples of male mice lacking IL12p40 (Fig EV3C–K).

Female APP23p40$^{-/-}$ mice show a reduction in soluble and insoluble $A\beta_{1-40}$ compared to APP23 mice

In contrast to male mice, IL12p40 deficiency in female APP23 mice had substantial effects on Aβ levels. In the TBS and Triton-X soluble protein fractions, a 38% and a 45% decrease in $A\beta_{1-40}$ levels could be detected in female APP23 versus APP23p40$^{-/-}$ mice (Fig 6A). No effect was seen on SDS-soluble Aβ (Fig 6A) and aggregated Aβ

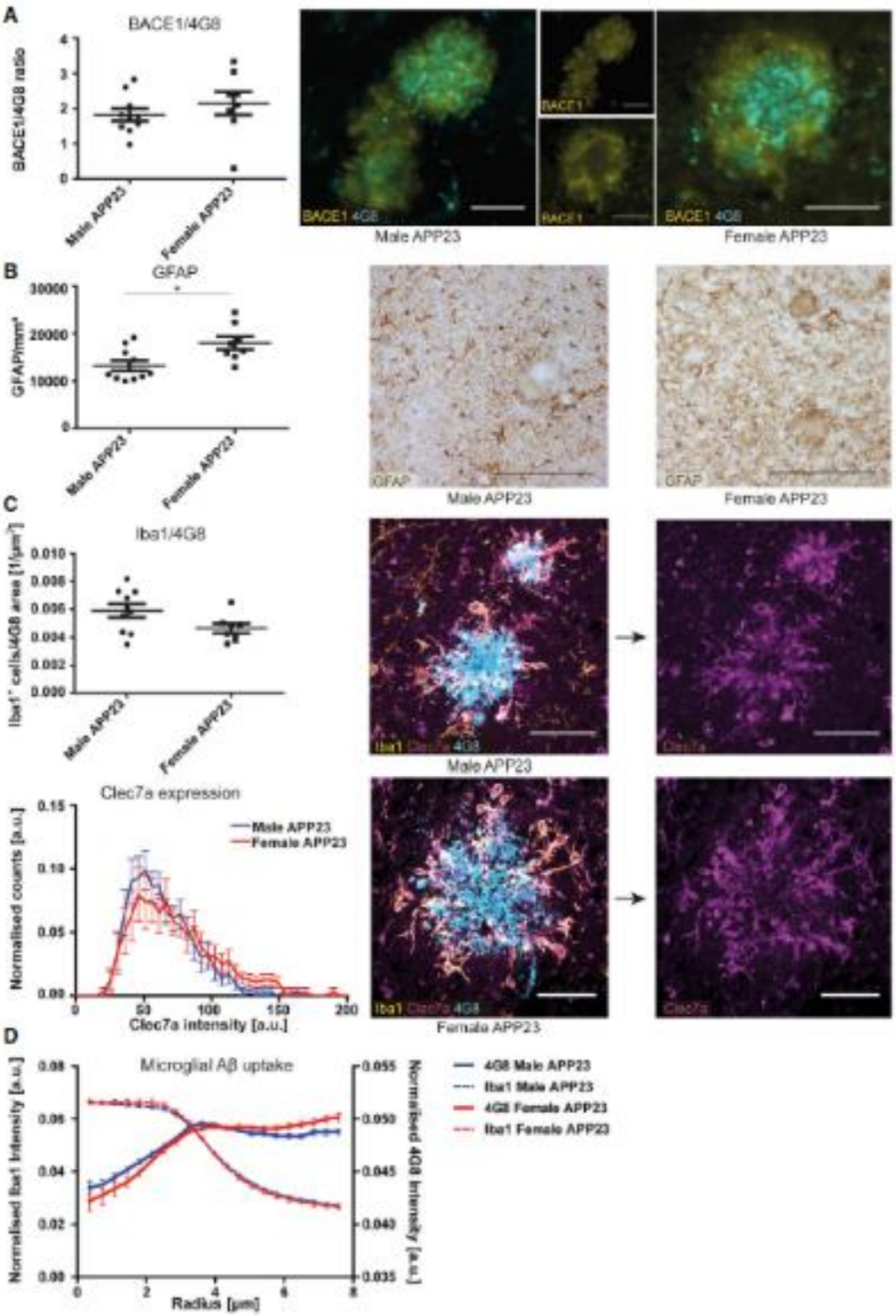
A
BACE1/4G8
BACE1/4G8 ratio
Male APP23
Female APP23
BACE1 4G8
BACE1
Male APP23
Female APP23
B
GFAP
GFAP/mm²
Male APP23
Female APP23
GFAP
Male APP23
Female APP23
C
Iba1/4G8
Iba1⁺ cells/4G8 area [1/µm²]
Male APP23
Female APP23
Iba1 Clec7a 4G8
Male APP23
Iba1 Clec7a 4G8
Female APP23
Clec7a
Clec7a expression
Male APP23
Female APP23
Normalised counts [a.u.]
Clec7a intensity [a.u.]
D
Microglial Aβ uptake
Normalised Iba1 Intensity [a.u.]
Normalised 4G8 Intensity [a.u.]
Radius [µm]
4G8 Male APP23
Iba1 Male APP23
4G8 Female APP23
Iba1 Female APP23

Figure 2.

Figure 2. Female APP23 mice have higher astrocyte numbers than male mice.

A Histological analysis of plaque-associated BACE1 immunoreactivity in male (n = 10) and female (n = 8) APP23 mice. BACE1 area covered was normalised to 4G8-positive area covered of the same image (left). Right: representative images, scale bar = 50 μm. Mean ± SEM, statistical analysis: two-tailed unpaired t-test, P = 0.3724.

B Stereological quantification of the number of cortical GFAP-positive astrocytes in male (n = 10) and female (n = 8) APP23 mice (left). Right: representative images of GFAP staining, scale bar = 200 μm. Mean ± SEM, statistical analysis: two-tailed unpaired t-test, *P = 0.0134.

C Quantification of activated microglia within 30 μm from plaque borders. Top: numbers of Iba1-positive microglia were normalised to the size of the nearest 4G8-positive plaque and quantified in male (n = 10) and female (n = 8) APP23 mice. Mean ± SEM, statistical analysis: two-tailed unpaired t-test, P = 0.0576. Bottom: histogram representing Clec7a staining intensity within plaque-associated Iba1-positive microglia in male (n = 10) and female (n = 8) APP23 mice. Mean ± SEM, statistical analysis: two-tailed unpaired t-test with Bonferroni correction for each single bin, P = $N.S.$. Right: representative images, scale bar = 40 μm.

D Radial intensity profiles of Iba1 and 4G8 around the centre of the nucleus of plaque-associated Iba1-positive microglia in male (n = 10) and female (n = 8) APP23 mice. Iba1 intensity declines until a radius of ~6 μm, marking the cell periphery. 4G8 intensity peaks inside the cell (~4 μm), but stays high outside the cell. This is very likely due to the close proximity to 4G8-positive plaques. Mean ± SEM, statistical analysis: two-tailed unpaired t-test with Bonferroni correction for the number of binned radii shows no significant difference between both 4G8 traces.

Source data are available online for this figure.

as measured by filter assays (Fig 6E; Appendix Fig S3). As in male mice, $A\beta_{1-42}$ levels were not affected by a lack of IL12p40 (Appendix Fig S2B) as were the expression levels of APP, BACE1, Neprilysin and IDE (Fig EV4A and B).

To confirm whether these changes also affected the amount of deposited Aβ, brain sections of female APP23 and APP23p40$^{-/-}$ mice were stained with 4G8, pFTAA and Congo Red. The percentage of the cortical area covered by 4G8-, pFTAA- and Congo Red-positive plaques was unchanged in female APP23 mice lacking or harbouring IL12p40 (Fig 6B–D), contrary to the findings in male mice. The ratio of diffuse versus core plaques also was not influenced by a lack of IL12p40 (Appendix Fig S2D). Plaque-associated BACE1 immunoreactivity, cortical astrocyte number, the number of activated plaque-associated microglia and microglial Aβ uptake were all unchanged in female APP23p40$^{-/-}$ mice (Fig 7A–D).

Analysis of pro- and anti-inflammatory cytokines (IFNγ, IL-10, IL-1β, IL-2, IL-4, IL-5, IL-6, TNF-α, CXCL1) in plasma showed reduced expression of IL-5 and IL-6 as well as an increased expression of IL-1β and CXCL1 in female APP23p40$^{-/-}$ mice when compared to APP23 mice. In brain homogenates, a twofold decrease in CXCL1 protein levels was noted in APP23p40$^{-/-}$ mice (Fig EV4C–K).

Discussion

Using the Aβ-producing APP23 mouse model of AD-like pathology, we identified specific gender differences in plaque accumulation, amyloid composition and aggregation characteristics, astrogliosis as well as brain and plasma cytokine levels. We further show that the deletion of the IL12p40 subunit, which is the essential component of the cytokines IL-12 and IL-23, differentially affects pathology in age-matched male and female mice.

Given that male and female APP23 mice are known to show varying levels of pathology and behavioural deficits, most studies using APP23 mice analyse male and female animals independently [31,32]. Previously observed sex differences in spatial learning paradigms may be explained by hormonal variances [50], yet an influence of hormones upon plaque pathology has not been described in

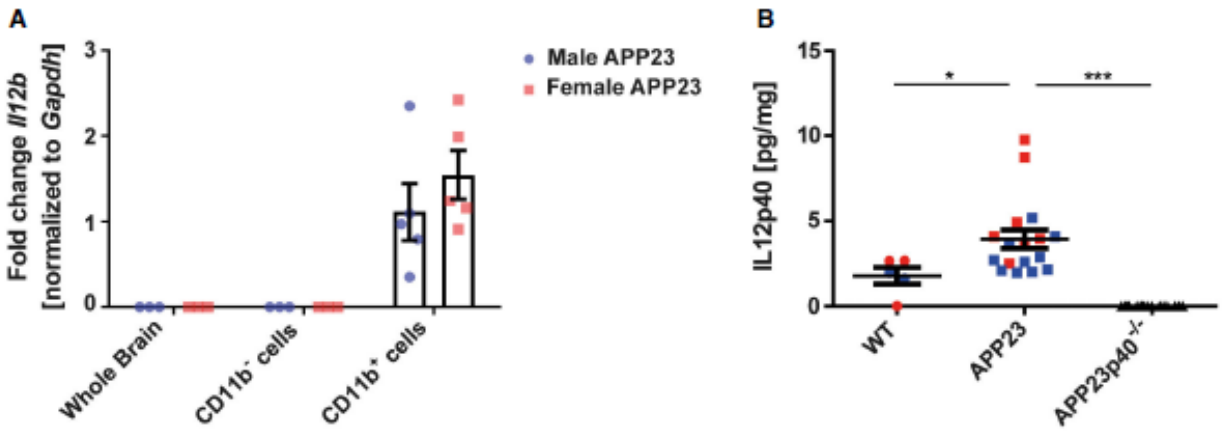

Figure 3. APP23 mice have increased microglia-specific Il12b/IL12p40 levels in the brain.

A Gene expression analysis of Il12b in whole brain (n = 3 per gender, Il12b undetected), Cd11b-negative non-microglial cells (n = 3 per gender, Il12b undetected) and CD11b-positive microglia (n = 5 per gender, P = 0.3540) in male and female APP23 mice. Gapdh expression was used as an internal reference gene. Mean ± SEM, statistical analysis: two-tailed unpaired t-test for each fraction.

B ELISA measurements of the IL12p40 concentration in the TBS-soluble protein fraction derived from wild-type (WT) (n = 5), APP23 (n = 17) and APP23p40$^{-/-}$ (n = 16) mice. Male mice are depicted by blue squares, while female mice are shown as red squares. Mean ± SEM, statistical analysis: one-way ANOVA, Tukey post hoc test, *P = 0.0276, ***P = < 0.0001.

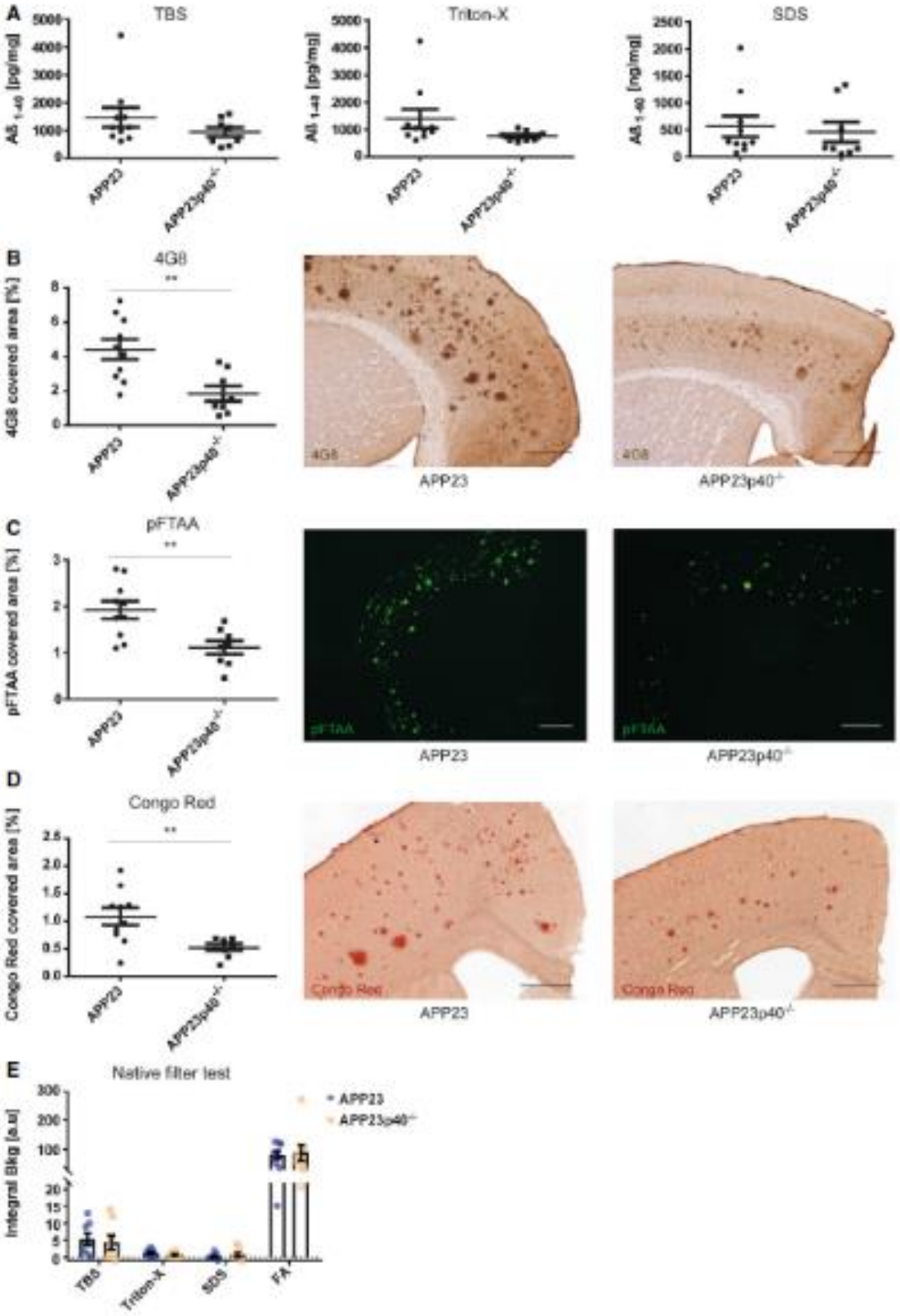
A
TBS
Triton-X
SDS
Aβ1-40 [pg/mg]
Aβ1-40 [ng/mg]
APP23
APP23p40-/-
B
4G8
4G8 covered area [%]
4G8
APP23
APP23p40-/-
C
pFTAA
pFTAA covered area [%]
pFTAA
APP23
APP23p40-/-
D
Congo Red
Congo Red covered area [%]
Congo Red
APP23
APP23p40-/-
E
Native filter test
Integral Bkg [a.u]
APP23
APP23p40-/-
TBS
Triton-X
SDS
FA

Figure 4.

Figure 4. In male APP23 mice, IL12p40 deficiency reduces Aβ plaque deposition but not does not affect biochemical characteristics of Aβ.

A Mesoscale analysis for the $Aβ_{1–40}$ protein in the TBS ($P = 0.2298$), Triton-X ($P = 0.1329$) and SDS ($P = 0.7184$) fractions of brain homogenates from male APP23 ($n = 10$) and APP23p40$^{-/-}$ ($n = 8$) mice. Total protein concentration of each sample was used as an internal reference. Mean ± SEM, statistical analysis: two-tailed unpaired *t*-test.

B Stereological analysis of cortical area covered by 4G8-positive plaques (left) and representative images of 4G8-staining in APP23 ($n = 10$) and APP23p40$^{-/-}$ ($n = 8$) mice (right), scale bar = 500 μm. Mean ± SEM, statistical analysis: two-tailed unpaired *t*-test, $^{**}P = 0.0039$.

C Fluorescence intensity-based analysis of pFTAA-positive area covered in the cortex of APP23 ($n = 10$) and APP23p40$^{-/-}$ ($n = 8$) mice (left) and representative images for each genotype (right), scale bar = 1 mm. Mean ± SEM, statistical analysis: two-tailed unpaired *t*-test, $^{**}P = 0.0051$.

D Stereological analysis of cortical area covered by Congo Red-positive plaques in APP23 ($n = 10$) and APP23p40$^{-/-}$ ($n = 8$) mice (left) and representative images (right), scale bar = 500 μm. Mean ± SEM, statistical analysis: two-tailed unpaired *t*-test, $^{**}P = 0.0070$.

E Native filter assay analysis of TBS ($P = 0.7124$), Triton-X ($P = 0.3170$), SDS ($P = 0.4833$) and formic acid (FA) ($P = 0.8144$) fractions from APP23 ($n = 8$) and APP23p40$^{-/-}$ ($n = 8$) mouse brain homogenates. Mean ± SEM, statistical analysis: two-tailed unpaired *t*-test between the same fractions.

this mouse model to date. Since none of the studies assessing plaque pathology in APP23 mice undertook thorough comparative analyses of aged male and female mice [31,50–52], and as recent reports highlight differences in the innate immune response between males and females including differences in male and female microglia [25–28], we undertook gender-specific analyses of various pathological readouts where we observed robust differences between male and female mice at late stages of pathology (21 months). Female APP23 mice showed a twofold higher pathology in both biochemical and histological analyses of Aβ accumulation compared to male mice, indicating faster disease progression. Furthermore, Aβ aggregation properties differed between genders since in female mice increased amounts of Aβ aggregates were found in SDS- and FA-extracted protein fractions. In male mice, aggregates were mainly found in TBS- and FA-soluble fractions. Previous studies have shown that the vast majority of Aβ plaques in APP23 mice in an age range of 14–24 months are densely aggregated core plaques and that diffuse plaques only appear in very old mice [29,39,53]. Contrary to these reports, diffuse Aβ plaques, as visualised by immunohistochemistry, constituted the majority of plaques in our analyses of 21-month-old male and female mice, their levels being four times as high as core plaques. We also did not observe any gender-specific differences in plaque-associated BACE1 immunoreactivity, a surrogate marker of neuritic dystrophy [40–43]. Additionally, female APP23 mice, in accordance with the increase in plaque burden, also showed higher numbers of cortical astrocytes and increased levels of CXCL1 (also known as KC/CRO or GRO1) in the brain, which positively correlated with $Aβ_{1–40}$ pathology. It is of note that in a mouse model of multiple sclerosis, astrocyte-specific induction of CXCL1 augmented disease progression via recruitment of neutrophils [54], while in an AD-like mouse model, blocking the entry of neutrophils into the brain was shown to have a beneficial effect upon pathogenesis [55]. CXCL1, as one of the differentially regulated cytokines in male versus female APP23 mice lacking or harbouring IL12p40, may thus not only present a possible (non-exclusive) explanation for the gender-specific differences in AD pathology, but may also qualify as an interesting target to study in AD pathogenesis. While the cytokine signatures in brain and plasma of male and female APP23 mice seem to differ, we could not observe any gender-specific differences in the number of plaque-associated microglia, their expression of Clec7a, a marker of activated microglia in various disease contexts [47,48] and Aβ uptake, suggesting that altered microglial functions are not the cause of gender-specific pathogenesis in this mouse model.

We previously reported that genetic deletion or pharmacological blockage of the pro-inflammatory IL12p40 in the APPPS1 mouse model led to a marked decrease in plaque pathology at both early and late stages of Aβ deposition (4 and 8 months, respectively) as well as a reduction in cognitive deficits [18]. This study also found that the IL12p40 subunit was expressed by microglia, describing for the first time a role of IL-12/IL-23 signalling in AD carried out by glial cells in the CNS. Given that the APPPS1 mouse model is characterised by a rapid accumulation of Aβ deposits, it may not fully represent the rather slow Aβ accumulation and disease progression that typically is described for sporadic human AD. Our data using the APP23 AD-like mouse model now show that a lack of IL12p40 similarly leads to a reduction in Aβ burden in a mouse model with a rather slow disease course. We therefore provide further evidence of the involvement of IL-12 and/or IL-23 signalling in AD pathogenesis, which also strengthens the hypothesis that the blockage of certain pro-inflammatory factors secreted by glia can have beneficial

Figure 5. Lack of IL12p40 does not affect plaque-associated BACE1 immunoreactivity or glial properties in male APP23 mice.

A Histological analysis of plaque-associated BACE1 immunoreactivity in male APP23 ($n = 10$) and APP23p40$^{-/-}$ ($n = 8$) mice. BACE1 area covered was normalised to 4G8-positive area covered of the same image (left). Right: representative images, scale bar = 50 μm. Mean ± SEM, statistical analysis: two-tailed unpaired *t*-test, $P = 0.1780$.

B Stereological quantification of the number of cortical GFAP-positive astrocytes in male APP23 ($n = 10$) and APP23p40$^{-/-}$ ($n = 8$) mice (left). Right: representative images of GFAP staining, scale bar = 200 μm. Mean ± SEM, statistical analysis: two-tailed unpaired *t*-test, $P = 0.3148$.

C Quantification of activated microglia within 30 μm from plaque borders. Top: numbers of Iba1-positive microglia were normalised to the size of the nearest 4G8-positive plaque and quantified in male APP23 ($n = 10$) and APP23p40$^{-/-}$ ($n = 8$) mice. Mean ± SEM, statistical analysis: two-tailed unpaired *t*-test, $P = 0.1925$. Bottom: histogram representing Clec7a staining intensity within plaque-associated Iba1-positive microglia in male APP23 ($n = 10$) and APP23p40$^{-/-}$ ($n = 8$) mice. Mean ± SEM, statistical analysis: two-tailed unpaired *t*-test with Bonferroni correction for each single bin, P = N.S. Right: representative images, scale bar = 40 μm.

D Radial intensity profiles of Iba1 and 4G8 around the centre of the nucleus of plaque-associated Iba1-positive microglia in male APP23 ($n = 10$) and APP23p40$^{-/-}$ ($n = 8$) mice. Iba1 intensity declines until a radius of ~6 μm, marking the cell periphery. 4G8 intensity peaks inside the cell (~4 μm), but stays high outside the cell. This is very likely due to the close proximity to 4G8-positive plaques. Mean ± SEM, statistical analysis: two-tailed unpaired *t*-test with Bonferroni correction for the number of binned radii shows no significant difference between both 4G8 traces.

Source data are available online for this figure.

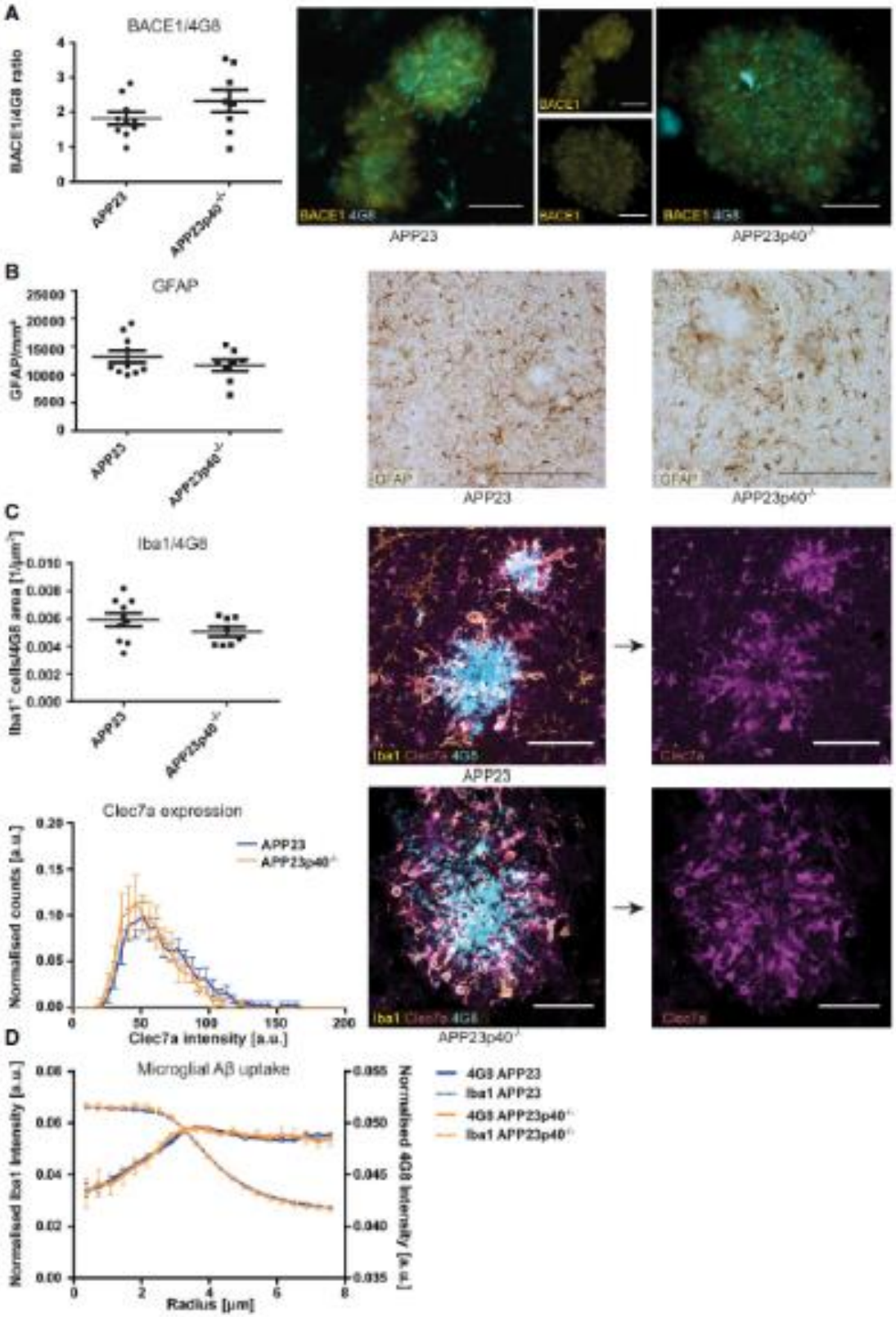
A
BACE1/4G8
BACE1/4G8 ratio
APP23
APP23p40-/-
BACE1 4G8
BACE1
APP23
APP23p40-/-
B
GFAP
GFAP/mm²
APP23
APP23p40-/-
GFAP
APP23
APP23p40-/-
C
Iba1/4G8
Iba1+ cells/4G8 area [1/µm²]
APP23
APP23p40-/-
Iba1 Clec7a 4G8
Clec7a
APP23
APP23p40-/-
Clec7a expression
Normalised counts [a.u.]
Clec7a intensity [a.u.]
APP23
APP23p40-/-
Iba1 Clec7a 4G8
Clec7a
APP23p40-/-
D
Microglial Aβ uptake
Normalised Iba1 intensity [a.u.]
Normalised 4G8 intensity [a.u.]
Radius [µm]
4G8 APP23
Iba1 APP23
4G8 APP23p40-/-
Iba1 APP23p40-/-

Figure 5.

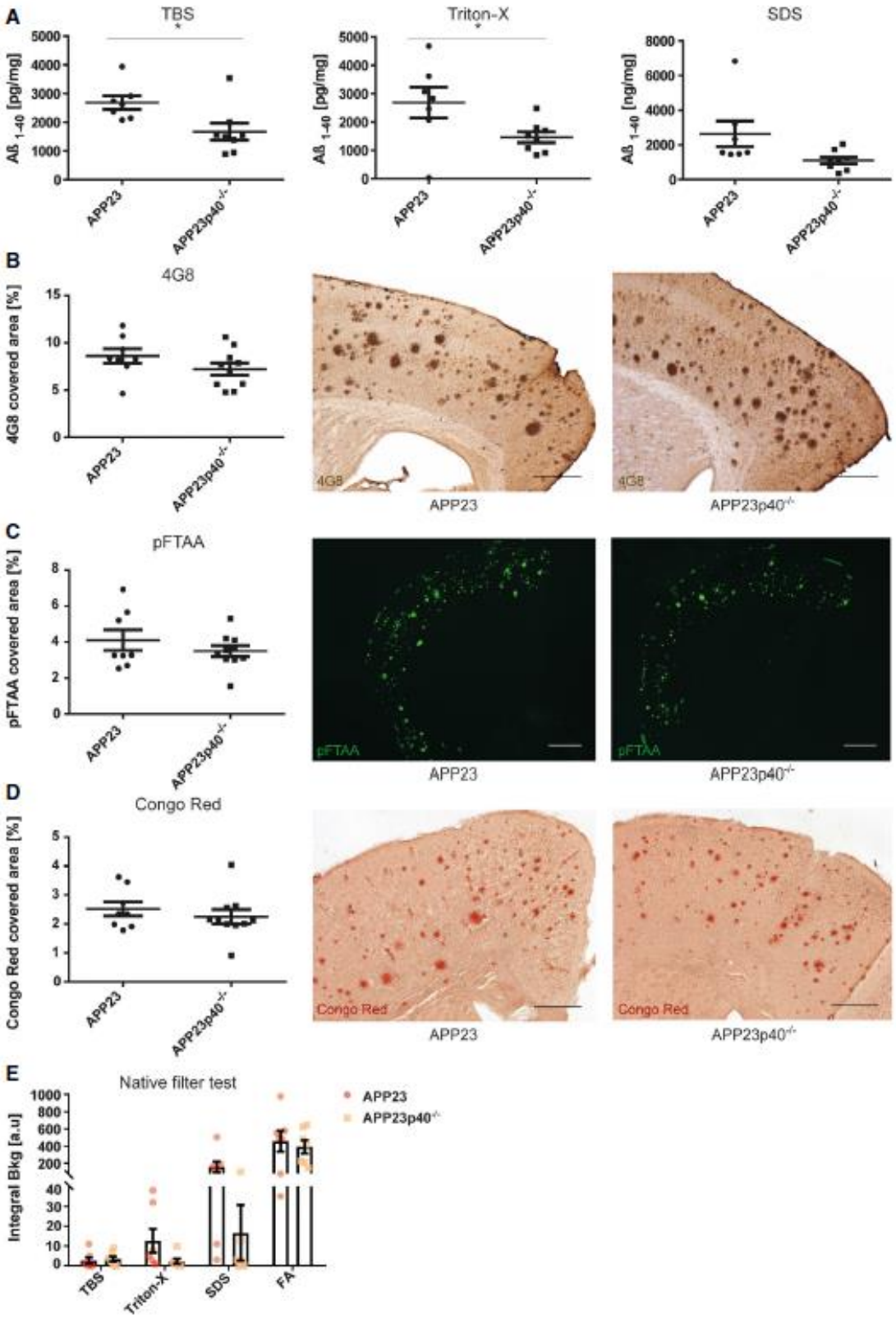

Figure 6.

Figure 6. In female APP23 mice, IL12p40 deletion leads to a reduction in soluble $A\beta_{1-40}$ but not Aβ plaque load.

A Mesoscale analysis for the $A\beta_{1-40}$ protein in the TBS (*P = 0.0208), Triton-X (*P = 0.0440) and SDS (P = 0.0540) fractions of brain homogenates from APP23 (n = 7) and APP23p40$^{-/-}$ (n = 8) mice. Total protein concentration of each sample was used as an internal reference. Mean ± SEM, statistical analysis: two-tailed unpaired t-test.

B Stereological analysis of cortical area covered by 4G8-positive plaques (left) and representative images of 4G8-staining in APP23 (n = 8) and APP23p40$^{-/-}$ (n = 10) mice (right), scale bar = 500 μm. Mean ± SEM, statistical analysis: two-tailed unpaired t-test, P = 0.1831.

C Fluorescence intensity-based analysis of pFTAA-positive area covered in the cortex of APP23 (n = 8) and APP23p40$^{-/-}$ (n = 10) mice (left) and representative images for each genotype (right), scale bar = 1 mm. Mean ± SEM, statistical analysis: two-tailed unpaired t-test, P = 0.3406.

D Stereological analysis of cortical area covered by Congo Red-positive plaques in APP23 (n = 8) and APP23p40$^{-/-}$ (n = 10) mice (left) and representative images (right), scale bar = 500 μm. Mean ± SEM, statistical analysis: two-tailed unpaired t-test, P = 0.4542.

E Native filter assay analysis of TBS (P = 0.6823), Triton-X (P = 0.1146), SDS (P = 0.0508) and formic acid (FA) (P = 0.6608) fractions from APP23 (n = 7) and APP23p40$^{-/-}$ (n = 7) mouse brain homogenates. Mean ± SEM, statistical analysis: two-tailed unpaired t-tests between the same fractions.

effects upon Aβ pathology. The importance of IL-12/IL-23 signalling in AD is supported further by other studies demonstrating that targeting IL12p40 via small interfering RNA in the SAMP8 AD-like mouse model of accelerated ageing induced a reduction in cerebral Aβ as well as reduced neuronal loss and cognitive function [33]. Analysis of genetic data within the Han Chinese population also indicated specific polymorphisms in the IL-12/IL-23 pathway as risk factors for late-onset AD [56,57]. Additionally, increased levels of IL-23 and/or IL-12 were found in serum and plasma [19,58] and a correlation was made between IL12p40 CSF levels and cognitive performance in AD patients [18]. Given that IL-12/IL-23 has been shown to be regulated in MCI and AD subjects [18–20] and biologicals that inhibit IL-12 and/or IL-23 have already been approved by the US Food and Drug Administration (FDA) for other diseases such as psoriasis and Crohn's disease, the immediate suitability for repurposing existing drugs targeting these innate immune molecules in a first clinical AD trial is obvious.

In addition to previous data assessing the effect of a lack of IL12p40 on Aβ plaque burden in AD-like mice, we noted differential effects of IL-12/IL-23 deficiency in age-matched female and male APP23 mice. Compared to APP23 mice, male APP23p40$^{-/-}$ mice showed a significant reduction in diffuse and core plaques when histologically assessing cortical plaque burden, while $A\beta_{1-40}$ levels and Aβ aggregation properties were not altered. Contrary to male mice, female APP23p40$^{-/-}$ mice did have reduced levels of soluble $A\beta_{1-40}$ when compared to APP23 mice, though cortical plaque burden appeared to not be affected. In both male and female mice, the observed changes in Aβ pathology upon IL12p40 deficiency were not mediated by differential APP expression or Aβ processing. Interestingly, despite the differences in Aβ pathology, BACE1-positive dystrophic neurites, the number of cortical astrocytes or plaque-associated microglia were not affected upon IL12p40 deletion, including the expression of microglial Clec7a and Aβ uptake. These observations suggest that microglial IL12p40 does not seem to excerpt its detrimental effect upon Aβ pathology by modulating microglial functions. Alternatively, an indirect effect of IL12p40-mediated intercellular signalling could take place given that the IL12p40 receptor was found to be expressed on non-microglial cells in an AD model [18]. Since IL12p40 deficiency does not affect Aβ processing, it could act upon other cell types by restoring cellular metabolism and thus intracellular degradation of Aβ or by modulating peripheral cells that might affect Aβ deposition such as neutrophils via CXCL1 [55]. The gender-specific effects of IL12p40 deletion upon Aβ pathology could also be explained by the underlying pathological differences between male and female APP23 mice at the age of 21 months. Pathology in female APP23 mice could already be so advanced that potential effects of lack of IL12p40 are overshadowed by the abundance of Aβ deposits. In male APP23 mice, on the other hand, fewer Aβ aggregates at a given stage are present which is why effects of IL12p40 deficiency on plaque accumulation are still observable.

In summary, we show that genetic ablation of the IL-23/IL-12 p40 subunit has a different effect on plaque and cellular pathology in age-matched male and female APP23 mice, a mouse model of slow Aβ accumulation with gender-specific temporal pathogenesis. While in female APP23 mice, deletion of IL-12/IL-23 signalling specifically decreased soluble $A\beta_{1-40}$ levels, the pathology in male mice was characterised by a reduction in cortical Aβ plaque load. Our results provide important evidence on the role of IL-12 and IL-23 signalling in a mouse model of amyloid deposition, which adds to data suggesting a detrimental effect of this signalling cascade

Figure 7. Lack of IL12p40 but does not affect plaque-associated BACE1 immunoreactivity or gliosis in female APP23 mice.

A Histological analysis of plaque-associated BACE1 immunoreactivity in female APP23 (n = 8) and APP23p40$^{-/-}$ (n = 10) mice. BACE1 area covered was normalised to 4G8-positive area covered of the same image (left). Right: representative images, scale bar = 50 μm. Mean ± SEM, statistical analysis: two-tailed unpaired t-test, P = 0.5402.

B Stereological quantification of the number of cortical GFAP-positive astrocytes in female APP23 (n = 8) and APP23p40$^{-/-}$ (n = 8) mice (left). Right: representative images of GFAP staining, scale bar = 200 μm. Mean ± SEM, statistical analysis: two-tailed unpaired t-test, P = 0.1579.

C Quantification of activated microglia within 30 μm from plaque borders. Top: numbers of Iba1-positive microglia were normalised to the size of the nearest 4G8-positive plaque and quantified in female APP23 (n = 8) and APP23p40$^{-/-}$ (n = 10) mice. Mean ± SEM, statistical analysis: two-tailed unpaired t-test, P = 0.8240. Bottom: Histogram representing Clec7a staining intensity within plaque-associated Iba1-positive microglia in female APP23 (n = 8) and APP23p40$^{-/-}$ (n = 10) mice. Mean ± SEM, statistical analysis: two-tailed unpaired t-test with Bonferroni correction for each single bin, P = N.S. Right: representative images, scale bar = 40 μm.

D Radial intensity profiles of Iba1 and 4G8 around the centre of the nucleus of plaque-associated Iba1-positive microglia in female APP23 (n = 8) and APP23p40$^{-/-}$ (n = 10) mice. Iba1 intensity declines until a radius of ~6 μm, marking the cell periphery. 4G8 intensity peaks inside the cell (~4 μm), but stays high outside the cell. This is very likely due to the close proximity to 4G8-positive plaques. Mean ± SEM, statistical analysis: two-tailed unpaired t-test with Bonferroni correction for the number of binned radii shows no significant difference between both 4G8 traces.

Source data are available online for this figure.

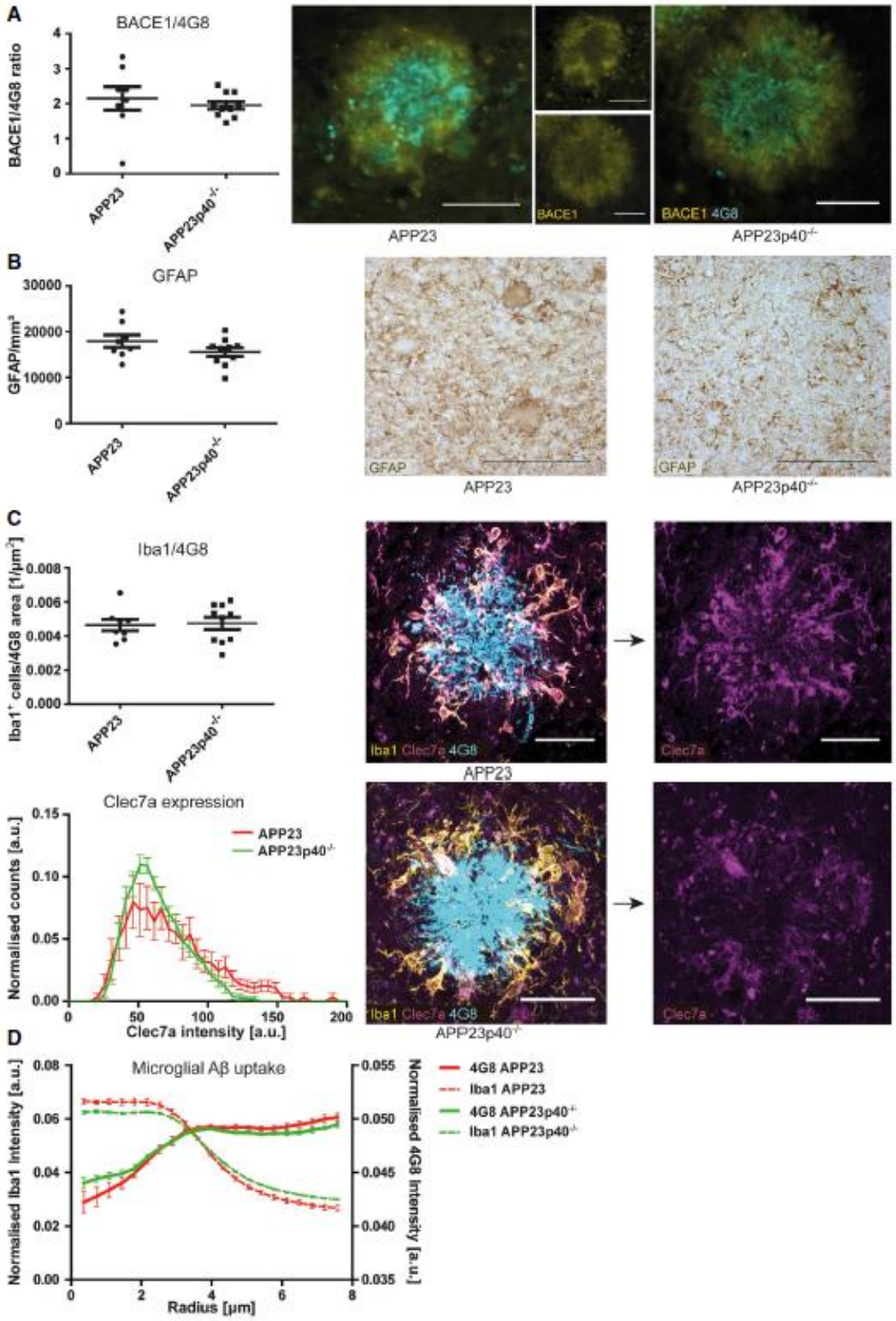

Figure 7.

[18–20,33,56–58]. While future research aimed at successfully targeting IL12p40 in AD implies the need to dissect its downstream mechanisms and to identify whether it is IL-12 or IL-23 specifically that influences AD pathogenesis, it will be equally interesting to address whether this signalling pathway also plays a gender-specific role in other CNS proteinopathies such as Parkinson's disease or tau-driven pathologies.

Materials and Methods

Animals

We crossed heterozygous APP23$^{+/-}$ mice (Tg(Thy1-APPKM670/671NL)23) [29], termed APP23 throughout this manuscript, to mice lacking the IL12p40 gene *Il12b*, termed *Il12p40*$^{-/-}$ mice [47], generating APP23p40$^{-/-}$ mice and APP23 littermate controls. Cohorts of male and female APP23 mice were compared to each other and used as control groups in comparison to APP23p40$^{-/-}$ littermates. Thus, data points of male and female APP23 mice shown in Figs 1A–E, 2A–D, EV2A–I and S1A–B served also as references in Figs 4A–E, 5A–D, EV3C–K and S2A and C analysing male APP23 mice as well as in Figs 6A–E, 7A–D, EV4C–K and S2B and D analysing female APP23 mice. Mice were group-housed under specific pathogen-free conditions on a 12-h light/dark cycle; food and water were provided *ad libidum*. We did not observe any differences in mortality between male and female APP23 and APP23p40$^{-/-}$ mice. All animal experiments were performed in accordance with the national animal protection guidelines approved by the regional offices for health and social services in Berlin (LaGeSo, licence number O 0132/09).

Tissue processing

Transgenic APP23 and APP23p40$^{-/-}$ mice and littermate controls were aged to 21 months. For tissue collection, mice were deeply anaesthetised and transcardially perfused with PBS. Venous blood was collected from the right atrium into EDTA-coated tubes. After centrifugation, the plasma supernatant was collected, snap-frozen in liquid nitrogen and stored at −80°C. Plasma samples could not be collected for all experimental animals. Brains were rapidly removed from the skull and divided into half sagittally, and the cerebellum was removed. One hemisphere was snap-frozen in liquid nitrogen and stored at −80°C until further processing for biochemical analysis, and the other hemisphere was fixed in 4% paraformaldehyde over night at 4°C. Subsequently, the hemisphere was immersed in 30% sucrose for at least 24 h until sectioning for immunohistochemical analysis. For some animals, the fresh frozen hemispheres were not available for further biochemical analyses. For RNA analysis, tissue from male and female APP23 mice aged 648–764 days was processed as described below.

RNA isolation of brain fractions

For RNA analysis, the left hemisphere was used to isolate microglia and the microglia-negative fraction from fresh tissue while the right hemisphere was snap-frozen in liquid nitrogen to generate RNA from whole brain. Microglia were isolated using magnetic-activated cell sorting (MACS) according to manufacturer's protocol. In brief, tissue was dissociated using the Neural Tissue Dissociation Kit (P) (Miltenyi Biotec, 130-092-628) on a gentleMACS Octo Dissociator with Heaters (Miltenyi Biotec, 130-096-427) and the resulting single-cell suspension labelled with CD11b MicroBeads (Miltenyi Biotec, 130-093-634) and passed through LS columns (Miltenyi Biotec, 130-042-401) to positively select for microglia. The CD11b-negative flow-through was also collected as the microglia-negative brain fraction. Both cell fractions were pelleted via centrifugation, snap-frozen and stored at −80°C until further use. For whole brain RNA, the frozen right hemisphere was homogenised in RLT buffer (RNeasy Mini Kit, Qiagen, 74106) using M tubes (Miltenyi Biotec, 130-093-236) on the gentleMACS Octo Dissociator with Heaters (Miltenyi Biotec, 130-096-427) before continuing with the downstream RNA isolation protocol. For RNA isolation, the RNeasy Mini Kit (Qiagen, 74106) was used and cDNA was generated using the High-Capacity cDNA Reverse Transcription Kit (Thermo Fisher, 4368813) according to manufacturer's protocols.

Quantitative real-time PCR

Gene expression analysis was performed on 12 ng cDNA per reaction using the TaqMan Fast Universal Master Mix (Applied Biosystems, 4364103) and TaqMan primers for *Il12b* (Thermo Fisher, Mm00434174_m1) and *Gapdh* (Thermo Fisher, Mm99999915_g1). Quantitative PCR analysis was performed on a QuantStudio 6 Flex Real-Time PCR System (Applied Biosystems). Data were analysed using the Double Delta Ct method to determine fold change expression changes between samples. The number of mice per group analysed was as follows: for CD11b-positive cell fractions: female APP23 $n = 5$, male APP23 $n = 5$; for whole brain and CD11b-negative samples: female APP23 $n = 3$, male APP23 $n = 3$.

Histology

Formalin-fixed and sucrose-treated hemispheres were frozen and cut coronally in serial sections at 40 µm using a cryostat (Thermo Scientific HM 560). Sections were kept in cryoprotectant (0.65 g $NaH_2PO_4 \times H_2O$, 2.8 g Na_2HPO_4 in 250 ml ddH_2O, pH 7.4 with 150 ml ethylene glycol, 125 ml glycerine) at 4°C until staining. For immunohistochemistry, sections were washed in PBS, mounted on SuperFrost Plus slides (R. Langenbrink), dried and blocked in PBS with 0,3% Triton X-100 and 10% normal goat serum (NGS) for 1 h, before incubation with Aβ-specific antibody anti-4G8 targeting aa. 17–24 of human Aβ (1:1,000 dilution, Covance, SIG39320) or astrocyte-specific antibody anti-GFAP (1:1,000 dilution, Dako, Z0334) over night at 4°C in PBS with 0.3% Triton X-100 and 5% NGS. Next, sections were quenched with 0.5% H_2O_2 for 30 min at room temperature, washed and then incubated with peroxidase-conjugated goat anti-mouse secondary antibody (1:100 dilution, Dianova, 115-035-068) or peroxidase-conjugated goat anti-rabbit secondary antibody (1:100 dilution, Jackson ImmunoResearch, 111-035-003) in PBS with 0.3% Triton X-100 and 5% NGS for 1 h at room temperature. The staining was developed using diaminobenzidine (DAB) substrate (Sigma-Aldrich). Sections were counterstained with matured haematoxylin, followed by signal development in tap water. Subsequently, sections were dehydrated in ascending ethanol concentrations (70, 80, 96, 100%) and xylene and embedded with

hydrophobic mounting medium (Roti Histokitt, Carl Roth). Immunofluorescent co-labelling of anti-4G8 (1:1,000 dilution, Covance, SIG39320) and anti-BACE1 (1:500 dilution, Abcam, ab108394) was performed as above with primary antibody incubation for 48 h at 4°C and incubation with secondary antibodies Alexa Fluor 568 goat anti-rabbit IgG (H+L) (1:500 dilution, Invitrogen, A11011) and Alexa Fluor 647 goat anti-mouse IgG (H+L) (1:500 dilution, Invitrogen, A21236) for 2 h at room temperature. Immunofluorescent labelling of anti-4G8 (1:1,000 dilution, Covance, SIG39320), anti-Iba1 (1:500 dilution, Wako, 019-19741) and marker of activated microglia anti-Clec7a (Dectin-1) (1:30 dilution, InvivoGen, mabg-mdect) was modified to include a 10 min permeabilisation step at room temperature in TBS with 0.2% Triton-X. For all following steps, no Triton-X was added to the solutions. Blocking was performed in TBS with 10% NGS and antibody incubations in TBS with 5% NGS. Again, primary antibodies were incubated for 48 h at 4°C and secondary antibodies Alexa Fluor 488 goat anti-mouse IgG (H+L) (1:500 dilution, Invitrogen, A11001), Cy™3 AffiniPure Donkey Anti-Rat IgG (H+L) (1:500 dilution, Jackson ImmunoResearch, 712-165-153) and Alexa Fluor 647 goat anti-rabbit IgG (H+L) (1:500 dilution, Invitrogen, A21244) were incubated for 2 h at room temperature. Following fluorescent immunostaining, sections were counterstained with DAPI (1:2,500 dilution, Sigma-Aldrich, 10236276001) and embedded with fluorescence mounting medium (Dako, S3023).

Congo Red staining [37] was performed on mounted and dried sections counterstained with matured haematoxylin. Sections were incubated in stock solution I (0.5 M NaCl in 80% ethanol, 0.01% hydrous NaOH) for 20 min and in stock solution II (8.6 mM Congo Red in stock solution I, 0.01% NaOH) for 45 min. Subsequently, sections were rinsed in 80% EtOH and xylene and embedded with hydrophobic mounting medium.

For staining with pentameric formyl thiophene acetic acid (pFTAA) [36], sections were washed in PBS, stained for 30 min with 2 µg/ml pFTAA in PBS and counterstained with 4′,6-diamidino-2-phenylindole (DAPI) (1:5,000, Sigma-Aldrich). Sections were embedded in fluorescent mounting medium (Agilent).

Stereological analysis of Aβ plaque burden and cortical astrocyte number

For quantifying Aβ plaque load and astrocytes number, the Stereo Investigator system (MBF Bioscience) mounted on an Olympus BX53 microscope, equipped with the QImaging camera COLOR 12 BIT and a stage controller MAC 6000 was used. Quantification of cortical area covered by 4G8-positive or Congo Red-positive Aβ plaques was undertaken using the Stereo Investigator 64-bit software (MBF Bioscience) (settings: 10× objective, counting frame 90 × 90 µm, scan grid size 450 × 450 µm, Cavalieri grid spacing 10 µm). For counting cortical astrocytes, the Optical Fraction Fractionator tool of the Stereo Investigator 64-bit software (MBF Bioscience) was used (settings: 40× objective, counting frame 75 × 75 µm, scan grid size 500 × 500 µm). The values from "Estimated Population using User Defined Section Thickness" and "Measured Volume (µm³)" were divided and used to calculate the number of cells per cortical volume. For quantification of pFTAA-positive plaques, the Olympus cellSens Dimension software was used. Sections were exposed at 400 ms, and a region of interest (ROI) was selected around the cortex. The image was converted to grey scale, and the same threshold was applied to obtain the area fraction of pFTAA-positive signal (%). For each stain, 10 serial coronal sections per brain were used for analysis. The number of mice per group analysed was as follows: female APP23 $n = 8$, female APP23p40$^{-/-}$ $n = 10$, male APP23 $n = 10$ and male APP23p40$^{-/-}$ $n = 8$.

Analysis of BACE1/4G8 ratio

Images of BACE1/4G8 co-labelled sections were taken on an Olympus BX53 microscope, equipped with the QImaging camera COLOR 12 BIT and controlled by the Olympus cellSens Dimension software. Per animal, images were taken from 10 serial coronal sections and three regions per section. In ImageJ, we performed a batch conversion of raw TIFF images as contrast-optimised, greyscale JPEG files, and using a custom R script, we extracted the generated histograms and used these to calculate the respective proportion of stained and unstained pixels. A fixed analysis threshold was chosen based on variance and mean image intensity of all analysed images belonging to the BACE1 antibody and 4G8 antibody staining, respectively. Quality of the histological stainings and image material was estimated by a cross-comparison of each image's characteristics to (i) all other images of the same animal and (ii) all other images of the same experimental group and all images that did not meet the defined acceptable range of 2*SD were excluded from downstream analysis (10.7% of images total). The median BACE1/4G8 ratio of 16–30 images per animal was taken for analysis, and the mean and SEM of all animals from one group was plotted. The number of mice per group analysed was as follows: female APP23 $n = 8$, female APP23p40$^{-/-}$ $n = 10$, male APP23 $n = 10$ and male APP23p40$^{-/-}$ $n = 8$. The R script has been deposited on Github (https://github.com/eedep/Image-processing).

Quantification of Clec7a-positive plaque-associated microglia and Aβ uptake

Three-dimensional image stacks (1 µm step size, 40× objective) of 4G8/Clec7a/Iba1-stained sections were taken on a Leica TCS SP5 confocal laser scanning microscope controlled by LAS AF scan software (Leica Microsystems, Wetzlar, Germany). Per animal, 10 serial coronal sections and three regions per section were used for analysis. The number of mice per group analysed was as follows: female APP23 $n = 8$, female APP23p40$^{-/-}$ $n = 10$, male APP23 $n = 10$ and male APP23p40$^{-/-}$ $n = 8$.

The expression levels of Iba1 and Clec7a, 4G8 positive plaques, radial intensity profiles, cell numbers and distances to the nearest plaque (Figs 2C, 5C and 7C) were quantified from maximum projections of the confocal stacks. The quantification was performed in an automated manner using custom-written ImageJ macros (segmentation) [59] and python scripts (radial profiles and other statistics), which can be found on GitHub (https://github.com/ngimber/AlzheimersWorkflow). Data were pooled by calculating the median from all images per animal and plotting the mean and SEM of all animals from one group. Data that are displayed as a histogram were binned image-wise. Histograms and radial intensity profiles were normalised (divided by its own integral) and then pooled as mentioned above.

Segmentation (ImageJ)

Nuclei were segmented from blurred DAPI channels (Gaussian blur, sigma = 720 nm) by histogram-based thresholding (Otsu binarisation) [60] followed by watershed segmentation of the Euclidean distance map of the binary image using ImageJ. Plaques were segmented from the blurred 4G8 channel (Gaussian blur, sigma = 7.2 μm) followed by Otsu binarisation. Only objects above 720 μm² were regarded as plaques.

Quantification (Custom Python scripts)

The mean intensities within segmented nuclear regions (s. above) were used as a measure for Iba1 and Clec7a expression levels. Cells were classified as Iba1-positive/-negative by auto-thresholding (Otsu's method on all cell-specific expression levels within one image). Only Iba1-positive cells were used for further analysis (e.g. Clec7a expression levels, cell numbers, distances to the nearest plaque and radial intensity profiles). The size of the nearest plaques was determined for each cell based on the segmented regions mentioned above. Radial intensity profiles were calculated for all channels around the centre of mass of the segmented nucleus.

Brain homogenisation

For analysis of protein levels, frozen hemispheres were subjected to a 4-step protein extraction protocol, using buffers with increasing stringency [34]. In brief, hemispheres were homogenised consecutively in Tris-buffered saline (TBS) buffer (20 mM Tris, 137 mM NaCl, pH = 7.6), Triton-X buffer (TBS buffer containing 1% Triton X-100), SDS buffer (2% SDS in ddH_2O) and FA (70% formic acid in ddH_2O). Immediately before use, cOmplete™ Mini Protease Inhibitor Cocktail Tablets (Roche, 1 tablet per 10 ml) were added to all buffers. Initial homogenisation occurred mechanically by consecutive passing the solution through a 2-ml syringe and cannulas with decreasing diameter (G23, G27 and G30). Brain extracts were incubated 30 min on ice (except SDS homogenate, which was incubated at RT) and centrifuged at 100,000 *g* for 1 h at 4°C. The supernatant was collected, aliquoted, snap-frozen in liquid nitrogen and stored at −80°C until further use. The remaining pellet was re-suspended in subsequent buffers. Protein concentrations of each fraction were determined using the Quantipro BCA Protein Assay Kit (Pierce) according to the manufacturer protocol using the Photometer Tecan Infinite® 200M (Tecan).

ELISA analysis

An IL-12/IL-23 total p40 enzyme-linked immunosorbent assay (ELISA) (eBioscience) was performed according to manufacturer's instructions. Undiluted TBS brain homogenate was analysed in duplicate. Absorption was read at 450 and 570 nm (for wavelength correction) on a microplate reader (Infinite® 200M, Tecan) and analysed using the Magellan Software (Tecan).

Quantification of Aβ levels

Brain extracts of all TBS, Triton-X and SDS fractions were analysed for Aβ40 and Aβ42 levels using the 96-well MultiSpot Human 6E10 Aβ Triplex Assay Kit (Meso Scale Diagnostics, MSD). In brief, samples were analysed in duplicate and were diluted to fit the standard curve (Aβ Peptide 3-Plex). After blocking the MSD plate with 1% Blocker A Solution, the detection antibody solution and sample or calibrator were added and incubated for 2 h. After washing the plate with 0.05% Tween-20 in PBS, 2× Reading Buffer was added to the wells and the plate was analysed on a MS6000 machine (MSD). The number of mice per group analysed was as follows: female APP23 $n = 7$, female APP23p40$^{-/-}$ $n = 8$, male APP23 $n = 10$ and male APP23p40$^{-/-}$ $n = 8$.

Quantification of cytokines

Pro- and anti-inflammatory markers [IFNγ, IL-10, IL-1β, IL-2, IL-4, IL-5, IL-6, TNF-α, CXCL1 (KC/GRO)] were analysed in the TBS fraction of brain homogenates and plasma samples using the 96-well 10-plex Pro-inflammatory Panel 1 (mouse) Mesoscale Kit according to manufacturer's instructions (MSD In brief, undiluted TBS homogenate, plasma samples diluted 1:100 or the calibrator was added in duplicate to the MSD plate and incubated for 2 h. After washing in 0.05% Tween-20 in PBS, the detection antibody solution was added and incubated for further 2 h. After washing the plate with 0.05% Tween-20 in PBS, 2× Reading Buffer was added to the wells and the plate was analysed on a MS6000 machine (MSD). The number of mice per group analysed was as follows: female APP23 $n = 7$, female APP23p40$^{-/-}$ $n = 8$, male APP23 $n = 10$ and male APP23p40$^{-/-}$ $n = 8$.

Western blot analysis

For the quantification of BACE1, neprilysin and insulin-degrading enzyme (IDE), the Triton-X fraction of brain homogenates (30 μg/lane) was separated by SDS–PAGE using 10% Tris-Glycine gels. For quantifying 6E10, the SDS fraction of brain homogenates (30 μg/lane) was separated by SDS–PAGE using Novex™ 10–20% Tricine protein gels (Invitrogen, EC66255BOX). Proteins were transferred by wet blotting onto a nitrocellulose membrane.

Membranes were blocked with 3% milk powder and stained with the anti-Aβ 6E10 antibody (1:2,000, BioLegend, 803002), anti-BACE1 (1:1,000, Abcam, ab108394), anti-Neprilysin (CD10) (1:500, Invitrogen, PA5-29354), anti-IDE (1:1,000, Merck, PC730) and either anti-β-Actin (1:50,000, Sigma, A1978) or anti-GAPDH (1:500, Merck, MAB374). Blots pre-stained with anti-IDE were stripped using the Abcam Mild Stripping protocol in order to re-stain with anti-Neprilysin. Secondary staining was performed using the ECL HRP-linked anti-mouse antibody (1:5,000, GE Healthcare, NA931) or ECL HRP-linked anti-rabbit antibody (1:5,000, GE Healthcare, NA934) and for visualisation of the bands the SuperSignal® West Femto Chemiluminescent Substrate (Thermo Fisher) for the detection of horseradish peroxidase activity was used. For quantification, the intensities of the corresponding bands for each protein were determined with ImageJ and the amount of the respective protein was normalised either to the β-actin or GAPDH protein content. For the analysis of BACE1, Neprilysin and IDE, some of the loaded Triton-X samples did not contain enough protein sufficient for analysis (based on GAPDH content). These specific samples were removed from the analysis.

Filter retardation test

A native filter test was applied to analyse size and stability of Aβ aggregates on non-denatured samples [modified from 38]. In brief,

brain homogenates from all four protein fractions (10 µg total protein per dot) were filtered in triplicate through a 0.2-µm cellulose acetate membrane. Synthetic pre-fibrillar Aβ was used as a positive control and NSP buffer (10 mM K_3PO_4, 10 mM NaCl pH 7.4) as a negative control. Filters were washed in PBS and incubated with the 6E10 antibody (1:2,000, BioLegend, 803002), followed by a mouse secondary HRP-conjugated antibody (Sigma, A0168), to allow chemiluminescent detection of the aggregated proteins remaining on the filter. Membranes were exposed for 1 min, and signals were analysed using the Aida program. A detailed setup of the membrane can be found in Appendix Fig S2.

Statistics, data analysis, study design and data availability

General

Data were generated based on multiple exploratory histological and biochemical analyses aimed at generating hypotheses and biostatistical planning for future confirmatory studies. Data analysis, processing, descriptive and formal statistical testing were done according to the current customary practice of data handling using Excel 2016, GraphPad PRISM 5.0, ImageJ, Python 3.7.4 and R version 3.5.1 "Feather Spray" (code available via Github). To display data in a consistent manner, graphs were generated using PRISM, while correlation graphs were done by the use of ggplot2 in R. All data generated or analysed during this study are included in this article.

Statistics

Student's *t*-test was used for pairwise comparison between two experimental groups. For Clec7a column analysis, a Bonferroni correction for each single bin was applied. Pearson *r*-value and *P*-value for correlations were identified using correlation analysis. One-way ANOVA testing was applied for comparison of more than two groups, with post hoc analysis using Tukey's multiple comparison test. Statistical significance is indicated as follows: $*P \leq 0.05$, $**P \leq 0.01$ and $***P \leq 0.001$.

Expanded View for this article is available online.

Acknowledgements

This work was supported by the Deutsche Forschungsgemeinschaft (DFG, German Research Foundation) under Germany's Excellence Strategy—EXC-2049—390688087, as well as under SFB TRR 43, SFB TRR 167 and HE 3130/6-1 to F.L.H., SFB 958/Z02 to J.S., by the German Center for Neurodegenerative Diseases (DZNE) Berlin, and by the European Union (PHAGO, 115976; Innovative Medicines Initiative-2; FP7-PEOPLE-2012-ITN: NeuroKine). We are indebted to Eilís Perez for generating correlation graphs and to Kiara Freitag for assistance with graphical illustrations. Synopsis image was created with Biorender.com.

Author contributions

PE and JO performed experiments and analysed data; EEW and AB performed filter retardation tests and analyses; EB performed histological stainings and generated confocal images; GY-D performed stereological analyses; BCR wrote the custom R script for analysing the BACE1/4G8 ratio; NG and JS analysed confocal images for plaque-associated microglia and Clec7a intensity as well as 4G8-positive microglia; FLH and SP designed and supervised the study; PE prepared figures. All authors wrote, revised and approved the manuscript.

Conflict of interest

The authors declare that they have no conflict of interest.

References

1. Montine TJ, Phelps CH, Beach TG, Bigio EH, Cairns NJ, Dickson DW, Duyckaerts C, Frosch MP, Masliah E, Mirra SS *et al* (2012) National Institute on Aging–Alzheimer's Association guidelines for the neuropathologic assessment of Alzheimer's disease: a practical approach. *Acta Neuropathol* 123: 1 – 11
2. Jack CR, Albert MS, Knopman DS, Mckhann GM, Sperling RA, Carrillo MC, Thies B, Phelps CH (2011) Introduction to the recommendations from the National Institute on Aging-Alzheimer's Association workgroups on diagnostic guidelines for Alzheimer's disease. *Alzheimers Dement* 7: 257 – 262
3. McKhann GM, Knopman DS, Chertkow H, Hyman BT, Jack CR, Kawas CH, Klunk WE, Koroshetz WJ, Manly JJ, Mayeux R *et al* (2011) The diagnosis of dementia due to Alzheimer's disease: recommendations from the National Institute on Aging-Alzheimer's Association workgroups on diagnostic guidelines for Alzheimer's disease. *Alzheimers Dement* 7: 263 – 269
4. Jack CR, Knopman DS, Jagust WJ, Petersen RC, Weiner MW, Aisen PS, Shaw LM, Vemuri P, Wiste HJ, Weigand SD *et al* (2013) Tracking pathophysiological processes in Alzheimer's disease: an updated hypothetical model of dynamic biomarkers. *Lancet Neurol* 12: 207 – 216
5. Gordon BA, Blazey TM, Su Y, Hari-Raj A, Dincer A, Flores S, Christensen J, Mcdade E, Wang G, Xiong C *et al* (2018) Spatial patterns of neuroimaging biomarker change in individuals from families with autosomal dominant Alzheimer's disease: a longitudinal study. *Lancet Neurol* 17: 241 – 250
6. Ashe KH, Zahs KR (2010) Probing the biology of Alzheimer's disease in mice. *Neuron* 66: 631 – 645
7. Prokop S, Miller KR, Heppner FL (2013) Microglia actions in Alzheimer's disease. *Acta Neuropathol* 126: 461 – 477
8. Akiyama H, Barger S, Barnum S, Bradt B, Bauer J, Cole GM, Cooper NR, Eikelenboom P, Emmerling M, Fiebich BL *et al* (2000) Inflammation and Alzheimer's disease. *Neurobiol Aging* 21: 383 – 421
9. Bradshaw EM, Chibnik LB, Keenan BT, Ottoboni L, Raj T, Tang A, Rosenkrantz LL, Imboywa S, Lee M, Von Korff A *et al* (2013) CD33 Alzheimer's disease locus: altered monocyte function and amyloid biology. *Nat Neurosci* 16: 848 – 850
10. Guerreiro R, Wojtas A, Bras J, Carrasquillo M, Rogaeva E, Majounie E, Cruchaga C, Sassi C, Kauwe JSK, Younkin S *et al* (2013) TREM2 variants in Alzheimer's disease. *N Engl J Med* 368: 117 – 127
11. Heppner FL, Ransohoff RM, Becher B (2015) Immune attack: the role of inflammation in Alzheimer disease. *Nat Rev Neurosci* 16: 358
12. Grathwohl SA, Kalin RE, Bolmont T, Prokop S, Winkelmann G, Kaeser SA, Odenthal J, Radde R, Eldh T, Gandy S *et al* (2009) Formation and maintenance of Alzheimer's disease β-amyloid plaques in the absence of microglia. *Nat Neurosci* 12: 1361 – 1363
13. Spangenberg EE, Lee RJ, Najafi AR, Rice RA, Elmore MR, Blurton-Jones M, West BL, Green KN (2016) Eliminating microglia in Alzheimer's mice prevents neuronal loss without modulating amyloid-beta pathology. *Brain* 139: 1265 – 1281
14. Heneka MT, Kummer MP, Stutz A, Delekate A, Schwartz S, Vieira-Saecker A, Griep A, Axt D, Remus A, Tzeng T-C *et al* (2013) NLRP3 is activated in Alzheimer's disease and contributes to pathology in APP/PS1 mice. *Nature* 493: 674 – 678

15. Chakrabarty P, Li A, Ceballos-Diaz C, Eddy JA, Funk CC, Moore B, DiNunno N, Rosario AM, Cruz PE, Verbeeck C *et al* (2015) IL-10 alters immunoproteostasis in APP mice, increasing plaque burden and worsening cognitive behavior. *Neuron* 85: 519 – 533
16. Guillot-Sestier M-V, Doty KR, Gate D, Rodriguez J, Leung BP, Rezai-Zadeh K, Town T (2015) Il10 deficiency rebalances innate immunity to mitigate Alzheimer-like pathology. *Neuron* 85: 534 – 548
17. Spangenberg E, Severson PL, Hohsfield LA, Crapser J, Zhang J, Burton EA, Zhang Y, Spevak W, Lin J, Phan NY *et al* (2019) Sustained microglial depletion with CSF1R inhibitor impairs parenchymal plaque development in an Alzheimer's disease model. *Nat Commun* 10: 3758
18. Vom Berg J, Prokop S, Miller KR, Obst J, Kalin RE, Lopategui-Cabezas I, Wegner A, Mair F, Schipke CG, Peters O *et al* (2012) Inhibition of IL-12/IL-23 signaling reduces Alzheimer's disease-like pathology and cognitive decline. *Nat Med* 18: 1812 – 1819
19. Hu WT, Holtzman DM, Fagan AM, Shaw LM, Perrin R, Arnold SE, Grossman M, Xiong C, Craig-Schapiro R, Clark CM (2012) Plasma multianalyte profiling in mild cognitive impairment and Alzheimer disease. *Neurology* 79: 897 – 905
20. Wood LB, Winslow AR, Proctor EA, Mcguone D, Mordes DA, Frosch MP, Hyman BT, Lauffenburger DA, Haigis KM (2015) Identification of neurotoxic cytokines by profiling Alzheimer's disease tissues and neuron culture viability screening. *Sci Rep* 5: 16622
21. Mielke MM, Vemuri P, Rocca WA (2014) Clinical epidemiology of Alzheimer's disease: assessing sex and gender differences. *Clin Epidemiol* 6: 37 – 48
22. Mazure CM, Swendsen J (2016) Sex differences in Alzheimer's disease and other dementias. *Lancet Neurol* 15: 451 – 452
23. Mayeda ER (2019) Examining sex/gender differences in risk of Alzheimer's disease and related dementias: challenges and future directions. *Am J Epidemiol* 188: 1224 – 1227
24. Klein SL, Flanagan KL (2016) Sex differences in immune responses. *Nat Rev Immunol* 16: 626
25. Nissen JC (2017) Microglial function across the spectrum of age and gender. *Int J Mol Sci* 18: 561
26. Guneykaya D, Ivanov A, Hernandez DP, Haage V, Wojtas B, Meyer N, Maricos M, Jordan P, Buonfiglioli A, Gielniewski B *et al* (2018) Transcriptional and translational differences of microglia from male and female brains. *Cell Rep* 24: 2773 – 2783.e2776
27. Villa A, Gelosa P, Castiglioni L, Cimino M, Rizzi N, Pepe G, Lolli F, Marcello E, Sironi L, Vegeto E *et al* (2018) Sex-specific features of microglia from adult mice. *Cell Rep* 23: 3501 – 3511
28. Mathys H, Davila-Velderrain J, Peng Z, Gao F, Mohammadi S, Young JZ, Menon M, He L, Abdurrob F, Jiang X *et al* (2019) Single-cell transcriptomic analysis of Alzheimer's disease. *Nature* 570: 332 – 337
29. Sturchler-Pierrat C, Abramowski D, Duke M, Wiederhold K-H, Mistl C, Rothacher S, Ledermann B, Bürki K, Frey P, Paganetti PA *et al* (1997) Two amyloid precursor protein transgenic mouse models with Alzheimer disease-like pathology. *Proc Natl Acad Sci USA* 94: 13287 – 13292
30. Radde R, Bolmont T, Kaeser SA, Coomaraswamy J, Lindau D, Stoltze L, Calhoun ME, Jäggi F, Wolburg H, Gengler S *et al* (2006) Aβ42-driven cerebral amyloidosis in transgenic mice reveals early and robust pathology. *EMBO Rep* 7: 940 – 946
31. Sturchler-Pierrat C, Staufenbiel M (2000) Pathogenic mechanisms of Alzheimer's disease analyzed in the APP23 transgenic mouse model. *Ann NY Acad Sci* 920: 134 – 139
32. Kelly P, Bondolfi L, Hunziker D, Schlecht H-P, Carver K, Maguire E, Abramowski D, Wiederhold K-H, Sturchler-Pierrat C, Jucker M (2003) Progressive age-related impairment of cognitive behavior in APP23 transgenic mice. *Neurobiol Aging* 24: 365 – 378
33. Tan M-S, Yu J-T, Jiang T, Zhu X-C, Guan H-S, Tan L (2014) IL12/23 p40 inhibition ameliorates Alzheimer's disease-associated neuropathology and spatial memory in SAMP8 mice. *J Alzheimers Dis* 38: 633 – 646
34. Kawarabayashi T, Younkin LH, Saido TC, Shoji M, Ashe KH, Younkin SG (2001) Age-dependent changes in brain, CSF, and plasma amyloid β protein in the Tg2576 transgenic mouse model of Alzheimer's disease. *J Neurosci* 21: 372 – 381
35. Dickson TC, Vickers JC (2001) The morphological phenotype of β-amyloid plaques and associated neuritic changes in Alzheimer's disease. *Neuroscience* 105: 99 – 107
36. Åslund A, Sigurdson CJ, Klingstedt T, Grathwohl S, Bolmont T, Dickstein DL, Glimsdal E, Prokop S, Lindgren M, Konradsson P *et al* (2009) Novel pentameric thiophene derivatives for *in vitro* and *in vivo* optical imaging of a plethora of protein aggregates in cerebral amyloidoses. *ACS Chem Biol* 4: 673 – 684
37. Puchtler H, Sweat F, Levine M (1962) On the binding of Congo red by amyloid. *J Histochem Cytochem* 10: 355 – 364
38. Wanker EE, Scherzinger E, Heiser V, Sittler A, Eickhoff H, Lehrach H (1999) Membrane filter assay for detection of amyloid-like polyglutamine-containing protein aggregates. *Method Enzymol* 309: 375 – 386
39. Calhoun ME, Wiederhold K-H, Abramowski D, Phinney AL, Probst A, Sturchler-Pierrat C, Staufenbiel M, Sommer B, Jucker M (1998) Neuron loss in APP transgenic mice. *Nature* 395: 755
40. Zhao J, Fu Y, Yasvoina M, Shao P, Hitt B, O'connor T, Logan S, Maus E, Citron M, Berry R *et al* (2007) β-Site amyloid precursor protein cleaving enzyme 1 levels become elevated in neurons around amyloid plaques: implications for Alzheimer's disease pathogenesis. *J Neurosci* 27: 3639 – 3649
41. Sadleir KR, Kandalepas PC, Buggia-Prévot V, Nicholson DA, Thinakaran G, Vassar R (2016) Presynaptic dystrophic neurites surrounding amyloid plaques are sites of microtubule disruption, BACE1 elevation, and increased Aβ generation in Alzheimer's disease. *Acta Neuropathol* 132: 235 – 256
42. Peters F, Salihoglu H, Pratsch K, Herzog E, Pigoni M, Sgobio C, Lichtenthaler SF, Neumann U, Herms J (2019) Tau deletion reduces plaque-associated BACE1 accumulation and decelerates plaque formation in a mouse model of Alzheimer's disease. *EMBO J* 38: e102345
43. Leyns CEG, Gratuze M, Narasimhan S, Jain N, Koscal LJ, Jiang H, Manis M, Colonna M, Lee VMY, Ulrich JD *et al* (2019) TREM2 function impedes tau seeding in neuritic plaques. *Nat Neurosci* 22: 1217 – 1222
44. Stalder M, Phinney A, Probst A, Sommer B, Staufenbiel M, Jucker M (1999) Association of microglia with amyloid plaques in brains of APP23 transgenic mice. *Am J Pathol* 154: 1673 – 1684
45. Bornemann KD, Wiederhold K-H, Pauli C, Ermini F, Stalder M, Schnell L, Sommer B, Jucker M, Staufenbiel M (2001) Aβ-induced inflammatory processes in microglia cells of APP23 transgenic mice. *Am J Pathol* 158: 63 – 73
46. Burbach GJ, Hellweg R, Haas CA, Del Turco D, Deicke U, Abramowski D, Jucker M, Staufenbiel M, Deller T (2004) Induction of brain-derived neurotrophic factor in plaque-associated glial cells of aged APP23 transgenic mice. *J Neurosci* 24: 2421 – 2430
47. Keren-Shaul H, Spinrad A, Weiner A, Matcovitch-Natan O, Dvir-Szternfeld R, Ulland TK, David E, Baruch K, Lara-Astaiso D, Toth B *et al* (2017) A unique microglia type associated with restricting development of Alzheimer's disease. *Cell* 169: 1276 – 1290.e1217
48. Krasemann S, Madore C, Cialic R, Baufeld C, Calcagno N, El Fatimy R, Beckers L, O'Loughlin E, Xu Y, Fanek Z *et al* (2017) The TREM2-APOE

pathway drives the transcriptional phenotype of dysfunctional microglia in neurodegenerative diseases. *Immunity* 47: 566 – 581.e569

49. Magram J, Connaughton SE, Warrier RR, Carvajal DM, Wu C-Y, Ferrante J, Stewart C, Sarmiento U, Faherty DA, Gately MK (1996) IL-12-deficient mice are defective in IFNγ production and type 1 cytokine responses. *Immunity* 4: 471 – 481
50. D'Hooge R, de Deyn PP (2001) Applications of the Morris water maze in the study of learning and memory. *Brain Res Rev* 36: 60 – 90
51. Kuo YM, Beach TG, Sue LI, Scott S, Layne KJ, Kokjohn TA, Kalback WM, Luehrs DC, Vishnivetskaya TA, Abramowski D *et al* (2001) The evolution of Abeta peptide burden in the APP23 transgenic mice: implications for A beta deposition in Alzheimer disease. *Mol Med* 7: 609 – 618
52. Schieb H, Kratzin H, Jahn O, Möbius W, Rabe S, Staufenbiel M, Wiltfang J, Klafki HW (2011) β-Amyloid peptide variants in brains and cerebrospinal fluid from amyloid precursor protein (APP) transgenic mice – comparison with human alzheimer amyloid. *J Biol Chem* 286: 33747 – 33758
53. Janssen L, Keppens C, De Deyn PP, Van Dam D (2016) Late age increase in soluble amyloid-beta levels in the APP23 mouse model despite steady-state levels of amyloid-beta-producing proteins. *BBA-Mol Basis Dis* 1862: 105 – 112
54. Grist JJ, Marro BS, Skinner DD, Syage AR, Worne C, Doty DJ, Fujinami RS, Lane TE (2018) Induced CNS expression of CXCL1 augments neurologic disease in a murine model of multiple sclerosis via enhanced neutrophil recruitment. *Eur J Immunol* 48: 1199 – 1210
55. Zenaro E, Pietronigro E, Della Bianca V, Piacentino G, Marongiu L, Budui S, Turano E, Rossi B, Angiari S, Dusi S *et al* (2015) Neutrophils promote Alzheimer's disease-like pathology and cognitive decline via LFA-1 integrin. *Nat Med* 21: 880 – 886
56. Liu Y, Yu J-T, Zhang W, Zong Y, Lu R-C, Zhou J, Tan L (2014) Interleukin-23 receptor polymorphisms are associated with Alzheimer's disease in Han Chinese. *J Neuroimmunol* 271: 43 – 48
57. Zhu X-C, Tan L, Jiang T, Tan M-S, Zhang W, Yu J-T (2014) Association of IL-12A and IL-12B polymorphisms with Alzheimer's disease susceptibility in a Han Chinese population. *J Neuroimmunol* 274: 180 – 184
58. Chen JM, Jiang GX, Li QW, Zhou ZM, Cheng Q (2014) Increased serum levels of interleukin-18, -23 and -17 in Chinese patients with Alzheimer's disease. *Dement Geriatr Cogn* 38: 321 – 329
59. Schneider CA, Rasband WS, Eliceiri KW (2012) NIH Image to ImageJ: 25 years of image analysis. *Nat Methods* 9: 671 – 675
60. Otsu NA (1979) Threshold selection method from gray-level histograms. *IEEE Trans Syst Man Cybern B Cybern* 9: 62 – 66

For reasons of data protection, my CV is not published in the electronic version of my work.

Mein Lebenslauf wird aus datenschutzrechtlichen Gründen in der elektronischen Version meiner Arbeit nicht veröffentlicht.

For reasons of data protection, my CV is not published in the electronic version of my work.

Mein Lebenslauf wird aus datenschutzrechtlichen Gründen in der elektronischen Version meiner Arbeit nicht veröffentlicht.

List of publications

Eede, P.*, Obst, J.*, Benke, E., Yvon-Durocher, G., Richard, B. C., Gimber, N., Schmoranzer, J., Böddrich, A., Wanker, E. E., Prokop, S.* & Heppner, F. L.* (2020). Interleukin-12/23 deficiency differentially affects pathology in male and female Alzheimer's disease-like mice. *EMBO Rep*, e48530.

Impact Factor: 8.383

Cossarizza, A., Chang, H. D., Radbruch, A., Acs, A., Adam, D., Adam-Klages, S., Agace, W. W., Aghaeepour, N., Akdis, M., Allez, M., Almeida, L. N., Alvisi, G., Anderson, G., Andra, I., Annunziato, F., Anselmo, A., Bacher, P., Baldari, C. T., Bari, S., Barnaba, V., Barros-Martins, J., Battistini, L., Bauer, W., Baumgart, S., Baumgarth, N., Baumjohann, D., Baying, B., Bebawy, M., Becher, B., Beisker, W., Benes, V., Beyaert, R., Blanco, A., Boardman, D. A., Bogdan, C., Borger, J. G., Borsellino, G., Boulais, P. E., Bradford, J. A., Brenner, D., Brinkman, R. R., Brooks, A. E. S., Busch, D. H., Buscher, M., Bushnell, T. P., Calzetti, F., Cameron, G., Cammarata, I., Cao, X., Cardell, S. L., Casola, S., Cassatella, M. A., Cavani, A., Celada, A., Chatenoud, L., Chattopadhyay, P. K., Chow, S., Christakou, E., Cicin-Sain, L., Clerici, M., Colombo, F. S., Cook, L., Cooke, A., Cooper, A. M., Corbett, A. J., Cosma, A., Cosmi, L., Coulie, P. G., Cumano, A., Cvetkovic, L., Dang, V. D., Dang-Heine, C., Davey, M. S., Davies, D., De Biasi, S., Del Zotto, G., Dela Cruz, G. V., Delacher, M., Della Bella, S., Dellabona, P., Deniz, G., Dessing, M., Di Santo, J. P., Diefenbach, A., Dieli, F., Dolf, A., Dorner, T., Dress, R. J., Dudziak, D., Dustin, M., Dutertre, C. A., Ebner, F., Eckle, S. B. G., Edinger, M., **Eede, P.,** Ehrhardt, G. R. A., Eich, M., Engel, P., Engelhardt, B., Erdei, A., Esser, C., Everts, B., Evrard, M., Falk, C. S., Fehniger, T. A., Felipo-Benavent, M., Ferry, H., Feuerer, M., Filby, A., Filkor, K., Fillatreau, S., Follo, M., Forster, I., Foster, J., Foulds, G. A., Frehse, B., Frenette, P. S., Frischbutter, S., Fritzsche, W., Galbraith, D. W., Gangaev, A., Garbi, N., Gaudilliere, B., Gazzinelli, R. T., Geginat, J., Gerner, W., Gherardin, N. A., Ghoreschi, K., Gibellini, L., Ginhoux, F., Goda, K., Godfrey, D. I., Goettlinger, C., Gonzalez-Navajas, J. M., Goodyear, C. S., Gori, A., Grogan, J. L., Grummitt, D., Grutzkau, A., Haftmann, C., Hahn, J., Hammad, H., Hammerling, G., Hansmann, L., Hansson, G., Harpur, C. M., Hartmann, S., Hauser, A., Hauser, A. E., Haviland, D. L., Hedley, D., Hernandez, D. C., Herrera, G., Herrmann, M., Hess, C., Hofer, T., Hoffmann, P., Hogquist, K., Holland, T., Hollt, T., Holmdahl, R., Hombrink, P., Houston, J. P., Hoyer, B. F., Huang, B., Huang, F. P., Huber, J. E., Huehn, J., Hundemer, M., Hunter, C. A., Hwang, W. Y. K., Iannone, A., Ingelfinger, F., Ivison, S. M., Jack, H. M., Jani, P. K., Javega, B., Jonjic, S., Kaiser, T., Kalina, T., Kamradt, T., Kaufmann, S. H. E., Keller, B., Ketelaars, S. L. C., Khalilnezhad, A., Khan, S., Kisielow, J., Klenerman, P., Knopf, J., Koay, H. F., Kobow, K., Kolls, J. K., Kong, W. T., Kopf, M., Korn, T., Kriegsmann, K., Kristyanto, H., Kroneis, T., Krueger, A., Kuhne, J., Kukat, C., Kunkel, D., Kunze-Schumacher, H., Kurosaki, T., Kurts, C., Kvistborg, P., Kwok, I., Landry, J., Lantz, O., Lanuti, P., Larosa, F., Lehuen, A., Leibundgut-Landmann, S., Leipold, M. D., Leung, L. Y. T., Levings, M. K., Lino, A. C., Liotta, F., Litwin, V., Liu, Y., Ljunggren, H. G., Lohoff, M., Lombardi, G., Lopez, L., Lopez-Botet, M., Lovett-Racke, A. E., Lubberts, E., Luche, H., Ludewig, B., Lugli, E., Lunemann, S., Maecker, H. T., Maggi, L., Maguire, O., Mair, F., Mair, K. H., Mantovani, A., Manz, R. A., Marshall, A. J., Martinez-Romero, A., Martrus, G., Marventano, I., Maslinski, W., Matarese, G., Mattioli, A. V., Maueroder, C., Mazzoni, A., Mccluskey, J., Mcgrath, M., Mcguire, H. M., Mcinnes, I. B., Mei, H. E., Melchers, F., Melzer, S., Mielenz, D., Miller, S. D., Mills, K. H. G., Minderman, H., Mjosberg, J., Moore, J., Moran, B., Moretta, L., Mosmann, T. R., Muller, S., Multhoff, G., Munoz, L. E., Munz, C., Nakayama, T., Nasi, M., Neumann, K., Ng, L.

G., Niedobitek, A., Nourshargh, S., Nunez, G., O'connor, J. E., Ochel, A., Oja, A., Ordonez, D., Orfao, A., Orlowski-Oliver, E., Ouyang, W., Oxenius, A., Palankar, R., Panse, I., Pattanapanyasat, K., Paulsen, M., Pavlinic, D., Penter, L., Peterson, P., Peth, C., Petriz, J., Piancone, F., Pickl, W. F., Piconese, S., Pinti, M., Pockley, A. G., Podolska, M. J., Poon, Z., Pracht, K., Prinz, I., Pucillo, C. E. M., Quataert, S. A., Quatrini, L., Quinn, K. M., Radbruch, H., Radstake, T., Rahmig, S., Rahn, H. P., Rajwa, B., Ravichandran, G., Raz, Y., Rebhahn, J. A., Recktenwald, D., Reimer, D., Reis, E. S. C., Remmerswaal, E. B. M., Richter, L., Rico, L. G., Riddell, A., Rieger, A. M., Robinson, J. P., Romagnani, C., Rubartelli, A., Ruland, J., Saalmuller, A., Saeys, Y., Saito, T., Sakaguchi, S., Sala-De-Oyanguren, F., Samstag, Y., Sanderson, S., Sandrock, I., Santoni, A., Sanz, R. B., Saresella, M., Sautes-Fridman, C., Sawitzki, B., Schadt, L., Scheffold, A., Scherer, H. U., Schiemann, M., Schildberg, F. A., Schimisky, E., Schlitzer, A., Schlosser, J., Schmid, S., Schmitt, S., Schober, K., Schraivogel, D., Schuh, W., Schuler, T., Schulte, R., Schulz, A. R., Schulz, S. R., Scotta, C., Scott-Algara, D., Sester, D. P., Shankey, T. V., Silva-Santos, B., Simon, A. K., Sitnik, K. M., Sozzani, S., Speiser, D. E., Spidlen, J., Stahlberg, A., Stall, A. M., Stanley, N., Stark, R., Stehle, C., Steinmetz, T., Stockinger, H., Takahama, Y., Takeda, K., Tan, L., Tarnok, A., Tiegs, G., Toldi, G., Tornack, J., Traggiai, E., Trebak, M., Tree, T. I. M., Trotter, J., Trowsdale, J., Tsoumakidou, M., Ulrich, H., Urbanczyk, S., Van De Veen, W., Van Den Broek, M., Van Der Pol, E., Van Gassen, S., Van Isterdael, G., Van Lier, R. a. W., Veldhoen, M., Vento-Asturias, S., Vieira, P., Voehringer, D., Volk, H. D., Von Borstel, A., Von Volkmann, K., Waisman, A., Walker, R. V., Wallace, P. K., Wang, S. A., Wang, X. M., Ward, M. D., Ward-Hartstonge, K. A., Warnatz, K., Warnes, G., Warth, S., Waskow, C., Watson, J. V., Watzl, C., Wegener, L., Weisenburger, T., Wiedemann, A., Wienands, J., Wilharm, A., Wilkinson, R. J., Willimsky, G., Wing, J. B., Winkelmann, R., Winkler, T. H., Wirz, O. F., Wong, A., Wurst, P., Yang, J. H. M., Yang, J., Yazdanbakhsh, M., Yu, L., Yue, A., Zhang, H., Zhao, Y., Ziegler, S. M., Zielinski, C., Zimmermann, J. & Zychlinsky, A. (2019). Guidelines for the use of flow cytometry and cell sorting in immunological studies (second edition). *Eur J Immunol* **49,** 1457-1973. Impact

Factor: 4.695

Kichev, A., **Eede, P.**, Gressens, P., Thornton, C. & Hagberg, H. (2017). Implicating Receptor Activator of NF-kappaB (RANK)/RANK Ligand Signalling in Microglial Responses to Toll-Like Receptor Stimuli. *Dev Neurosci* **39,** 192-206.

Impact Factor: 2.125

Acknowledgements

I would like to take this opportunity to express my gratitude towards the people who assisted me in pursuing my PhD.

Firstly, I would like to thank Prof. Dr. Frank Heppner for giving me the opportunity to undertake my PhD at the Department of Neuropathology, for his continuous support and guidance and for helping me become the scientist I am today. Thank you for continuing to give me pep talks even when being presented with negative data the majority of time.

I would like to say thank you to all the past and present members of the department that I had the pleasure of working with – you have always generated a joyful and collaborative working environment and I have learned so much from you. My special gratitude goes to the PhD girls Dr. Judith, Shirin, Kiara, Eileen and Alex for edible and mental support, the scientific and not-so-scientific discussions, steady Rotkäppchen and Berliner Luft supply and for always motivating me when things got tough. Thank you also to Janine and Adnan for our regular concert visits. I am also very grateful to Kelly and Juliane for supervising me during the first months in the lab, to the NeuroKine ITN consortium as well as to the students who have assisted my along the way. A special thank you to Marlene Foerster for patiently generating the data on the APPPS1;Nestin^{Cre};IL23R$^{fl/fl}$ mouse line.

To all the people I will list now: Thank you for always showing interest in my work, even though you never quite understood it.

My biggest thank you goes to my parents who have supported me in every step on the way leading up to this PhD. You have opened up countless opportunities for me, making me grow and become the person I am today and I know that you will always be there for me.

Merv, thank you for sticking with me even when I decided to move away for my PhD. Thank you for your patience, distractions, adventures, culinary extravaganzas and for making me see that taking things easy once in a while is not a bad thing.

Anna, Lena and Gulbi, what would I do without you? Thanks for always filling my heart with laughter and joy, supporting me and being silly with me – you are the best! Thanks as well to all my other friends spread across the world that always showed their support no matter how far away.